# Wave-Induced Currents Within Mangrove Forest

By

## Ahmad Azimi bin Kamaluddin

in partial fulfilment of the requirements for the degree of

**Master of Science**
in Hydraulic Engineering
with a specialisation in Coastal Engineering

at the Delft University of Technology,
to be defended publicly on Thursday November 9, 2017 at 9:30 AM.

Student number:     4519337
Thesis committee:   Prof.dr.ir Aarninkhof, S.G.J.    TU Delft, Chairman
                    Prof.dr.ir. Stive, M.J.F.        TU Delft
                    Prof.dr.ir. Uijttewaal, W.S.J.   TU Delft
                    Dr. Ye, Qinghua                  TU Delft
                    Zhang, R.                        TU Delft
                    ir. Tas, S.A.J.                  TU Delft

**TU**Delft

[This page is intentionally left blank]

# Preface

*In the name of Allah, the Beneficent, the Merciful.*

*All praise is due to Allah, the Lord of the Worlds.*

*The Beneficent, the Merciful.*

بِسْمِ اللهِ الرَّحْمنِ الرَّحِيمِ

الْحَمْدُ للّهِ رَبِّ الْعَالَمِينَ

الرَّحْمـنِ الرَّحِيمِ

[*Holy Quran 1:1-3*]

This master's thesis culminates the completion of my study in Master of Science in Hydraulic Engineering with a specialisation in Coastal Engineering in the prestigious Delft University of Technology. The two plus years leading up to this have been fruitful and have been full of new knowledge and experiences. This study has been heavily requiring to source theories that were learned in Ocean Waves and Coast Dynamics 1, as well as a good warmup to Delft3D from Coastal Dynamics 2.

No master's thesis, I believe, is absent of problems. This study is no exception. My major setback has been the validation of numerical model against measured data. Various trials and approaches have been made, thinking that I may have missed a thing or two. And numerous consultation with various experts have been made. Eventually, after crossing out each item in the checklist and with the help of the thesis committee, I arrived at the conclusion that this may be attributed to a limitation of one of the tools of the study. This has taught me the invaluable lesson that I have to be critical of all aspect of a study, be it the available measured data, literatures, empirical formulations, the modelling software, or my approaches and understandings. However, I cannot mask my nonfulfillment, that had I been able to run the simulations without the setbacks, with in mind of the huge potential of numerical models to predict various extrapolation and scenarios, perhaps the study would be able to present much more interesting findings. This compelling challenge may need to be undertaken by future master's thesis counterparts.

I would like to extend my gratitude to the thesis committee members who have been very helpful over the months: Prof.dr.ir Aarninkhof, S.G.J. in giving continuous support and guidance in the direction of the study; Prof.dr.ir. Stive, M.J.F. for giving a good form to the inception of the thesis scope of study and for the guidance on the (negative) findings of the model; Prof.dr.ir. Uijttewaal, W.S.J. for the constructive suggestions for improvements on report writing as well as in imparting the gravity of analytically and theoretically analysing measured and numerical data; Dr. Qinghua Ye who has been greatly helpful in the technicalities of Delft3D and in providing moral support; Rong Zhang who has been a great consult for the numerous problems I have been encountering with regards to the model and general work flow as well as for being empathetic when I made silly mistakes; ir. Tas, S.A.J. for providing constructive suggestions on my report and shedding light on important aspects that I may have otherwise overlooked. I wish you all the best in your future endeavours.

Last but not least, I would like to express my endless gratitude and love to my family and friends who have been there with their support and their comforting presence, through thick and thin. I wish you all the best in your endeavours, current and future.

*Ahmad Azimi bin Kamaluddin (Azimi)*
*Delft, November 2017*

# Abstract

Mangroves are tidal trees commonly observed along the sheltered shorelines of most tropical (from equator to 23.5° North and South latitude) and few subtropical (23.5° to 40° North and South latitude) countries. These plants are adapted to loose wet soils, saline habitats and periodic tidal submergence. With more attention paid into the approach of building with nature, natural coastal defence strategies are gaining more importance as an asset in addressing the coastal squeeze that is prevalent not only in urban areas, but also in agriculture and industrial areas that are located along the coastline. Mangroves are receiving more attention due to their coastal protective role against wave and hydrodynamic forcings as well as their ability to adapt to sea level rise. Mangrove vegetation attenuates and damps the hydrodynamics forcings by providing obstacles to the flows and creating drag. To date and to the knowledge of the author, no study has been conducted on interaction of the wave-induced currents with mangrove vegetation. This lack of relevant studies may be due to the fact that mangrove forests and the foreshore in front of the mangroves are usually of very gently sloping bed (varying in order of 1:300 to 1:1500). This means that in order to conduct physical model experiments to study wave-induced current within a mangrove forest, a very large wave basin is required in order to conduct modelling without using a very large scale factor difference between prototype and model. This is to ensure that the relevant processes are representing prototype as closely as possible, as well as to be measureable. Numerical modelling of the interaction of wave-induced current with mangrove vegetation is yet to be conducted due to the lack of measured data for validation, both field as well as experimental measurements. An experiment by Hulsbergen (1973) was selected as validation data for current study. The main objective of the study is to understand the difference of nearshore processes for (stationary) tidal gradient-driven and oblique wave-driven current for both with and without mimic mangrove vegetation. The scope of the study involves desktop analysis of the main validation data and other relevant and similar experiments, assessment of reliability of Delft3D for the study, validation against measured data, and simulation of various hydraulic conditions for condition with mangrove forest. Among questions answered in this study are the extent of wave-induced longshore current damping within mangrove forest, the significance of wave-induced longshore current within mangrove forest, the effects of bed slope and mangrove density on wave-induced current and the extent of model's reliability for current study. It was shown that the damping of wave-induced longshore current is more than 80% and the contribution of wave-induced current to the total velocity can be more than 70%. Of course, both of the above was specific to the bathymetry, mangrove properties and hydraulic conditions specified within current study. Furthermore, it was shown that bed slope and mangrove density affect wave-induced longshore current within the mangrove forest. It was also found that current model setup has its limitations.

# CONTENTS

# LIST OF FIGURES

# LIST OF TABLES

# LIST OF TABLES

# LIST OF SYMBOLS AND ACRONYMS

| | |
|---|---|
| $a$ | Wave amplitude [m] |
| $A$ | Roller area |
| $A_D$ | Area of pile normal to flow [m$^2$] |
| $b$ | Width of vegetation [m] |
| $c$ | Wave celerity [m/s] |
| $C$ | Chezy coefficient [m$^{1/2}$/s] |
| | Bottom drag coefficient |
| $c_f$ | Generalized non-dimensional friction factor [-] |
| $c_g$ | Group celerity [m/s] |
| $C_D$ | Drag coefficient [-] |
| $D$ | Dissipation |
| | Plant diameter [m] |
| $D_f$ | Dissipation due to bed friction |
| $D_r$ | Dissipation due to rolle |
| $D_w$ | Dissipation due to wave breaking |
| $E$ | Wave energy [kg/s$^2$] |
| $E_{kinetic}$ | Kinetic energy |
| $E_{potential}$ | Potential energy |
| $E_r$ | Roller energy |
| $f$ | Frequency [Hz] |
| $F_D$ | Force on pile over water depth |
| $F_x$ | Net force in x-direction (cross-shore) |
| $F_y$ | Net force in y-direction (alongshore) |
| $g$ | Gravity acceleration [m/s$^2$] |
| $h$ | Water depth [m] |
| $h_b$ | Depth at breaking [m] |
| $H$ | Wave height [m] |
| | Total water depth [m] |
| HC | Hydraulic Conditions |
| $H_s$ | Significant wave height [m] |
| H.W. | High water condition |
| $k$ | Wave number [rad/m] |
| $k_s$ | Equivalent geometrical roughness of Nikuradse [m] |
| $k_{st}$ | Roughness height by Strickler [m] |
| $K_{ref}$ | Refraction coefficient [-] |
| $K_{sh}$ | Shoaling coefficient [-] |
| $L$ | Wave length [m] |
| $L_E$ | Effective vegetation length scale [m] |
| $n$ | Ratio of group celerity to wave celerity [-] |
| | Manning's coefficient |
| N.A.P | *Normaal Amsterdams Peil* or Amsterdam Ordnance Datum |
| $p_{wave}$ | Wave-induced pressure |
| $P$ | Non-dimensional parameter representing the relative importance of the horizontal mixing |
| $P_{energy}$ | Total energy transport |
| $q_{drift}$ | Mass flux due to Stokes' drift |
| $Re$ | Reynolds number [-] |
| $R_d$ | Stem Reynolds number [-] |
| $s$ | Local depth gradient = $dh/dx$ |
| $S_{xx}$ | Transport of x-momentum in the x-direction (normal component) |
| $S_{xy}$ | Transport of x-momentum in the y-direction (shear component) |
| $S_{yy}$ | Transport of y-momentum in the y-direction (normal component) |
| $S_{yx}$ | Transport of y-momentum in the x-direction (shear component) |
| $S$ | Source term |

| | |
|---|---|
| $T$ | Period [s] |
| $T_p$ | Peak wave period [s] |
| $\bar{u}$ | Depth-averaged velocity [m/s] |
| $u_x, u_y$ | Particle velocity in *x*- and *y*-direction, respectively |
| $U_{below\ trough}$ | Undertow / return current |
| $U_0$ | Upstream uniform velocity [m/s] |
| $v_0$ | Maximum longshore current velocity [m/s] |
| $V$ | Longshore current velocity [m/s] |
| $V_{max}$ | Maximum longshore current velocity [m/s] |
| $x_B$ | Distance of breaking from waterline [m] |
| $X_m$ | Location of maximum longshore current velocity [m] |
| $\alpha$ | Beach slope |
| | Coefficient relating wave amplitude to water depth |
| $\beta$ | Slope of roller wave front |
| $\delta_0$ | Length of vortices extension into open channel [m] |
| $\delta_L$ | Penetration of vortices into vegetation patch [m] |
| $\rho$ | Density of water [kg/m$^3$] |
| $\rho u_x, \rho u_y$ | *x*- and *y*-momentum, respectively |
| $\eta$ | Surface elevation [m] |
| $\omega$ | Angular frequency [deg/s or rad/s] |
| $\pi$ | pi ≈ 3.142 [-] |
| $\theta$ | Wave direction with respect to shore normal [°] |
| $\theta_B$ | Angle of incidence at breaker line [°] |
| $\lambda$ | Characteristic lateral dimension of obstacle to the wavelength |
| | Areal concentration of stem [m$^{-1}$] |
| $\gamma$ | Ratio of breaking height to water depth at breaking [-] |
| $\xi$ | Iribarren parameter [-] |
| $\varphi_0$ | Deep water wave angle to the shore |
| $\bar{\tau}_{b,y}$ | Time-averaged bed shear stress in alongshore direction |
| $\nu$ | Molecular viscosity |
| $\nu_{T,H}$ | Eddy viscosity or turbulent viscosity [m$^2$/s] |

# 1 Introduction

Mangroves are tidal forests commonly observed along the sheltered shorelines of most tropical (from equator to 23.5° North and South latitude) and few subtropical (23.5° to 40° North and South latitude) countries.  Generally, in the region of higher latitudes, their counterpart, salt marshes occupy similar environmental conditions.  Situated between land and regions of tidal influence, the mangrove forest is host to numerous species of plants called mangroves.  These plants are adapted to loose wet soils, saline habitats and periodic tidal submergence.  In the more landward region, mangrove tree species grow alongside freshwater-adapted plants. Further landward (terrestrial) and in entirely freshwater regions, the freshwater species outcompete and dominate over mangrove plants.

With more attention paid into the approach of building with nature, natural coastal defence strategies are gaining more importance as an asset in addressing the coastal squeeze that is prevalent not only in urban areas, but also in agriculture and industrial areas that are located along the coastline. Mangroves are receiving more attention due to their coastal protective role against wave and hydrodynamic forcings as well as their ability to adapt to sea level rise. Various developments in the landward boundary of mangrove forests inhibit the expansion of mangrove in landward direction, provided the hydrodynamics and sediment conditions are favourable. Due to the above restrictions, most mangrove forests are able to only expand in the seaward or riverward front.

Although mangrove forests are generally found along low wave energy coastal and estuarine fringes, they are occasionally exposed to larger wind and swell waves during storm and high wind periods. Mangrove vegetation attenuates and damps the hydrodynamics forcings by providing obstacles to the flows and creating drag.

These various forcings against mangrove vegetation as well as the dissipation of the forcings and their interaction with the vegetation have been studied via laboratory, field and modelling methodologies. They include:
1. Wind-waves study by McIvor et al. (2012);
2. Swell waves and Infragravity waves study by van Rooijen et al. (2016);
3. Current flow and tidal forcings study by Horstman et al. (2013), Truong et al. (2017), Mazda et al. (2005);
4. Waves + following (parallel) current studies by Li and Yan (2007), Paul et al. (2012) and Hu et al. (2014); and
5. Storm surge of cyclone-induced hydrodynamics study Narayan et al. (2011) and McIvor et al. (2012)

However, to date and to the knowledge of the author, no study has been conducted on interaction of the wave-induced currents with mangrove vegetation.

A better understanding of the hydrodynamics of such intense ecosystem environment is crucial because it paves the way to better understanding of its interaction with the vegetation affects sedimentation, mass transfer and biological processes. There have been reports where sediment transport occurs in flows through densely vegetated surfaces, which shows that to a certain degree (Tsujimoto, 1999, Specht, 2002, Baptist 2005, Jordanova and James, 2003, cited by Kothyari 2009) the effects of flow (tidal, gravity, and wave-induced) to sediment suspension, movement and settling is non-trivial, but may be at different extent. This study is also motivated by the fact that numerous mangrove rehabilitations by replanting have been conducted and among key parameters in the success of the rehabilitation are waves and currents. Thus, it is necessary to investigate the significance of wave-induced current in vegetation patch such as mangrove forests to have an idea of its effects.

## 1.1  Problem Analysis

As mentioned in previous section, a knowledge gap exists where the interaction of wave-induced current with mangrove vegetation is yet to be studied, with the wave+following current being the closest to describe the phenomena. However, the following current studied by above-mentioned researches correspond to incident waves and background tidal currents that are perpendicular to the coast.

This lack of relevant studies may be due to the fact that mangrove forests and the foreshore in front of the mangroves are usually of very gently sloping bed (varying in order of 1:300 to 1:1500). This means that in order to conduct physical

model experiments to study wave-induced current within a mangrove forest, a very large wave basin is required in order to conduct modelling without using a very large scale factor difference between prototype and model. This is to ensure that the relevant processes are representing prototype as closely as possible, as well as to be measureable.

Numerical modelling of the interaction of wave-induced current with mangrove vegetation is yet to be conducted due to the lack of measured data for validation, both field as well as experimental measurements. Hence, the selection of the experiment by Hulsbergen (1973) as validation data for current thesis, as further elaborated in Section 3.1.

Following that, since no study of such nature has been conducted, it is still uncertain whether wave-induced current pose significant hydraulic interaction within the mangrove forest fields. This needs to be addressed to further understand the processes taking place within such important ecosystem.

Current study is conducted entirely in Delft University of Technology (TU Delft), The Netherlands, and no external organization is involved.

## **1.2**   Problem Formulation

The objective of current study is:
> To understand the difference of nearshore processes for (stationary) tidal gradient-driven and oblique wave-driven current for both with and without mimic mangrove vegetation.

Research questions:
1. What is the extent of the model's applicability for current study?
2. What is the extent of damping of wave-induced current within the vegetation?
3. What is the significance of the interaction of wave-induced longshore current with mangrove vegetation?
4. How is the nearshore current affected by varying vegetation properties such as bed slope and density?

The study objective is articulated into several research questions for measurable achievement. Research question No. 1 addresses the applicability of the numerical model software for current study. Research question No.2 looks into the percentage of reduction of wave-induced longshore current velocity within mangrove forest in comparison to both situations without any vegetation and with pile groyne. This also is being quantified by comparing against the damping of other hydraulic conditions. Research question No. 3 quantifies the contribution of wave-induced longshore current to the total velocity within surf zone (plain condition, pile groyne and mangrove forest). Research question No. 4 looks into the magnitude and distribution of wave-induced current for gentler bed slopes and for forest densities that fall within the range of regular mangrove forest properties. To achieve research questions No. 2-4, in-depth look into theories, literatures, the main validation data, other experiments, analytical calculation, and numerical modelling were necessary.

The findings from current thesis may be extrapolated and utilised for future studies into the effects of wave-induced current on the sediment dynamics and morphology. A general idea is that waves stir the sediment from the bed into the water column and currents transport the suspended sediments away. Furthermore, the findings from current thesis may be able to be used in assisting in the improvement of existing models' numerical and/or formulation aspects for the interaction of vegetation and hydraulics, which is constantly being undertaken in TU Delft and Deltares, The Netherlands. This understanding will lead to better management, and increased awareness of the importance, of coastal mangroves.

## **1.3**   Study Approach

Following the knowledge gap and lack of available insight into wave-induced current within mangrove forest, as well as the importance of coastal fringing mangrove forest not only to ecosystem, but also as coastal protection, which is in turn highly crucial in maintaining good social and economic climate of coastal regions, the most important and wide-ranging aspect that needs to be addressed and objective was formed from this. Research questions were formulated that breaks down the objective into aspects that need to be looked at systematically.

Literature reviews were conducted to better understand previous studies that have been conducted in relation to current study. A good number of literatures gave excellent look at the approaches they adopted, the theories they associate with, a wealth of discussions and give good insight into the numerous aspects that builds up into the understanding needed for the objective. A theoretical background was established on linear wave theory, wave-induced current, etc. They are sourced mostly from textbooks and other literatures.

Various methods are possible in studying the interaction of wave-induced current and the vegetation, i.e. by conducting field measurement, physical modelling and numerical modelling. Field measurement is opted out of due to the elaborate nature of the preparation, high capital needed and the measurement campaign itself, as well as due to the relative inflexibility in varying the boundary conditions and other parameters.
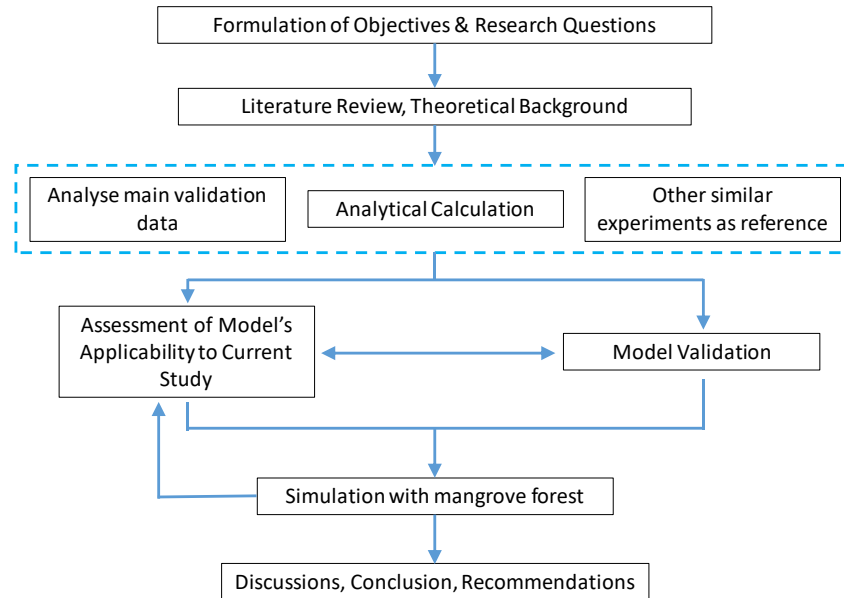


Figure 1        Study Approach

A physical modelling experiment on flow velocity and pattern for a coastline with permeable pile groynes has been conducted by Hulsbergen (1973). The measurements from the experiment will be used as main validation data. Their model setup is further elaborated in Section 3.1. As current study focuses only on the hydrodynamics of the interaction between the forcings and the mangrove vegetation, elaboration and application of Hulsbergen's study is largely focused on the model. An in-depth look into the result of the experiment was conducted, taking into account the theories established in the previous step.

Apart from the main validation dataset, references into other similar and relevant experiments were also made, mostly qualitatively. Comparisons were made between these experiments to establish areas of uncertainties, which mainly is prevalent in Hulsbergen's (1973) study due to the age of the experiment. To address uncertainties of the main validation dataset, an analytical calculation of wave-induced current was conducted concurrently using theories elaborated in the previous step. The result of analytical calculation was compared and discussed against main validation dataset and other experiments that are relevant and similar in nature.

For current study, numerical modelling was selected due to its flexible capability in varying the various parameters such as coastline profile, boundary conditions and vegetation properties. This allows the study into various scenarios and schematizations of interaction between wave-induced current. Delft3D-FLOW and -WAVE modules are used and are further elaborated in Section 1.4. The applicability of the model looks into the extent of its prediction against measured data and analytical calculation, as well as the model's limitation for different model settings and scenarios. Both will be different for different bathymetry and hydraulic conditions.  It is therefore very important to investigate the applicability of Delft3D for current study. This was conducted initially concurrent with validation stage against Hulsbergen's (1973) measured data which provides quite extensive information. After that, when different parameters of mangrove forest are varied, model robustness is also checked while discussing the results. Hence, the arrow that loops upward back from 'simulation with mangrove forest' to 'assessment of model's applicability to current study'.

Results and analysis were discussed during the Committee Meetings as well as during informal discussions with thesis committee and other academicians.

## 1.4    Scope of Study

Bed Slope

The foreshore slopes of muddy coastlines consist of wide variation. At Mekong Delta, the slope varies from as steep as about 1:300 to about 1:1000 (Figure 2), provided by Mathematical Modelling and GIS Department of Institute of Coastal and Offshore Engineering - Vietnam Academy for Water Resources (VAWR). Appendix A shows the respective profile cross-sections.
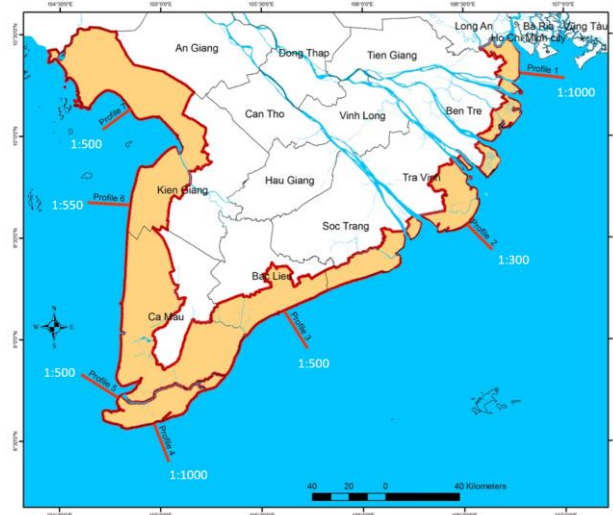


Figure 2       Locations of coastal profiles and their respective approximate slopes (Source: VAWR)
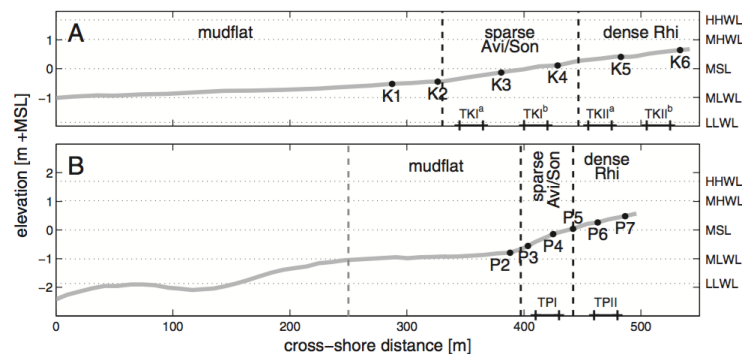


Figure 3       Elevation of mudflats and mangrove forest beds at west coast of southern Thailand facing the Andaman Sea (A) a transect at Kantang estuary; and (B) a transect at Palian estuary (Horstman et al., 2014)

Figure 3 shows the elevation of mudflats and mangrove forest beds at two transects located at the southwestern coast of Thailand facing the Andaman Sea. The transect at Kantang shows mudflat profile of about 1:600 and mangrove forest bed profile of about 1:200. Whereas, the transect at Palian shows mudflat profile of about 1:750 and mangrove forest bed profile of about 1:70. The above shows large variation in the slope profile of muddy coastline with coastal fringing mangrove forests.

A sensitivity analysis was conducted by Tas (2016) for extremely gentle slope of 1:1500 for both SWAN and SWASH (Figure 4). It can be seen that there is a very significant divergence between both models. This shows a lower confidence level for the performance of both numerical models for the wave processes in very gentle slope. Since current research focuses into the wave-induced current, which is due to wave energy dissipation and this is proportional to wave amplitude squared (Section 2.1), this further increases the uncertainty level.
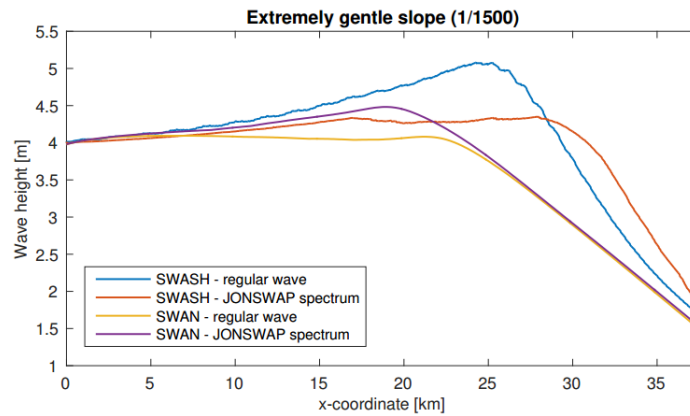
Figure 4      Comparison of the wave transformation of regular wave and JONSWAP spectrum on a slope of 1/1500 for SWAN and SWASH (Tas, 2016)

Due to the wide spectrum of bed profile for mangrove forest, as well as the low confidence level of current numerical models to be applied for extremely gentle slopes, for current research, mangrove forest with bed profile of Hulsbergen's (1973) experiment is investigated.

## Delft3D-FLOW and -WAVE Modules

Delft3D is developed by Deltares and is a fully integrated computer software suite for 3D computations for coastal, river and estuarine areas. The program is capable of simulations of flows, waves, sediment transports, water quality, morphological developments and ecology. Delft3D suite consists of multiple modules for different applications, including Delft3D-FLOW and Delft3D-WAVE.

Delft3D-FLOW is a multi-dimensional (2D or 3D), process based, hydrodynamic simulation program developed by Deltares that calculates non-steady flow and transport phenomena resulting from tidal and meteorological forcings. These forcings include flows driven by tide, wind, stratification and density gradients, as well as waves.

In schematization of the computational domain, the following options are available, summarized in the order from costly to fast computation time (Van der Linde, 2011):
1. 3D schematization;
2. Quasi-3D, this model computes the vertical velocity distribution at every grid point accounting for tidal forcing, wave breaking, wind and dissipation due to bottom friction;
3. 2D schematization consisting of averaging the width (2DV) or height (2DH); and
4. 1D schematization.

Horstman et al. (2013) has studied the tidal dynamics in mangroves whilst comparing between 3D and 2D models, and arrived at the conclusion that the 2DH model predicts tidal hydro- and sediment dynamics accurately resembling the 3D model prediction. With less computational demand required by 2D models, they are more efficient than 3D models. Plus, If the fluid is vertically homogeneous, a depth-averaged approach is appropriate (Delft3D manual, 2016). For current study, Delft3D is setup for 2DH schematization.

Waves computation in Delft3D-WAVE module is conducted by third generation SWAN (Simulating Waves Nearshore) model, which is capable of simulating the evolution of random, short-crested wind-generated waves in estuaries, tidal inlets, lakes, etc. State-of-the-art formulas are applied in SWAN to represent the physics, as well as being fully spectral in frequencies and directions. Orientation of computational grid is flexible as SWAN can compute waves propagating from all directions simultaneously.

In Delft3D, Flow and Wave modules can be coupled online. By doing so, both modules make dynamic two-way interaction. Both the effects of waves on current (via forcing, enhanced turbulence and enhanced bed shear stress) and the effect of flow on waves (via set-up, current refraction and enhanced bottom friction) are accounted for.

# 2  Theoretical Background

## 2.1.  Waves in Coastal Waters

Ocean waves consists of all the oscillations of the water surface generated in the ocean. The most important waves in shaping the coastal zone are short waves generated by wind and the longer tidal motion generated by the attractive forces of the sun and the moon on the water masses of the earth. A very simple representation and a general formula for the surface elevation of ocean waves is (Bosboom and Stive, 2015):

$$\eta = a \sin(\omega t - kx) = a \sin S(x, t)$$
<div align="right">Equation 1</div>

where, $a = \frac{H}{2}$ is the amplitude, $\omega = 2\pi f = \frac{2\pi}{T}$ is the angular frequency and $k = \frac{2\pi}{L}$ is the wave number. $H$ is the wave height in meter, $T$ is the wave period in second, $f$ is the frequency in Hz and $L$ is the wave length in meter.

The wave celerity or propagation speed of the deformations is $c = \frac{L}{T} = \frac{\omega}{k}$ in m/s. With dispersion relationship of

$$\omega^2 = gk \tanh kh$$
<div align="right">Equation 2</div>

the wave celerity at arbitrary depth is

$$c = \frac{g}{\omega} \tanh kh = \sqrt{\frac{g}{k}} \tanh kh = \frac{gT}{2\pi} \tanh kh$$
<div align="right">Equation 3</div>

with $h$ as the water depth in meter and $g$ as the gravity acceleration in m/s². Whereas, the group celerity is $c_g = nc$, with $n = \frac{1}{2}\left(1 + \frac{2kh}{\sinh 2kh}\right)$ from the dispersion relationship as the ratio of group celerity to wave celerity. $n = 0.5$ in deep water and $n = 1$ in very shallow water.

The dispersion relationship is an implicit expression in terms of wave number. This requires an iteration procedure to calculate the wave number in a given frequency and depth. A way to solve this is to utilise a look-up table or to use an explicit expression that approximates the solution closely. Eckart (1952) (cited by Holthuijsen, 2007) proposes an explicit approximation:

$$kh \approx \alpha(\tanh \alpha)^{-1/2} \qquad \text{with} \qquad \alpha = k_0 h = \frac{\omega^2 h}{g}$$
<div align="right">Equation 4</div>

which is exact for the limits of deep and shallow water (both $kh \to \infty$ and $kh \to 0$).

### Wave Energy

Waves consists of potential energy, $E_{potential}$, due to the work done against gravitation, and kinetic energy, $E_{kinetic}$, due to the movement of the particles (Holthuijsen, 2007). In linear wave theory approximations, $E_{potential} = E_{kinetic}$. Thus the total time-averaged wave-induced energy density is

$$E = E_{potential} + E_{kinetic} = \frac{1}{2}\rho g a^2 = \frac{1}{8}\rho g H^2$$
<div align="right">Equation 5</div>

The total energy transport,

$$P_{energy} = Enc = Ec_g$$
<div align="right">Equation 6</div>

shows that the wave energy is transported at the wave group velocity in the wave direction, which is normal to the wave crest, except for the in the case of the presence of ambient current.

### Energy Balance

Energy conservation equation by integrating over all frequencies and directions in an irregular wave field is (Bosboom and Stive, 2015):

$$\frac{\partial E}{\partial t} + \frac{\partial}{\partial x}\left(Ec_g \cos\theta\right) + \frac{\partial}{\partial y}\left(Ec_g \sin\theta\right) = S - D$$
<div align="right">Equation 7</div>

where the first term on the left hand side of the equation corresponds to change of energy, while the second and third terms correspond to import of energy in x-direction and y-direction respectively. The right hand side of the equation corresponds to gain of energy. $\theta$ is the wave direction with respect to shore normal, S is the generation term and D is the dissipation term.

The dissipation of wave energy can be caused by wave breaking, bottom friction, and interaction with vegetations. In small-scale coastal waters, wave generation, which is usually by energy transfer from wind, can be neglected. By assuming stationary wave condition, the term $\partial E/\partial t$ equals zero. Then the energy balance can be reduced to:

$$\frac{\partial}{\partial x}\left(Ec_g\cos\theta\right) + \frac{\partial}{\partial y}\left(Ec_g\sin\theta\right) = -D_f - D_w \qquad \text{Equation 8}$$

where $D_w$ denotes energy dissipation due to wave breaking and $D_f$ denotes energy dissipation due to bed friction.

## Shoaling

When a normally incident wave propagates towards a coastline with a gentle slope and no current, its wave length decreases with retained frequency, as the dispersion relationship remains valid. The phase speed, in turn, also decreases. This is called shoaling. The effect of shoaling will initially decrease and then increase the wave amplitude as it propagates towards the coast. The shoaling coefficient is

$$K_{sh} = \frac{a}{a_\infty} = \sqrt{\frac{c_{g,\infty}}{c_g}} = \sqrt{\frac{1}{\tanh kh}\frac{1}{2n}} \qquad \text{Equation 9}$$

where subscript $\infty$ denotes deep water parameter. The above shows that the coefficient is a function of $kh$ only, which explains the changes in the wave amplitude during the propagation towards the coast. This implies that the wave will subsequently rise to infinity at the waterline. However, in reality, the increase of wave height is halted by the dissipation of wave energy during wave breaking. Refraction may also play a role in the reduction of wave amplitude.

## Refraction

When a wave approaches a uniform coastline at an angle, the wave direction will gradually change due to the difference of water depth along a given crest of the wave. Consistent with the dispersion relationship, wave crests move faster in a deeper water than in shallow water, which means it moves over greater distance during a given passing of time. This orientates the wave to turn towards the coast, which is the region of lower propagation speed. This bending effect is called refraction.

According to Snell's law (Holthuijsen, 2007), the direction of wave rays (line normal to the crest) changes in proportion to the change of wave celerity:

$$\frac{\sin\theta}{c} = \frac{\sin\theta_{deepwater}}{c_{deepwater}} \qquad \text{Equation 10}$$

with $\theta$ denoting the angle of between the wave ray and the normal to depth contours. Due to conservation of energy, the effect of refraction on the wave amplitude is:

$$a = \sqrt{\frac{c_{g,\infty}}{c_g}}\sqrt{\frac{b_\infty}{b}}a_\infty \qquad \text{Equation 11}$$

The refraction coefficient from above is:

$$K_{ref} = \sqrt{\frac{b_\infty}{b}} \qquad \text{Equation 12}$$

Generally, if the wave rays converge, there will be an accumulation of wave energy and the wave amplitude will rise, and vice versa.

When a short wave comes into contact with current, a refraction phenomenon called current-refraction occurs (Bosboom and Stive, 2015). This occurs when the current velocity varies along a wave crest and will affect the wave celerity, amongst others (Section 2.4).

## Diffraction

Diffraction occurs when due to large variation of wave energy along wave crests, the energy is transferred along the crests. This happens when there is obstructions or abrupt changes in the bottom contours along the wave propagation path. When waves encounter an obstruction (for example, a breakwater), some part of the waves are reflected seaward while some propagate alongside the obstruction and bend and penetrate the leeward zone of the obstruction, which is called the shadow zone. Due to the lateral transfer of energy into the shadow zone, the wave height along the wave ray in the zone is lower than the incident wave height.

The extent of wave energy penetration in the shadow zone depends on the ratio of a characteristic lateral dimension of the obstacles (for example, the length of breakwater or the diameter of a pile), $\lambda$, to the wavelength, $L$ (Bosboom and

Stive, 2015). When a relatively thin pile is standing in waves with a large wavelength, $\lambda \ll L$, wave energy spreads behind the entire pile.

## Wave Breaking

Theoretically, the shoaling process will increase the wave height to infinity as the waves approach the coastal waterline. However, in reality the waves will break once they reach the physical limit of steepness. The wave crests will become unstable and will break when the particle velocity exceeds the wave celerity. In deepwater, this is called white-capping. In shallow water, this is called depth-induced breaking.

The limit of wave steepness is expressed by Miche (1994) (as cited by Bosboom and Stive, 2015) which is based in the Stokes wave theory:

$$\left[\frac{H}{L}\right]_{max} = 0.142 \tanh(kh) \qquad \text{Equation 13}$$

which reduces to $(H_0/L_0)_{max} = 0.142$ in deep water, when the white-capping will be induced. In shallow water Equation 13 becomes

$$\left[\frac{H}{L}\right]_{max} = 0.142 \frac{2\pi}{L} h \approx 0.88 \frac{h}{L} \qquad \text{Equation 14}$$

which is equivalent to the breaker index (individual waves start to break when the height becomes greater than a certain fraction of the water depth),

$$\gamma = \left[\frac{H}{h}\right]_{max} = \frac{H_b}{h_b} \approx 0.88 \qquad \text{Equation 15}$$

with $H_b$ as the breaking wave height and $h_b$ as the water depth at breaking point. For a non-linear wave for shallow water, the value is slightly different, i.e. $\gamma \approx 0.78$. In Rayleigh distribution, the maximum wave height $H_{max}$ in a record is equal to $2H_s$. Then, $H_s/h \approx 0.4-0.5$ based in Miche criterion.

The waves break differently for varying wave properties and bed slope angle. Battjes (1974) (as cited by Bosboom and Stive, 2015) presented Iribarren parameter in explaining the relationship:

$$\xi = \frac{\tan \alpha}{\sqrt{H_0/L_0}} \qquad \text{Equation 16}$$

with $\tan \alpha$ as the steepness of the beach while the steepness of the wave as a function of $L_0$, the wavelength in deep water. This differentiates the various breaker types, namely spilling, plunging, collapsing and surging breakers. Iribarren parameter indicates that the notion of 'steep' and 'gentle' are relative to the slope and wave properties.

A depth-varying breaker parameter proposed by Ruessink et al. (2003) is as following

$$\gamma_b = 0.76kh + 0.29 \qquad \text{Equation 17}$$

## Surface Roller

Surface roller acts as a temporary storage of energy and momentum (Bosboom and Stive, 2015). This process delays the dissipation of the wave energy, where upon breaking, the wave energy is converted into turbulent kinetic energy and subsequently is dissipated via the production of turbulence. This is taken into account by the usage of roller balance equation. The roller energy $E_r$, represents the amount of kinetic energy in a roller propagating at the shallow water speed, $c = \sqrt{gh}$.

It was shown by Reniers and Battjes (1997) that for an accurate prediction of longshore current, inclusion of roller model is necessary. A wave energy balance that includes a roller energy balance is (Mil-Homens, 2016),

$$\frac{d}{dx}\left(Ec_g \cos \theta\right) + \frac{d}{dx}\left(E_r c \cos \theta\right) = -D_r \qquad \text{Equation 18}$$

which can be separated into two independent equations, i.e. for wave energy and roller energy,

$$\frac{d}{dx}\left(Ec_g \cos \theta\right) = -D_b \qquad \text{Equation 19}$$

$$\frac{d}{dx}\left(E_r c \cos \theta\right) = D_w - D_r \qquad \text{Equation 20}$$

where $D_w$ is the energy dissipation due to wave breaking and $D_r$ is energy dissipation due to roller which is given by

$$D_r = 2 \frac{gE_r \beta}{c} \qquad \text{Equation 21}$$

where $\beta$ is the slope of the wave front which usually is 0.1, but no bigger than that value (Walstra et al., 1996). The roller energy,

$$E_r = \frac{\rho Ac^2}{2L} \qquad \text{Equation 22}$$

where $A$ is the roller area and $L$ is the wavelength corresponding to $T_p$. In Delft3D, the wave dissipation due to wave breaking uses the expression by Roelvink (1993) which includes the parameter $\alpha$, a calibration coefficient with the order $O(1.0)$.

## 2.2. Wave-Induced Longshore Current

Waves approaching the coastline at oblique angles will induce alongshore current in the surf zone (Figure 5). This current plays a significant role in the transport of sediment along the coastline and as such, is often dubbed as river of sand.
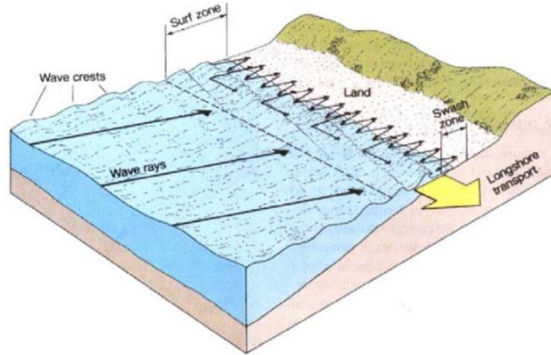


Figure 5 Alongshore current and transport induced by obliquely propagating waves (Source: Lecture slides of Coastal Dynamics 1 2016 [CIE4305])

The following sections provide brief background information regarding the generation of alongshore current in the surf zone. Firstly, radiation stress is explained, followed by the forces that induce the current.

Radiation Stresses

Waves carry energy and momentum across oceanic water body (Bosboom and Stive, 2015). Momentum is defined as the product of mass and velocity, or in other words, mass in motion or mass transport/ flux. Depth-integrated and wave-averaged flow (or flux) of momentum due to waves is called radiation stress. Longuet-Higgins and Stewart (1964) defined it as the excess of momentum due to the presence of waves. Wave forces are induced with the presence of spatial gradient of radiation stresses. These forces drive water level set-down and set-up, as well as longshore current for obliquely propagating waves.

Figure 6 shows the propagation of oblique waves with $\theta$ angle with respect to the shore normal line. $x$-axis denotes cross-shore while $y$-axis denotes alongshore direction. The radiation stress components are:

$$S_{xx} = \overline{\int_{-h_0}^{\eta} (\rho u_x)u_x dz} + \overline{\int_{-h_0}^{\eta} p_{wave} dz} \qquad \text{Equation 23}$$

$$S_{xy} = \overline{\int_{-h_0}^{\eta} (\rho u_x)u_y + \tau_{xy} dz} \qquad \text{Equation 24}$$

$$S_{yy} = \overline{\int_{-h_0}^{\eta} (\rho u_y)u_y dz} + \overline{\int_{-h_0}^{\eta} p_{wave} dz} \qquad \text{Equation 25}$$

$$S_{yx} = \overline{\int_{-h_0}^{\eta} (\rho u_y)u_x dz} \qquad \text{Equation 26}$$

Where,
$S_{xx}$ = Transport of $x$-momentum in the $x$-direction (normal component)
$S_{xy}$ = Transport of $x$-momentum in the $y$-direction (shear component)
$S_{yy}$ = Transport of $y$-momentum in the $y$-direction (normal component)
$S_{yx}$ = Transport of $y$-momentum in the $x$-direction (shear component)
$\rho u_x, \rho u_y$ = $x$- and $y$-momentum, respectively
$u_x, u_y$ = particle velocity in $x$- and $y$-direction, respectively
$p_{wave}$ = wave-induced pressure
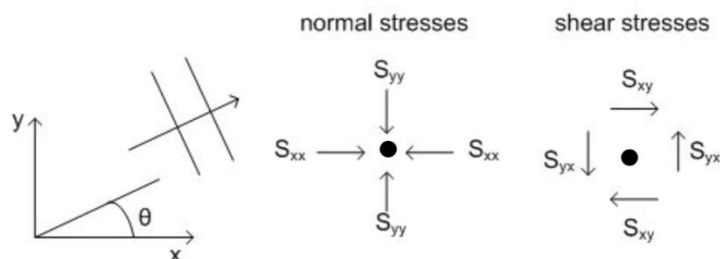


Figure 6 Radiation stress components for obliquely incident waves (Bosboom and Stive, 2015)

Using linear wave theory, general expressions can be obtained that are valid to second order. Equation 23 to Equation 26 are expressed as:

$$S_{xx} = \left(n - \frac{1}{2} + ncos^2\theta\right)E$$

Equation 27

$$S_{yy} = \left(n - \frac{1}{2} + nsin^2\theta\right)E$$

Equation 28

$$S_{xy} = S_{yx} = ncos\theta sin\theta E$$

Equation 29

Where,

$E$ = Wave energy in the water column per m$^2$

$n$ = Ratio of group velocity and phase velocity

## Wave Force

Wave-induced forces due to horizontal gradients of radiation stresses are expressed as:

$$F_x = -\left(\frac{dS_{xx}}{dx} + \frac{dS_{xy}}{dy}\right)$$

Equation 30

$$F_y = -\left(\frac{dS_{yy}}{dy} + \frac{dS_{yx}}{dx}\right)$$

Equation 31

Where,

$F_x$ = Net force in $x$-direction (cross-shore)

$F_y$ = Net force in $y$-direction (alongshore)

$\frac{dS_{xx}}{dx}$ = Cross-shore variations in the $x$-directed radiation normal stresses

$\frac{dS_{xy}}{dy}$ = Alongshore variations in the $y$-direction of the $x$-directed radiation shear stress

$\frac{dS_{yy}}{dy}$ = Alongshore variations in the $y$-directed radiation normal stresses

$\frac{dS_{yx}}{dx}$ = Cross-shore variations in the $x$-direction of the $y$-directed radiation shear stress

Equation 31 is responsible to drive alongshore current. Generally, the transfer of momentum from the wave motion to the mean flow in the alongshore direction gives rise to alongshore current. For an alongshore uniform coast (no variation in the y-direction), Equation 31 is simplified to:

$$F_y = -\frac{dS_{yx}}{dx}$$

Equation 32

This means that the cross-shore rate of variation of the shear component of the radiation stress $S_{yx}$ acts as driving force. Alongshore, the balancing force to restore equilibrium is supplied by bed shear stresses that develop when a longshore current is generated.

In deeper water, i.e. outside of the breaker zone, for linear waves the wave force equation can be written as:

$$F_y = -\frac{dS_{yx}}{dx} = -\frac{sin\theta}{c}\frac{d}{dx}Ec_gcos\varphi = \frac{D_w}{c_0}sin\varphi_0$$

Equation 33

Where,

$c$ = Wave celerity

$c_g$ = Wave group velocity

$D_w$ = Wave dissipation due to wave breaking

$c_0$ = Deep water wave celerity

$\varphi_0$ = Deep water wave angle to the shore

This shows that the alongshore driving force is a function of the dissipation of the wave energy. This dissipation of energy can be neglected outside of the surf zone, which means the radiation shear stress is constant, and no gradient of radiation shear stresses is present. Hence, the occurrence of the alongshore current in the surf zone due to the presence of energy dissipation due to wave breaking.

## Analytical Model for Longshore Current

In long uninterrupted coastlines, there is no hydraulic pressure gradient as happens in the cross-shore direction to balance the driving force. The counterforce restoring equilibrium is provided by bed shear stresses. The alongshore component of the momentum balance for steady state and uniform alongshore is:

$$F_y = -\frac{dS_{yx}}{dx} = \bar{\tau}_{b,y}$$

Equation 34

where $\bar{\tau}_{b,y}$ is the time-averaged bed shear stress in the alongshore direction,

$$\bar{\tau}_{b,y} = \frac{1}{\pi}\rho c_f\sqrt{gh}\frac{H}{h}V$$

Equation 35

where V is the depth-averaged longshore current velocity. The magnitude of depth-averaged longshore current velocity is a function of the dissipation, height and water depth. By balancing between the driving force and the resisting force, as well as for a constant $\gamma$,

$$V(x) = -\frac{5}{16}\pi\frac{\gamma}{c_f}g\frac{\sin\varphi_0}{c_0}h\frac{dh}{dx}$$                    Equation 36

A constant beach slope would render $\tan\alpha = -\frac{dh_0}{dx} \approx -\frac{dh}{dx}$. $c_f$ is a dimensionless coefficient relating the bed shear stress to the square of velocity. The Chezy coefficient, $C$, relates to $c_f$ as $c_f = g/C^2$. Equation 36 shows that the current velocity is maximum at the breaker line, where $h=h_b$. However, the formula above is unrealistic, as it does not take into account the effect of lateral dispersion of momentum by turbulence, which will smooth out the velocity gradients (Figure 7), especially at the breaker line (Longuet-Higgins, 1970). The figure shows the longshore current profiles for various values of $P$, which is non-dimensional parameter representing the relative importance of the horizontal mixing. $P$=0 means no horizontal mixing, which shows a zero mixing triangular profile with peak at the breaker line, similar to that of Equation 36. With higher value of $P$, the maximum velocity decreases and its location shifts landward.

Physically, this means the effect of increasing the horizontal mixing is to redistribute the momentum so that the fluid near the shoreline is dragged along at faster speed by the fluid farther offshore, but farther offshore the fluid is slowed down by the mass beyond the breaker line (Longuet-Higgins, 1970b).
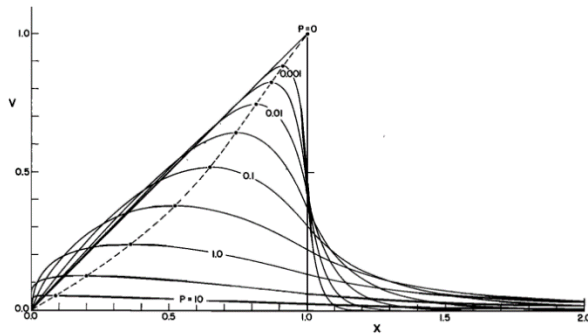


Figure 7    Longshore current velocity profile for varying values of $P$. $X = x/x_B$, where $x_B$ is the breaker distance from coastline. $V=v/v_0$, where $v_0$ is the maximum longshore current velocity for the case $P$=0 (Longuet-Higgins, 1970b).

By considering the effects of turbulence, the shear stress that acts on a surface parallel to the coast is (Bosboom and Stive, 2015,

$$S'_{yx} \cong h\rho\nu_{T,H}\frac{dV}{dx}$$                    Equation 37

where $\nu_{T,H}$ is the eddy viscosity or turbulent viscosity or horizontal diffusivity. The shear stress is related to velocity gradient through the eddy viscosity. It is a measure of turbulent fluid friction. In coastal waters, $\nu_T \gg \nu$, where $\nu$ is the molecular viscosity. Equation 34 now becomes (Bosboom and Stive, 2015),

$$\frac{D_w}{c_0}\sin\varphi_0 + \frac{d}{dx}\left(h\rho\nu_{T,H}\frac{dV}{dx}\right) = \bar{\tau}_{b,y}$$                    Equation 38

Generally, this reduces the maximum velocity and shifts the position of maximum velocity landward. Also, there will also be longshore current outside of the surf zone.

Equation 36 also does not take into account the effect of roller momentum, which shifts the maximum longshore current velocity shoreward. This can be modelled by including roller momentum into the alongshore momentum equation (Equation 38).

For irregular waves, there is no sharply defined breaker line. Similar to the effect of turbulence, the profile of longshore current velocity is wider and less sharply peaked (Bosboom and Stive, 2015).

An alternative formulation is provided by Longuet-Higgins (1970a & 1970b) for longshore current velocity:

$$V = \begin{cases} B_1 X^{p_1} + AX & 0 < X < 1 \\ B_2 X^{p_2} & 1 < X < \infty \end{cases}$$                    Equation 39

With,

$$B_1 = \frac{p_2-1}{p_1-p_2}A$$                    Equation 40

$$B_2 = \frac{p_1-1}{p_1-p_2}A$$                    Equation 41

$$p_1 = -\frac{3}{4} + \left(\frac{9}{16}+\frac{1}{P}\right)^{1/2}$$                    Equation 42

$$p_2 = -\frac{3}{4} - \left(\frac{9}{16}+\frac{1}{P}\right)^{1/2}$$                    Equation 43

$$A = \frac{1}{1 - \frac{5}{2}P}$$ 

<div align="right">Equation 44</div>

$$X = x/x_B$$

<div align="right">Equation 45</div>

$$V = v/v_0$$

<div align="right">Equation 46</div>

$$v_0 = \frac{5\pi}{8} \frac{\alpha}{C} \sqrt{gh_B} s \sin \theta_B$$

<div align="right">Equation 47</div>

$$P = \left(\frac{\pi}{2}\right)\left(\frac{sN}{\alpha C}\right)$$

<div align="right">Equation 48</div>

$x_B$ is the cross-shore location of the breaker line from the coastline, $s = dh/dx$ is the local depth gradient, $h_B$ is the water depth at breaker line, $\theta_B$ is the angle of incidence at the breaker line, $\alpha$ is a coefficient that relates the wave amplitude to water depth, $C$ the drag coefficient at the bottom, $N$ is a dimensionless constant, $P$ is a non-dimensional parameter representing the relative importance of the horizontal mixing as shown in Figure 7. Equation 47 is a variation of Equation 36, which is a momentum balance without the consideration of horizontal mixing ($P$=0). From Equation 39, it can be seen that the formulation is different for within breaker zone ($X < 1$) and for outside breaker zone ($X > 1$).

The maximum velocity location, $X_m$, and its corresponding magnitude, $V_{max}$, are,

$$X_m = \left[\frac{p_1 - p_2}{p_1(1 - p_2)}\right]^{\frac{1}{p_1 - 1}}$$

<div align="right">Equation 49</div>

$$V_{max} = \left(1 - \frac{1}{p_1}\right) A X_m$$

<div align="right">Equation 50</div>

## 2.3. Wave-Induced Cross-shore Current

Cross-shore current averaged over an entire water column for a stationary case should be zero (Bosboom and Stive, 2015). This is intuitively known because water neither piles up higher and higher against the coast nor flows towards deeper water. Thus, there is an offshore return current at lower elevation of a given point in cross-shore profile to compensate onshore-directed mass flux near the water surface. This means that the depth-averaged flow through each cross-section is zero. This return current is called undertow:

$$U_{below\ trough} = -\frac{q_{drift,x}}{\rho h} = -\frac{q_{drift} \cos \theta}{\rho h}$$

Where $q_{drift}$ is mass flux due to Stokes' drift.

Inside the surf zone, while moving towards coastline, the magnitude of $S_{xx}$ decreases rapidly due to wave breaking resulting in a negative gradient of $S_{xx}$ (Bosboom and Stive, 2015). This decrease means results in a force acting in landward direction. To achieve equilibrium of forces, a small difference in water level results, which is higher towards the waterline. This is called wave set-up, and it creates a seaward directed pressure force.

## 2.4. Wave-Current Interaction

When waves interact with current, energy is not conserved anymore, since transfer of energy between waves and current is possible (Bosboom and Stive, 2015, pp 158). In that case, another wave quantity, wave action $E/\omega$, will be conserved and the wave action balance rather than the energy balance should be solved. In the absence of current, the wave action balance reduces to the energy balance. This is taken into account in SWAN model.

If the waves meet a current, the wavelength, propagation velocity and wave height will be affected (Bosboom and Stive, 2015, pp 103). The propagation velocity and wavelength relative to a fixed reference frame will increase in the case of a current in the wave propagation direction. The wave height will decrease. And vice versa.

## 2.5. Current-Pile Interaction

The effect of a pile (or a cylinder or a vegetation stem) in a current flow can be taken into account with the simplified force on a pile over the water depth,

$$F_D = \frac{1}{2} C_D \rho u^2 A_D$$

where $C_D$ is the drag coefficient and $A_D$ is the area of the pile normal to the flow, which for a cylindrical pile is equal to the product of the diameter of the pile and the submergence height. $A_D$ is adjusted if the obstruction is a collective pile/cylinder/vegetation instead of a singular pile. This requires additional consideration for the number of stems, the frontal area of individual stems if the stems are varying in diameters and the coverage area of the collective of piles.

Mazda et al. (1997) have found that the drag coefficient for a mangrove forest is related to the Reynolds number Re that is defined using effective vegetation length scale, $L_E$., which is a representative estimate of characteristic length scale that includes information about the size of the obstacles (vegetation), the spacing between obstacles and water depth. For Re > 5 x $10^4$, the drag coefficient converges into a constant value of 0.4, while for Re < $10^4$, it reaches a value of up to 10.

Kothyari et al. (2009) has conducted an experimental study to measure the drag force of unsubmerged rigid vegetation stems. They formulated a formula to calculate drag coefficient as a function of areal concentration of stems, $\lambda$, and stem Reynolds number, $R_d$.

In 2DH simulation of Delft3D-FLOW, the consideration of vegetation is implemented with rigid vegetation model formulated by (Uittenbogaard, 2006, cited by Deltares, 2016). The model has been validated successfully against experimental flume data.  It accounts for the obstruction of momentum and turbulence exchange due to the area taken by the vegetation. The 2DH direct method takes into account the additional momentum generated by the vegetation induced friction force $F$,

$$F = \frac{1}{2}\rho_w C_D n D \bar{u}^2$$

<div align="right">Equation 51</div>

Where, $\rho_w$ is the water density in kg/m$^3$, $n$ is the number of plant elements per unit area [m$^{-2}$], $D$ is the plant diameter and $\bar{u}$ is the depth-averaged horizontal velocity. The 2DH approach does not take into account the vertical changes in vegetation geometry and the vertical fluxes in the momentum equation. Also, the 3D turbulence closures are not resolved.

## 2.6.  Current-Mangrove Forest Interaction

In contrast to flow in open channel, e.g. the main channel, the flow within a mangrove forest is largely a balance between the gradient (water level or pressure) and the drag force by vegetation, with the bed resistance acting in a much smaller degree. Flow velocity field is influenced by a canopy (community of vegetation) in individual element scale, due to the wakes generated by individual elements and branches, as well as in canopy scale, i.e. flow structure changes at the scale of the forest or meadow (Nepf, 2012a). In individual element scale, the branch and stem morphology of the vegetation can generate turbulence. Streets of vortices of same scale to the individual element are shed continuously. At canopy scale, the flow structure responds to the average flow resistance within the canopy, rather than the specific morphology of each element within the canopy. The generation of vortex drains energy from the mean flow and feeds it to the turbulent kinetic energy at the scale of individual elements (Nepf, 2012a).
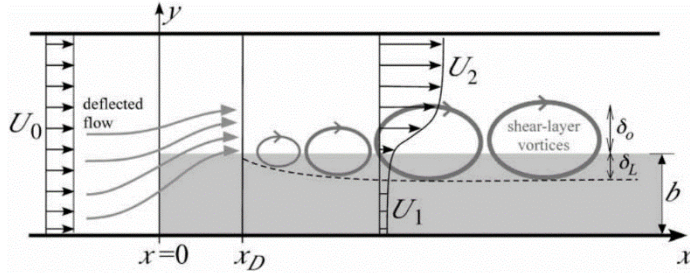


Figure 8      Plan view of a channel with long patch of emergent vegetation along the right bank (grey shading) (Zong and Nepf, 2010, adapted by Nepf, 2012b)

The plan view of development of flow with a patch of long (in streamwise direction) emergent vegetation with finite width is shown in Figure 8 (Nepf, 2012b). $b$ is the width of vegetation, $U_0$ is the upstream uniform velocity, $\delta_L$ is the vortices penetration into the vegetation patch, and $\delta_0$ is the length of vortices extension into the open channel, which is a function of water depth and bed friction. The vegetation provides high drag relative to bare bed (bed without vegetation).  This causes the flow to be deflected away from the patch until a distance of $X_D$ downstream, where the deflection is complete and shear layer with Kelvin-Helmholtz vortices develops along the lateral edge of the vegetation patch. These vortices dominate the mass and momentum exchange between the vegetation and the adjacent flow (White and Nepf, 2007, cited by Nepf 2012b), which is more than for the case of bare beds. According to Nepf (2012b), if the patch width, $b$, is greater than the penetration distance into the vegetation, $\delta_L$, turbulent stress does not penetrate to the centreline of the patch. $U_1$, the velocity within the patch is a function of potential gradient (bed and/or water surface slope) and vegetation drag. If $b < \delta_L$, the turbulent stress can reach the center of the patch and $U_1$ is a function of turbulent stress and vegetation drag.

Buckman (2013) stated that flow in an open channel with a patch of emergent vegetation has distinct flow regions. Within the canopy sufficiently far from boundaries (including the lateral edge of the vegetation patch), the velocity exhibits a uniform velocity profile (Figure 9a). At the lateral edge of the vegetation, the shear mixing layer as seen in Figure 8 is dominant. In the open channel, far from the boundaries as well, the flow exhibits logarithmic velocity profile.
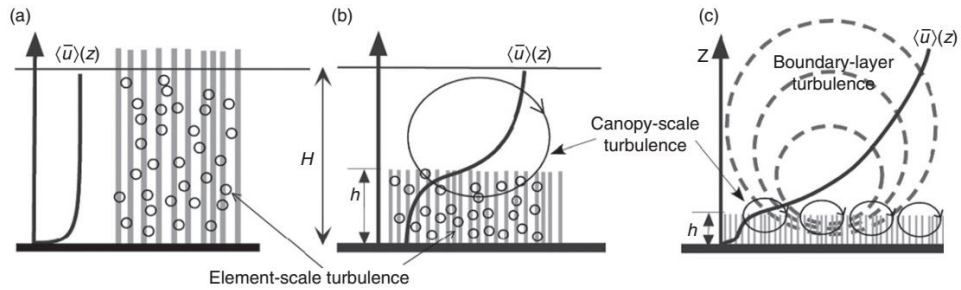
Figure 9      Vertical profiles of longitudinal (streamwise) velocity (Nepf, 2012a)

Various vertical profiles and turbulence scales can be observed for different submergence ratio of the vegetation as shown in  Figure 9 (Nepf, 2012a). $H$ is the flow depth, $h$ is the height of vegetation canopy, and $\langle\bar{u}\rangle(z)$ is the time-averaged spatial mean velocity in streamwise velocity as a function of depth (solid black line). In emergent canopy such as mangrove forest ($H/h$ = 1), the flow is driven predominantly by potential gradients from bed slope and water-surface slope. Turbulent stresses are generally much less significant within emergent canopy because the length scale of turbulent eddies within the canopy is small compared to the water depth. Turbulence is limited to the element scale (small circles inside the vegetation in Figure 9a). For shallow submergence (Figure 9b), $H/h$ < 5, the flow is driven by both potential gradients and turbulent stress. Canopy-scale and element-scale turbulences are generated at the top of and within the canopy. Figure 9c shows that flow in deeply submerged canopy ($H/h$ > 10) is driven mainly by the penetration of turbulent stress from above, that it, by the vertical turbulent transport of momentum from the overflow, with negligible contribution from pressure gradients.

Nepf (2012a) has shown that a nonlinear behaviour is seen for different canopy density under the same driving force, that is, the same potential and/or pressure gradient. As the vegetation density increases, the velocity within a canopy is less than in unvegetated region because the vegetation induces additional resistance. Nonlinearity is observed in the turbulence levels. As canopy density increases, the turbulence levels initially increase, but as the density further increase, the turbulence levels decrease. This is because with canopy, the turbulent kinetic energy consists of the competing effects of reduced velocity and increased turbulence production.

## 2.7. Flow with Permeable Pile Groyne
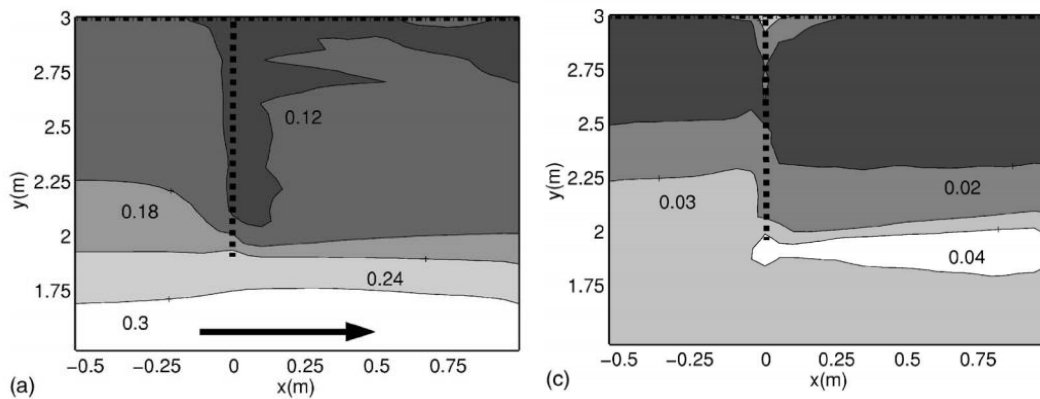


Figure 10      Around groyne tip of emerged pile groyne with 50% blocking. Left: Contours of velocity magnitude (m/s). Right: Contours of total turbulence intensity (m/s) (Uijttewaal, 2005)

A study was done by Uijttewaal (2005) on the effects of groyne layout on the flow in groyne fields. In the study, groyne field is defined as the gap between two groynes.  Various layouts were studied, including a full-length pile groyne with 50% blocking. Left plot of Figure 10 shows the velocity contours in the vicinity of the pile groyne head (dotted line). The highest velocity is seen at the bottom of the plot. Between the main channel flow and the rather stagnant water within the groyne field, mixing layer is observed, where large turbulence structure develop, which is also reflected by the right plot of Figure 10. It can be seen that the flow through the pile groyne exhibits a unidirectional flow in downstream groyne field (Uijttewaal, 2005). Formation of recirculating flow within the groyne field is prevented due to the momentum transfer by the water flowing through the piles. Thus, the flow through the groyne field is slow and rather uniform. This can be seen by the right plot of Figure 10. The turbulence intensity along the length of the groyne is uniform. A maximum of turbulence intensity is seen at downstream of the groyne tip. This is consistent with the high velocity gradient in the left plot.

Briele (2014) has conducted both analytical and numerical calculation on the effect of pile groynes to longitudinal water level. The balance of water level at upstream and downstream of a pile groyne is balanced by the longitudinal distance, incoming discharge, critical water depth, bottom friction and the drag coefficient of the piles. Both the analytical and numerical calculations show that water level is higher at upstream of a groyne than at its downstream, especially at the groyne's immediate vicinity where water piles up in front of the groyne and depresses behind it. In the cross-shore direction, the water level is constant due to the horizontal mixing, except for in the intermediate region of the pile groyne.

## **2.8.** Bed Roughness

The commonly used formulae for roughness of bed are the (Chezy) White-Colebrook formula (Equation 52) and Manning's formula (Equation 53).

$$C = 18 log_{10}\left(\frac{12H}{k_s}\right) \qquad\qquad \text{Equation 52}$$

$$C = \frac{\sqrt[6]{H}}{n} \qquad\qquad \text{Equation 53}$$

With $H$ is the total water depth, $n$ is the Manning coefficient, and $k_s$ is the Nikuradse equivalent roughness length. The Manning coefficient is $n = k_{st}^{1/6}/25$ (Strickler, 1923, cited by Huthoff and Augustijn, 2005) with $k_{st}$ the roughness height by Strickler. The above equations are empirical.

# 3 Data for Calibration and Validation

This chapter outlines available data for the purpose of validation. First, the study and data by Hulsbergen (1973), which is the main validation reference, is elaborated. Next, the experiment and results of Reniers and Battjes (1997) and of Trampenau (2000) are discussed. Both of these experiments will be referred to mostly qualitatively during the discussion of the numerical modelling result of current study.

## 3.1 Effects of Permeable Pile Groyne on Coastal Currents (Hulsbergen, 1973)

Hulsbergen has conducted a 3D physical modelling on the hydrodynamics along coastline with permeable pile groynes in a wave basin with uniform coast and contour lines. The objective of the study was to observe flow velocity reduction with respect to different pile groyne configurations. The study is selected as main validation dataset due to its potential applicability in current study, mainly due to the imposed waves at the offshore boundary to induce longshore current, in both with and without piles conditions, as well as extensive wealth of information. To address current Master Thesis research questions, for post-validation simulations, the coverage of the piles of the groynes is increased to mimic a mangrove forest condition. The length scale of $n$ = 40 and velocity scale of $n_v = \sqrt{40}$ were applied to scale the prototype down into the model. The following elaboration focuses on the setup of the model in the basin.

Figure 11 shows the plan layout of the setup and a typical cross-section of one of the pile groyne configurations. For the purpose of current study, the boundaries of the basin and in the numerical model are designated/nomenclated as following: South boundary where the land and pile groynes are located, North boundary where the wave makers are located, as well as West and East boundaries that are located to the left and right of the layout plan. The basin was 35.35 m long alongshore and 12.10 m long cross-shore. *Normaal Amsterdams Peil* (N.A.P.) or Amsterdam Ordnance Datum was designated as the reference datum for the setup. The slopes were 1:35 and 1:20 for above low water line (from -5 cm to +5 cm N.A.P.) and below low water line (from -25 cm to -5 cm N.A.P.), respectively. The bed level of the setup ranged from +5 cm to -25 cm, offshore-ward (wavemaker-ward) of which was horizontal bed at -25 cm N.A.P.

Figure 12 shows the schematization of eight pile groyne configurations that were tested in the study. The varied properties were length of groynes, spacing between groynes, and single- or double-layered groynes. The lengths of pile groyne are 3.5 m and 5 m from H.W. line (+0.05 m NAP). All the groynes were perpendicular (90°) to the high-water line. The piles of the groynes were of 0.625 cm in diameter. The piles centre-to-centre spacing ranged from 1.2 to 2.5 cm in the cross-shore direction, and for double-rowed pile groynes, 8.75 cm in the alongshore direction. The height of piles above bed was varying from 4.25 to 13.75 cm.
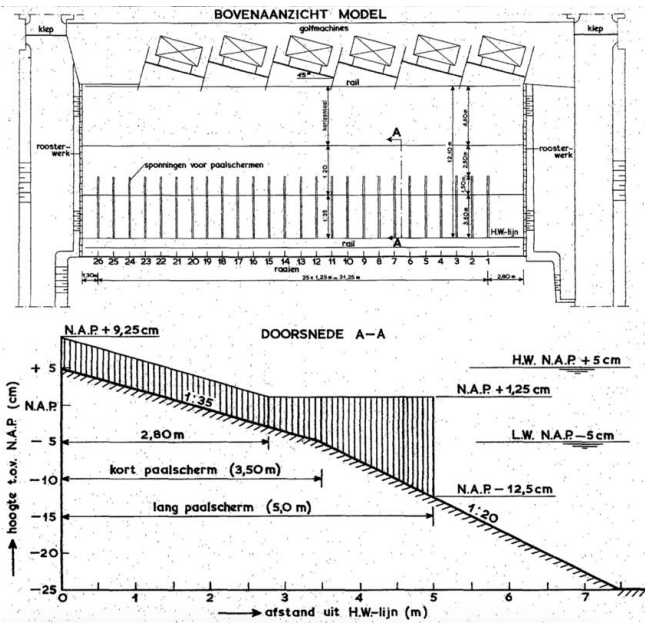
Figure 11        Permeable pile groyne model setup (Hulsbergen, 1973)
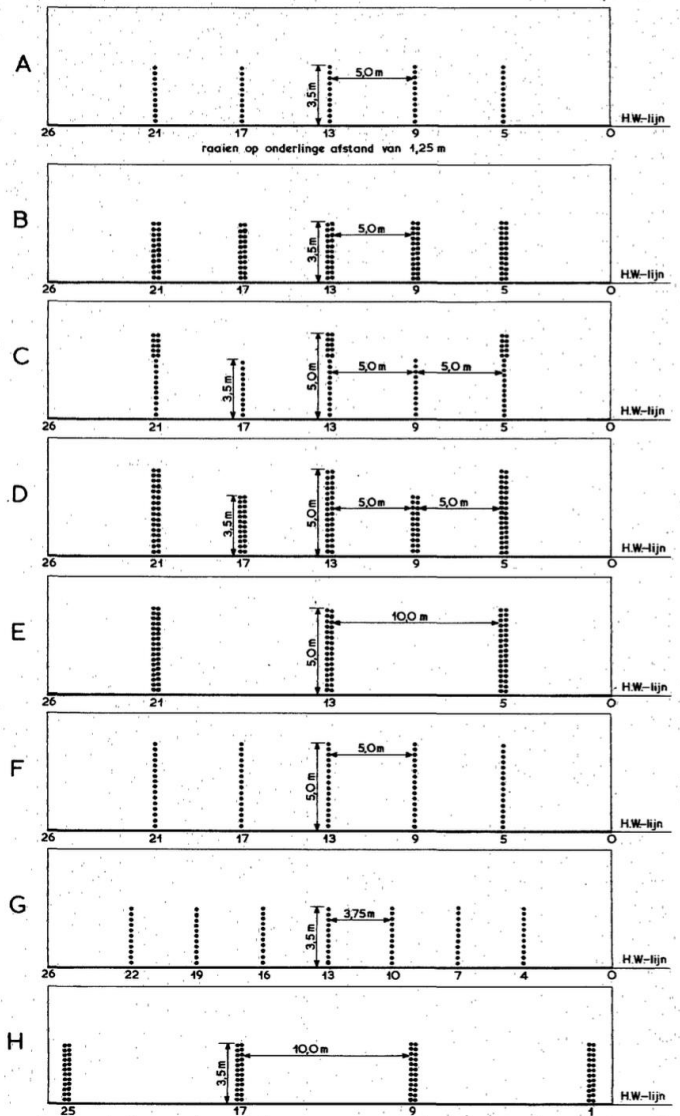


Figure 12    Pile groynes schematizations (Hulsbergen, 1973)

Six hydraulic conditions (HC) were considered in the wave basin experiment (Table 1). The main hydraulic conditions imposed are (stationary) tidal flow from two directions as well as oblique waves. The tidal flow is considered stationary because constant value is used. Two water levels were used, high-water (H.W.) and low-water (L.W.) conditions. Tidal flows used were 250 and 450 l/s for H.W. and L.W. conditions, respectively. Regular waves were induced by 6 wavemakers with wave height of 3 cm, wave period of 1.04 s and wave direction propagating from 15° clockwise from shore normal.

Table 1        Hydraulic conditions (Hulsbergen, 1973)

| No. | Water Level | Flow (l/s) | Wave Period (s) | Wave Height (cm) | Wave Direction (°) | Flow Direction |
|-----|-------------|------------|------------------|-------------------|---------------------|-----------------|
| 1 | H.W. | 450 | | No waves | | → → |
| 2 | H.W. | 450 | | No waves | | ← ← |
| 3 | H.W. | 450 | 1.04 | 3.0 | 15 | → ←--● |
| 4 | H.W. | 450 | 1.04 | 3.0 | 15 | ← ←--● |
| 5 | H.W. | 0 | 1.04 | 3.0 | 15 | ←--● |
| 6 | L.W. | 250 | | No waves | | → |

| H.W. | = High water | → | = Flow direction |
| L.W. | = Low water | ←--● | = Wave-induced current direction |

No water level measurement was conducted for insight into the water setdown and setup in the cross-shore direction. As an alternative, measured data by Reniers and Battjes (1997) is used qualitatively (Section 3.2). No flow guide was installed in the offshore boundary (along the wave makers). This may cause shearing of flow due to big gradient of current velocity. This will be addressed in the numerical modelling by adaptation of the numerical model domain.

Validation against this dataset

Analysis of the results from the experiment by Hulsbergen (1973) is conducted to understand the processes captured by the measurements (Chapter 5). This is so that the relevant parameters can be translated well in the numerical modelling. This paves the path to later understanding the processes that occur within mangrove forest to address research questions 1 and 2.

First of all, current study involves numerical model simulation of conditions without pile groyne, with pile groynes and with pile groynes as mimic vegetation, all conducted for both steady and wave-driven flows. This will provide fundamental insights into the processes for the different conditions, and will be able to provide observation on which parameters will be important for further subsequent investigation.

A numerical model will be set up to mimic the experiment conducted by Hulsbergen (1973). From Table 1, hydraulic conditions (HC) 1, 4 and 5 are chosen. The selection is conducted based on the relevance of the hydraulic conditions on current thesis and based on availability of measured data for validation purposes. Hulsbergen stated that calibration of HC 1 was better than that of HC 2. With that reasoning, they conducted subsequent experiments without HC 2. In current study, interchangeable reference to HC1 will be 'flow-only', to HC4 will be 'wave+following current', and to HC5 will be 'wave-only'.

Table 2      Chosen Hydraulic conditions for current study from Table 1

| No. | Water Level | Flow (l/s) | Wave Period (s) | Wave Height (cm) | Wave Direction (o) | Flow Direction |
|-----|-------------|------------|-----------------|------------------|--------------------|----------------|
| 1 | H.W. | 450 | | No waves | | → → |
| 4 | H.W. | 450 | 1.04 | 3.0 | 15 | ← ←--● |
| 5 | H.W. | 0 | 1.04 | 3.0 | 15 | ←--● |
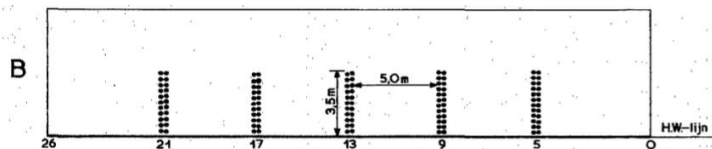


Figure 13      Chosen pile groyne configuration for current study from Figure 12

Figure 13 shows the chosen pile configuration, pile groyne configuration B. The spacings between the double-layered groynes are 5.0 m and the length of the groynes is 3.5 m. The piles representing groyne are of 0.625 cm in diameter and are spaced 1.2 cm centre-to-centre cross-shore and 8.75 cm alongshore. The height of piles above bed is ranging from 4.25 to 6.25 cm.

The numerical simulations involve model validation with measured data of Hulsbergen's experiment. Table 3 shows the summary of proposed simulations. The respective validation data is appended in Appendix B. The validation includes cross-shore velocity distribution, current patterns, as well as wave breaking locations and heights. For simulations without available validation data, the simulations are treated as exploratory in nature. Alternatively, current patterns and velocity distributions will be assessed qualitatively.

Table 3      Proposed validations and simulations

| Pile configuration | Hydraulic Condition | Proposed validation |
|--------------------|---------------------|---------------------|
| Without pile groyne / mimic mangrove forest | Constant flow (HC 1) | Figure B. 1 |
| | Constant flow and wave-driven flow (HC 4) | Figure B. 2, Figure B. 3, Figure B. 4 |
| | Wave-driven flow (HC 5) | Figure B. 3, Figure B. 4 |
| With pile groyne configuration B | Constant flow (HC 1) | Figure B. 5 |
| | Constant flow and wave-driven flow (HC 4) | Figure B. 6, Figure B. 7 |
| | Wave-driven flow (HC 5) | (No data for validation) |
| With mimic mangrove forest | Constant flow (HC 1) | |
| | Constant flow and wave-driven flow (HC 4) | (No data for validation) |
| | Wave-driven flow (HC 5) | |

Due to the availability of measured data for validation for a relatively steep bed slope and lack of such data for very gentle slopes (order of 1:300 to 1:1000), current study focuses on the nearshore processes in such relatively steep profile, which is the steep end of the spectrum.

## 3.2  Reniers and Battjes (1997)

Reniers and Battjes (1997) conducted longshore current experiment on barred and non-barred beaches. The setup is as shown in Figure 14. The basin size is approximately 25 m x 40 m. Following Visser (1991), a pump system was installed to recirculate the wave-induced longshore current to obtain alongshore uniformity. The multipaddle type wave maker was installed in an oblique angle from the coastline. Wave guides were installed at both of the sides from the wave maker to the extent of the inflow and outflow opening, in order to prevent wave diffraction and alongshore variation of wave set-up.

The bed profile (Figure 14) consists of a concrete slope of 1:20 at offshore, a Gaussian bar profile with crest height of about 0.1 m which has a 1:8 slope on the seaward side. At shoreward of the bar, the bed profile was set to 1:10 slope.
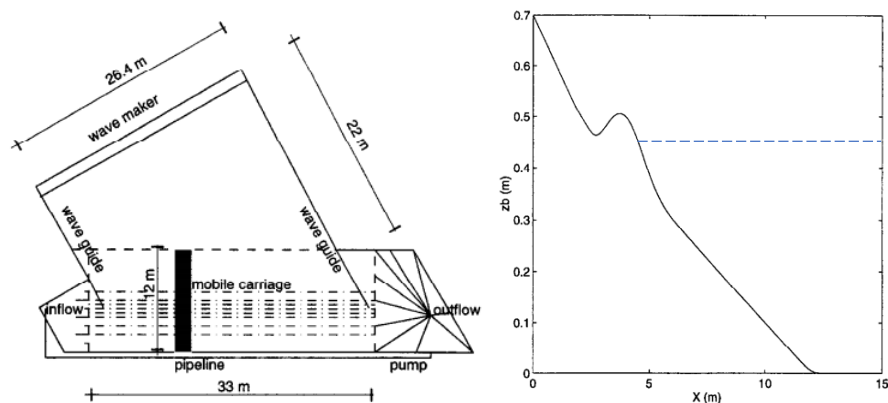


Figure 14         Left: Laboratory setup. Right: Bed profile. Water level is set as constant at 0.55m (adapted from Reniers and Battjes, 1997)

It has been shown by Visser (1991) that the current recirculation could contribute to the larger measured velocities outside of the surf zone than for an experiment setup where return flows are minimized so as to obtain virtually uniform alongshore distribution. Figure 15 shows the relation of total longshore current flow rate, $Q$, pumped current flow rate, $Q_p$, and return flow rate, $Q_r$ (Visser, 1980 and 1982, cited by Visser 1991). $Q_{pu}$ is the value of pumped flow rate that corresponds with nearly uniform longshore current flow rate, $Q_u$. The diagram shows that lower $Q_p$ values will cause the flow rate $Q$ to grow alongshore. The surplus $Q-Q_p$ returns offshore and raises $Q_r$. Conversely, for $Q_p > Q_{pu}$, the excess will generate a circulation flow between the wave guides (by convection and lateral friction) which will also increase $Q_r$.
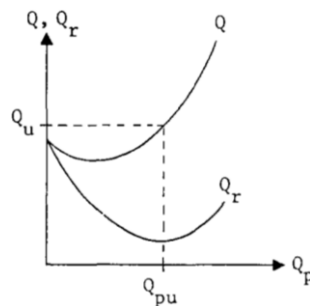


Figure 15     Relation of total longshore current, $Q$, pumped current, $Q_p$, and return, $Q_r$, flow rates (Visser, 1991)

In parallel, according to Reniers and Battjes (1997), the current recirculation is to be zero if the pumped discharge at the lateral boundaries is similar to the discharge forced by waves. However, due to lateral mixing, a small recirculation remains. If the pumped discharge is smaller, a part of the wave-induced flow is forced to recirculate in the basin. Recirculation also occurs if the pumped discharge is larger due to convection and lateral friction. If pumped discharge is not near optimal discharge, a strong offshore directed flow will occur along the wave guide at the downstream end of the basin.

Reniers and Battjes (1997) experiment SA219 is used as basis of qualitative comparison for current study. The bed profile is non-barred (Figure 14) by maintaining a constant water level of 0.45m, thus the coastline is situated at the offshore face of the bar. The regular incident wave height is 0.08 m, wave period is 1 s, and wave direction is 30° from shore normal. Velocity was measured at one third of water depth from the bottom to approximate depth-averaged velocity by assuming a logarithmic velocity profile.
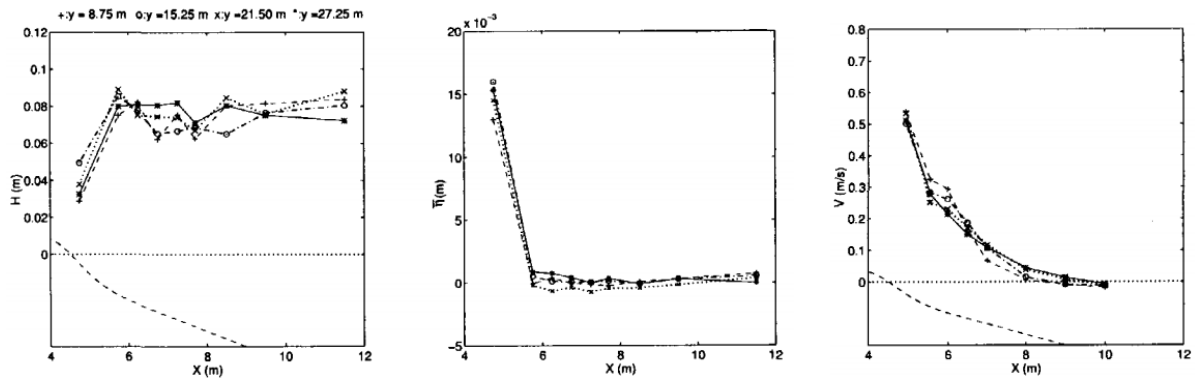


Figure 16     Measurement of test SC219 (Regular waves, non-barred profile) (Reniers and Battjes, 1997)

Figure 16 shows the measurement result of non-barred beach with imposed regular waves. Although the wave height varies in the deeper water, the waves break at the same location. Water level setup is observed at the waterline. Maximum current velocity occurs close to the shoreline, but due to the vertical clearance limitation of measuring device, velocity measurement at shallower water was not feasible. It then is uncertain if the shoreward-most velocity measurement represent the maximum velocity.

This study is not adopted as main validation dataset due to absence of measurement data for a condition with pile groyne. Such measurement is necessary for incremental understanding of wave-induced current within mangrove forest, due to practical similarity in nature between the two. In turn, the findings in this study is very useful as a qualitative reference for current study.

## 3.3   Trampenau (2000)

Trampenau (2000) conducted a series of laboratory tests to understand the hydraulic functioning of permeable pile groins in comparison to impermeable groynes. He tested incrementally varied groyne permeability from 0% (impermeable) to 50% (highly permeable). Also, the ratio of groin length to the width of surf zone is varied. The hydraulic conditions imposed are uniform longshore current and other tests using oblique waves. The model setup for oblique waves is shown in Figure 17. Similar in principle to the setup of Reniers and Battjes (1997), wave guides and flow guides are installed. Also the inflow of water is controlled by means of inductive flowmeter. This will ensure the cross-shore profile of longshore current to be uniform in alongshore direction.
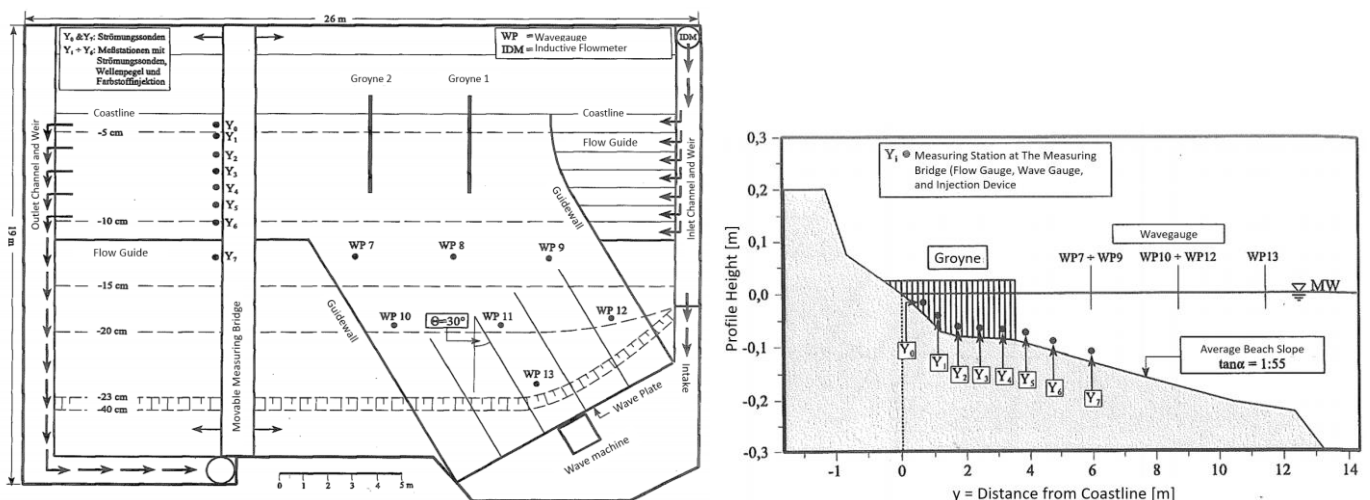


Figure 17               Laboratory setup (Adapted from Trampenau, 2000)
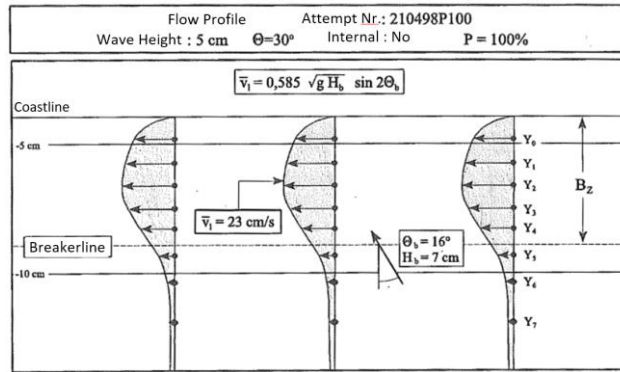
Figure 18          Flow profiles generated by the wave-induced current (wave parameters: *H* = 5 cm and *Θ* = 30°) (Adapted from Trampenau, 2000)

A longshore current profile for a condition without pile groyne (reference condition with permeability = 100%) is shown in Figure 18 for a wave height of 5 cm with direction of propagation of 30°. The velocity peak of the longshore current is situated approximately halfway through the surzfone, which is more shoreward than the breaker line. Due to horizontal mixing, there is also longshore current outside of the breaker line. This study is not adopted as the main validation dataset due to lack of cross-shore measurement of velocity for the various hydraulic conditions and pile groyne configurations, which is very important for current study objectives. Results from this study are very useful as qualitative referral for current study.

# 4 Analytical Calculation

This chapter elaborates on the analytical calculation of longshore current and the comparison with the measured data. The boundary data and bed level profile used are similar to that by Hulsbergen (1973) as elaborated in Section 3.1. Equation 39 to Equation 50 are utilized. Cross-shore distributions of calculated wave height is shown in Figure 19, while of calculated longshore current velocity are shown in Figure 20 for both with and without horizontal mixing.

Hulsbergen (1973) measured the longshore current velocity in hydraulic condition by visually observed surface floats. Surface current velocity is higher than depth-averaged velocity. Thus, the measured data is corrected for depth-averaged values by assuming a logarithmic vertical velocity profile. The formulas introduced by Longuet-Higgins (1970a & 1970b) are estimation of depth-averaged longshore current velocity.

The breaker line is located at 1.75 m from waterline at water depth of 0.05 m (Figure 19). The calculated breaking wave height is 0.033 m, which approximates well to the average breaking wave height measured by Hulsbergen (H=0.032 m). The breaking location also agrees well with that of average by Hulsbergen of 1.85 m from waterline. Without horizontal mixing, the calculated longshore current velocity is maximum at the breaker line with magnitude of 0.21 m/s (red line in Figure 20). The velocity drops linearly with position that is closer towards the coastline.

$N$ value represents a dimensionless constant that relates the coefficient, $\mu_e$ of the horizontal eddy viscosity with offshore distance and typical velocity. The $N$ value ranges from 0 to 0.016. Three values were calculated for, i.e. $N$ = 0.001, 0.01 and 0.016. Smaller value of $N$ (dashed orange line) reduces the effect of horizontal mixing as can be seen from the longshore current outside the surfzone that is closing to zero velocity and the higher peak within the surfzone as well as the peak shifting closer to the breaker line. The opposite applies to higher value of $N$ (i.e. $N$ = 0.016). $N$ value that is as low as 0.001 is not deemed correct for this case as can be seen with the sharp reduction of velocity at outside of the breaker line. With such low value of $N$, the profile of the longshore current approaches more like that of without horizontal mixing. It is believed that by choosing an $N$ value from either of the extreme ends of the allowable range renders that the mixing due to turbulence effect to not be resolved correctly. Thus, mid-range value of $N$ is thought to be a good balance.

Using Equation 49 and Equation 50, the maximum longshore current velocity is 0.11 m/s at about 1.2 m from HW line.

The measurement data by Hulsbergen (1973) for Hydraulic Condition (HC) 5 (wave-only) without pile groyne is shown with black asterisks in Figure 20. In the following paragraphs, the comparison of analytical calculation with the measured data by Hulsbergen is only done for analytical calculation with horizontal mixing accounted for with $N$=0.008 (blue line in Figure 20.

Generally, the measured cross-shore profile of longshore current is in similar distribution to that of the analytical calculation (blue line). Also, cross-shore profiles of longshore current for both analytical calculation and Hulsbergen's (1973) measured data are consistent with that measured by Trampenau (2000) in Figure 18. Within the surfzone, the value of the measured peak longshore current velocity is approximately equal to that of the analytical calculation. However, the location of the analytically calculated longshore current peak is slightly shoreward by about 0.25 m in comparison to that of measured data.

It can be seen in Table 6 that the standard deviation of the measured longshore current velocity for HC5 can be as high as 35%. This significant variation alongshore is believed to be attributed to the significant variation of breaking wave height and locations (Figure B. 3) recirculation current. It is possible that this spatial variation of breaking location provide some difference with the analytical calculation. However, it is also to be noted that the formulation by Longuet-Higgins makes several simplification on the coefficients, such as the N and $\alpha$ values. These are constants with inherent relations between the horizontal eddy viscosity with offshore distance and typical velocity, and between wave amplitude to water depth, respectively. Also, $C$, the drag coefficient at the bottom is a constant.

Given the above, the result of the analytical calculation and the measured data agree reasonably. Thus, the result of analytical calculation will also be used as reference for validation, specifically, the calculated wave height cross-shore distribution for HC5.

**Cross-shore Distribution of Calculated Wave Height**
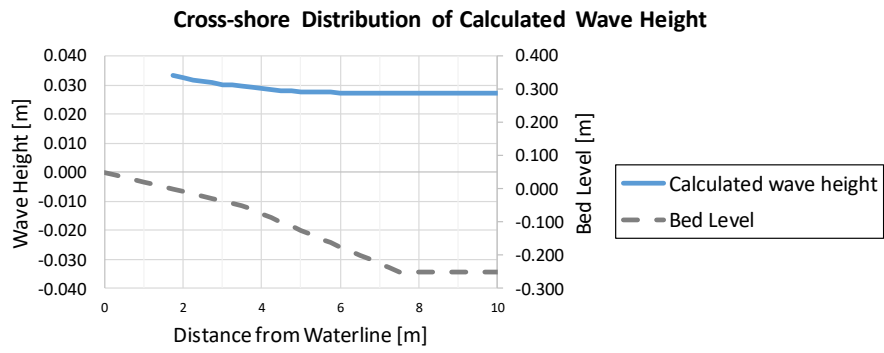
Figure 19          Cross-shore distribution of calculated wave height

**Cross-shore Distribution of Longshore Current Velocity**
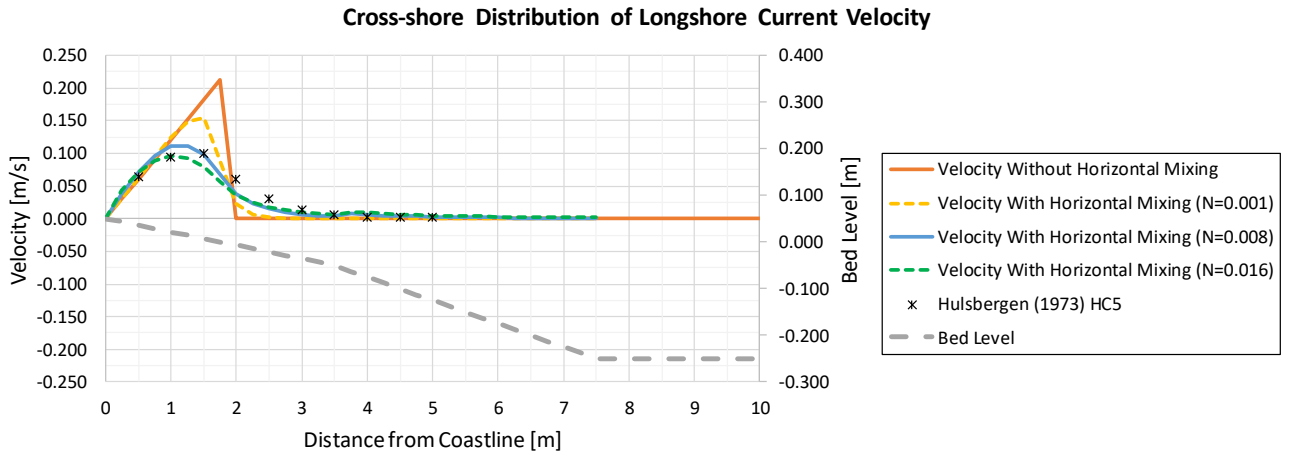
Figure 20          Longshore current velocity profile for with and without horizontal mixing

# 5 Analysis of Validation Data

In addressing research questions 1 and 2, various analyses are necessary to formulate incremental understanding on the processes occurring within mangrove forest with wave-induced current. The experiment by Hulsbergen (1973) is analysed by comparing the measurement data for the various conditions as following (Sections 5.1 to 5.5):

1. Current only – with and without pile groyne conditions
2. Without groyne – current-only and current+wave conditions
3. Without groyne – wave-only and current+wave conditions
4. With groyne – current-only and current+wave conditions
5. Current+wave – with and without groyne conditions

In understanding the processes, some references may be made to theoretical books and studies conducted by other researchers. For the purpose of discussions, the cross-shore distance from H.W. line is denoted with x-coordinate (e.g. x=3.5m).

A summary is provided at the end of the chapter.

## 5.1 Current Only – With and Without Pile Groyne Conditions

This corresponds to Hydraulic Condition 1 of the experiment by Hulsbergen (1973) as shown in Table 4. Measurements were available for with and without pile groyne B. Measurement for without pile groynes were done for a total of 11 transects and was averaged. It was not mentioned whether the 11 transect measurements were conducted simultaneously or one after the other. However, the usual practise is to measure one transect after the other, because if they were done simultaneously, the number of equipment would be need to be big, which can be very expensive. Furthermore, having numerous equipment within the water body might induce unwanted disturbances within the flow field. In contrast, one measurement transect was done for condition with pile groyne B. The location of the measurement was not mentioned, but it is assumed that the measurement location is the middlepoint between two groynes, as that would be logistically most feasible. The measurements are shown in Table 4 and Figure 21. Measurements for both were done with photographically recorded surface floats. The measurement was conducted between 0.5 m to 8 m from waterline. The extent of pile groyne B is shown by the pink line (0 m < x < 3.5m).

Table 4    Measurement results for Hydraulic Condition 1

| Distance from H.W. line (m) | Without Pile Groyne (No Waves) Flow = 450 l/s (→) | | With Pile Groyne B (No Waves) Flow = 450 l/s (→) | |
|---|---|---|---|---|
| | Average velocity (cm/s) | Calculated Standard deviation (cm/s) | Velocity (cm/s) | Standard deviation (cm/s) |
| 0.5 | 2.6 | - | - | - |
| 1.0 | 4.9 | - | - | - |
| 1.5 | 7.3 | - | 2.2 | - |
| 2.0 | 8.0 | - | 3.3 | - |
| 2.5 | 8.8 | - | 4.5 | - |
| 3.0 | 11.0 | - | 5.4 | - |
| 3.5 | 12.0 | - | 9.5 | - |
| 4.0 | 13.4 | - | 13.6 | - |
| 4.5 | 14.9 | - | 16.1 | - |
| 5.0 | 16.9 | - | 18.0 | - |
| 5.5 | 18.4 | - | 19.0 | - |
| 6.0 | 18.8 | - | 19.9 | - |
| 6.5 | 18.4 | - | 20.0 | - |
| 7.0 | 19.6 | - | 20.9 | - |
| 7.5 | 19.9 | - | 22.0 | - |
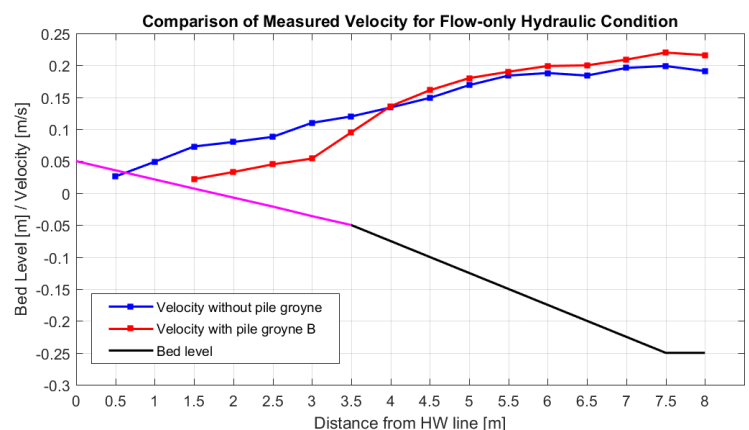


Figure 21    Measured velocity for Hydraulic Condition 1. Pink line shows the cross-shore coverage of pile groyne B.

| 8.0 | 19.1 | - | 21.6 | - |
|---|---|---|---|---|

For without pile groynes (blue line), the measured velocity ranges from 2.6 cm/s at nearshore to 19.9 cm/s at the deeper water region. As more roughness is experienced by flow at the shallow region in the nearshore part, the velocity gradually decreases as it gets closer to waterline.

For the condition of with pile groyne configuration B (red line), the pile groynes are located from H.W. line to x=3.5 m. Within the pile groyne region, the flow velocity is lower than that of without pile groyne condition. In general, the difference between both conditions in that region is about 3 cm/s. This is consistent with the findings by Trampenau (2000) that for a pile groyne with permeability of more than or equal to 20%, current still predominantly flows through in-between the pile cylinders. At about x=4.0 m, the velocity magnitude is about the same. This means that the mixing layer is about 0.5 m wide. In the deeper water region, the condition with pile groyne has higher velocity magnitude than without pile groyne condition, due to conservation of momentum.

Condition with pile groyne (Red line) measurement stops at x=1.5m with velocity magnitude of 2.2 cm/s. Measurement with photographically recorded surface floats is done by having photos taken at 11m elevation and records are done with time intervals of 3 or 6 seconds. At such distance, there is bound to be a low limit to the measured velocity. In the case of this laboratory setup, it could be 2 cm/s. Any closer to shore, it is assumed that the movement of the surface floats is too small for measurement. This assumption is supported by the fact that the measurement with blue line (condition without pile groyne) is available up till x=0.5m with magnitude of 2.6 cm/s. A look at all Hulsbergen's measured data supports this as well.

The rows of pile groynes, although permeable, create horizontal constriction in the cross-section of the flow. From Schiereck (2012), Figure 22a shows schematics of the flow with horizontal constriction, Figure 22b represents velocity (vertically averaged over turbulence period), Figure 22c represents relative turbulence (related to the local value of ū), Figure 22d represents the absolute value of the peak velocity. It can be seen that the velocity is reduced in the stagnant region, which in the case of with pile groyne B, the reduction is of smaller magnitude. The increase of absolute velocity and average velocity in the mixing layer region is represented by the x>3.5 m up to a short distance offshore in Figure 21. This is attributed to the acceleration in that region. It is to be noted that the study in Figure 22 was done in a flume, thus a horizontal bottom throughout the cross-section of the flume is assumed.
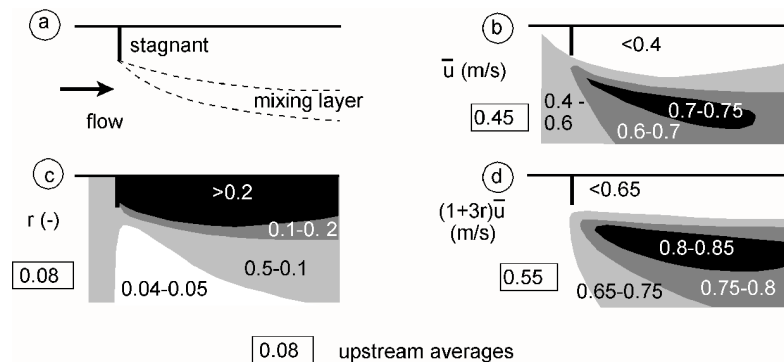


Figure 22     Flow characteristics for a horizontal constriction (Schiereck, 2012)

## 5.2    Without Groyne – Current-only and Current+Wave Conditions

This corresponds to Hydraulic Conditions 1, 3 and 4 of the experiment by Hulsbergen (1973). Measurements were done for a total of 16 sections and were averaged. Similarly, it was assumed that one transect was measured at a time. The measurement data are shown in Table 5 and Figure 23. Figure B. 8 shows the velocity profiles for the measurement of 16 sections. HC 1 was measured with photographically recorded surface floats, while HC3 and HC4 were measured with visually observed surfaced floats. Due to the nature of observation by visual, the measurement for HC3 and HC4 may have significant variation, as can be seen by the significant standard deviation (Table 5), which for some points can be up to 50% of the magnitude of average velocity. Further variation is contributed by the varying breaking wave height and breaking locations in alongshore direction (Figure B. 3).

Table 5        Measurement results for without groyne condition

| Distance from H.W. line (m) | HC 1 (No Waves) Flow = 450 l/s (→) | | HC 3 H = 0.03 m T = 1.04 s Dir = 15° Flow = 450 l/s (←) | | HC 4 H = 0.03 m T = 1.04 s Dir = 15° Flow = 450 l/s (→) | |
|---|---|---|---|---|---|---|
| | Average velocity (cm/s) | Standard deviation (cm/s) | Average velocity (cm/s) | Standard deviation (cm/s) | Average velocity (cm/s) | Standard deviation (cm/s) |
| 0.5 | 2.6 | - | 10.1 | 5.0 | 8.6 | 4.6 |
| 1.0 | 4.9 | - | 12.3 | 3.6 | 14.8 | 3.5 |
| 1.5 | 7.3 | - | 11.3 | 3.1 | 17.1 | 4.1 |
| 2.0 | 8.0 | - | 7.5 | 5.9 | 11.9 | 2.2 |
| 2.5 | 8.8 | - | 1.4 | 3.1 | 11.4 | 1.7 |
| 3.0 | 11.0 | - | -3.1 | 4.9 | 11.8 | 1.5 |
| 3.5 | 12.0 | - | -9.4 | 3.7 | 13.5 | 0.7 |
| 4.0 | 13.4 | - | -13.7 | 3.0 | 14.1 | 1.2 |
| 4.5 | 14.9 | - | -16.7 | 3.0 | 14.0 | 1.2 |
| 5.0 | 16.9 | - | -18.6 | 1.6 | 15.0 | 1.2 |
| 5.5 | 18.4 | - | -19.9 | 1.5 | 16.4 | 1.6 |
| 6.0 | 18.8 | - | -18.2 | 1.5 | 17.7 | 1.8 |
| 6.5 | 18.4 | - | -18.2 | 1.9 | 17.9 | 1.1 |
| 7.0 | 19.6 | - | -18.8 | 1.5 | 18.8 | 1.9 |
| 7.5 | 19.9 | - | -19.8 | 1.5 | 18.9 | 1.6 |
| 8.0 | 19.1 | - | -18.5 | 1.7 | 17.2 | 1.3 |

NOTE: positive values indicate flow in westward direction, and vice versa.
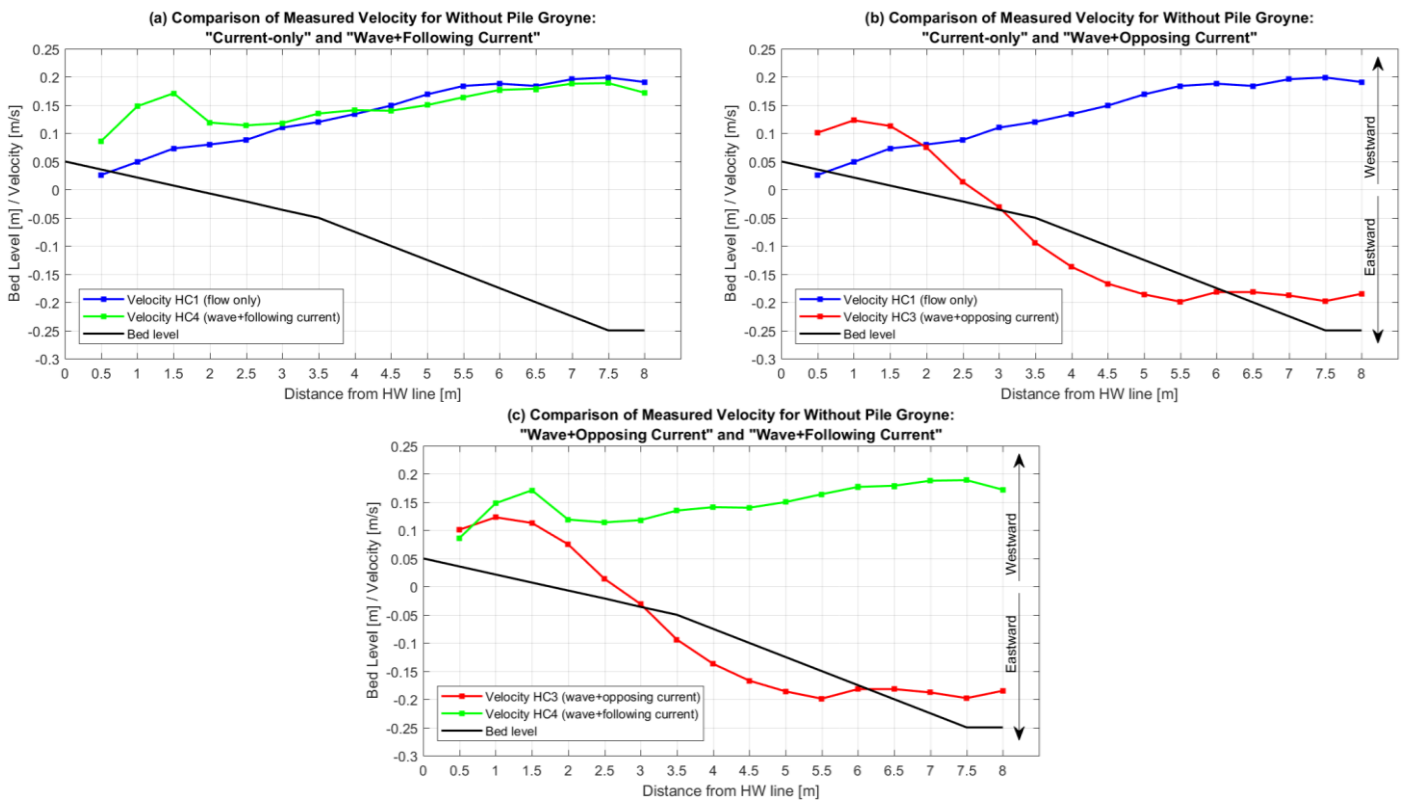


Figure 23    Measured longshore velocity for without pile groyne condition: "Current-only" and current+wave conditions. Negative values indicate eastward flow direction, vice versa.

In Figure 23a, velocity profile for HC1 (blue line) and HC4 (green line) show almost similar distribution for x=3m to 8m. The velocity profiles diverged for x<3m. This means that the contribution of longshore current for HC4 is between coastline and x=3m. The magnitude of the longshore velocity is about 17 cm/s. The velocity of HC1 drops steadily towards waterline.

In Figure 23b, a comparison between flow-only (blue line) and wave+opposing current (red line) is shown. In deeper water, x>3m, the flow of HC3 (red line) is headed eastward due to the pressure gradient of tidal flow. Between x=0m and x=3m, the current flows westward due to contribution of wave-induced current. The longshore velocity peaks at 12 cm/s.

In Figure 23c, a comparison between wave+following current (green line) and wave+opposing current (red line) is shown. What is starkly apparent is that the magnitude of longshore current velocity for HC4 is higher than for HC3. This may be explained by the interaction of waves and current propagating in the same direction. According to Schiereck (2012), the influence of waves is taken into account by adding current and orbital velocity vectorially at a level:

$$u_{c-t} = \frac{\sqrt{g}}{\kappa C} u_c$$

<div align="right">Equation 54</div>

$$u_{b-t} = \frac{1}{\kappa}\sqrt{\frac{c_f}{2}} u_b sin(\omega t)$$

<div align="right">Equation 55</div>

Where $\kappa \approx 0.4$ and $u_b$ is the maximum orbital velocity at the bottom. The results are:

$$u_r = \sqrt{\frac{g}{\kappa^2 C^2} u_c^2 + \frac{c_f}{2\kappa^2} u_b^2 sin^2(\omega t) + 2\frac{\sqrt{g}}{\kappa C} u_c \frac{1}{\kappa}\sqrt{\frac{c_f}{2}} u_b sin(\omega t) sin(\phi)}$$

<div align="right">Equation 56</div>

Where angle $\varphi$ is the angle between wave and current direction (Figure 24). According to Equation 56, the maximum velocity due to wave-current interaction occurs when the angle $\varphi$ is 90°, that is when the wave direction is parallel to the flow. This is consistent with the elaboration in Section 2.4. Which also means that if the direction is opposite, then the velocity is minimum. From Table 5, high standard deviations are recorded for x=2m to x=4.5m. This could be due to high mixing by turbulence in that region because of very high velocity shear. What is quite inconsistent with theory is that the velocity peak for HC3 is closer to the waterline than that of HC4. The opposite is true for theory (Section 2.4). This is perhaps a result to measurement data uncertainty as can be seen by the high standard deviations in Table 5.
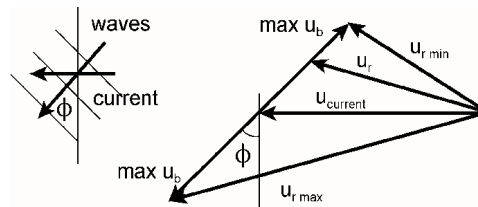


Figure 24          Combined wave-current action (Schiereck, 2012)

## 5.3 Without Groyne – Wave-only and Current+Wave Conditions

This analysis corresponds to Hydraulic Conditions 3, 4 and 5 of the experiment by Hulsbergen (1973. The measurements were done for a total of 16 sections and were averaged. Similarly, it was assumed that one transect is measured at a time. The measurements are shown in Table 6 and Figure 25. Figure B. 8 shows the velocity profiles for the 16 sections. All three HC3, HC4 and HC5 were measured with visually observed surface floats. No measurements were done for HC5 for x>5.5m because there is no flow velocity beyond that point.

Table 6      Measurement results for without groyne condition

| Distance from H.W. line (m) | HC 3 H = 0.03 m T = 1.04 s Dir = 15° Flow = 450 l/s (←) | | HC 4 H = 0.03 m T = 1.04 s Dir = 15° Flow = 450 l/s (→) | | HC 5 H = 0.03 m T = 1.04 s Dir = 15° (No Flow) | |
|---|---|---|---|---|---|---|
| | Average velocity (cm/s) | Standard deviation (cm/s) | Average velocity (cm/s) | Standard deviation (cm/s) | Average velocity (cm/s) | Standard deviation (cm/s) |
| 0.5 | 10.1 | 5.0 | 8.6 | 4.6 | 11.1 | 3.8 |
| 1.0 | 12.3 | 3.6 | 14.8 | 3.5 | 14.1 | 3.8 |
| 1.5 | 11.3 | 3.1 | 17.1 | 4.1 | 14.2 | 2.5 |
| 2.0 | 7.5 | 5.9 | 11.9 | 2.2 | 8.2 | 2.5 |
| 2.5 | 1.4 | 3.1 | 11.4 | 1.7 | 4.0 | 2.7 |
| 3.0 | -3.1 | 4.9 | 11.8 | 1.5 | 1.9 | 1.7 |
| 3.5 | -9.4 | 3.7 | 13.5 | 0.7 | 0.7 | 1.1 |
| 4.0 | -13.7 | 3.0 | 14.1 | 1.2 | 0.2 | 0.6 |
| 4.5 | -16.7 | 3.0 | 14.0 | 1.2 | 0.2 | 0.6 |
| 5.0 | -18.6 | 1.6 | 15.0 | 1.2 | 0.2 | 0.6 |
| 5.5 | -19.9 | 1.5 | 16.4 | 1.6 | - | - |
| 6.0 | -18.2 | 1.5 | 17.7 | 1.8 | - | - |

| Distance from H.W. line (m) | HC 3 H = 0.03 m T = 1.04 s Dir = 15° Flow = 450 l/s (←) | | HC 4 H = 0.03 m T = 1.04 s Dir = 15° Flow = 450 l/s (→) | | HC 5 H = 0.03 m T = 1.04 s Dir = 15° (No Flow) | |
|---|---|---|---|---|---|---|
| | Average velocity (cm/s) | Standard deviation (cm/s) | Average velocity (cm/s) | Standard deviation (cm/s) | Average velocity (cm/s) | Standard deviation (cm/s) |
| 6.5 | -18.2 | 1.9 | 17.9 | 1.1 | - | - |
| 7.0 | -18.8 | 1.5 | 18.8 | 1.9 | - | - |
| 7.5 | -19.8 | 1.5 | 18.9 | 1.6 | - | - |
| 8.0 | -18.5 | 1.7 | 17.2 | 1.3 | - | - |

NOTE: positive values indicate flow in westward direction, and vice versa.
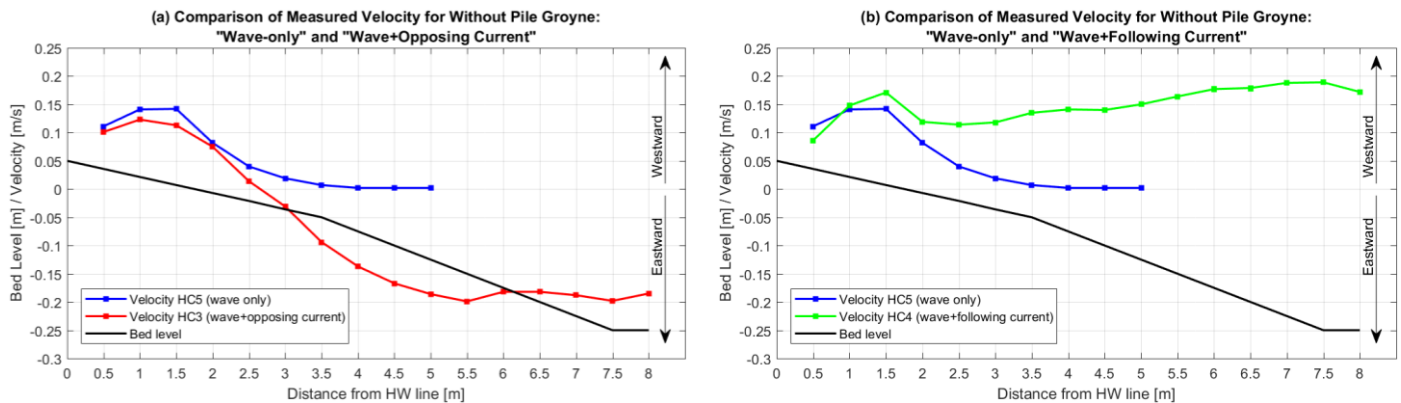


Figure 25      Measured longshore velocity for without pile groyne condition: Wave-only and current+wave conditions

In Figure 25a, a comparison between wave-only (blue line) and wave+opposing current (red line) is shown. HC5 (wave-only) shows that longshore current velocity contribution starts at x=3.5m shoreward. As expected, the longshore velocity magnitude in the surf zone is highest in wave+following current (green line in Figure 25b), followed by wave-only (blue line) and then wave+opposing current (red line). As explained in Section 5.2, this could be because the following current velocity in HC4 adds up to the wave-induced current. In contrast, the opposite current flow in HC3 reduces the velocity of its wave-induced current.

## 5.4   With Groyne – Current-only and Current+Wave Conditions

This corresponds to Hydraulic Conditions 1, 3 and 4 of the experiment by Hulsbergen (1973). However, measurements for with pile groyne B configuration were only conducted for HC 1 and 4. For HC3, flow field (flow pattern) measurement with dye is available. For HC1, the measurement was done for a cross-section, while for HC4, the measurement was done for 5 sections, and thus the standard deviation was able to be derived from the provided data. HC1 was measured with photographically recorded surface floats and HC 4 was measured with visually observed surface floats. The measurement results are shown in Table 7 and Figure 26. Pile groyne B configuration extends from x=0m (H.W. line) to x=3.5m.

Table 7        Measurement results for with groyne condition

| Distance from H.W. line (m) | HC 1 | | HC 4 | |
| | (No Waves) Flow = 450 l/s (→) | | H = 0.03 m T = 1.04 s Dir = 15° Flow = 450 l/s (→) | |
| | Velocity (cm/s) | Standard deviation (cm/s) | Average velocity (cm/s) | Calculated standard deviation (cm/s) |
|---|---|---|---|---|
| 0.5 | - | - | 6.7 | 0.3 |
| 1.0 | - | - | 8.6 | 1.7 |
| 1.5 | 2.2 | - | 11.2 | 2.4 |
| 2.0 | 3.3 | - | 7.3 | 1.7 |
| 2.5 | 4.5 | - | 4.2 | 1.9 |
| 3.0 | 5.4 | - | 4.2 | 1.4 |
| 3.5 | 9.5 | - | 5.5 | 1.0 |
| 4.0 | 13.6 | - | 10.0 | 3.5 |
| 4.5 | 16.1 | - | 14.1 | 4.3 |
| 5.0 | 18 | - | 14.8 | 1.1 |
| 5.5 | 19 | - | 16.2 | 0.6 |
| 6.0 | 19.9 | - | 17.5 | 1.4 |
| 6.5 | 20 | - | 20.4 | 1.7 |
| 7.0 | 20.9 | - | 21.1 | 0.9 |
| 7.5 | 22 | - | 19.7 | 1.7 |
| 8.0 | 21.6 | - | 18.9 | 0.3 |
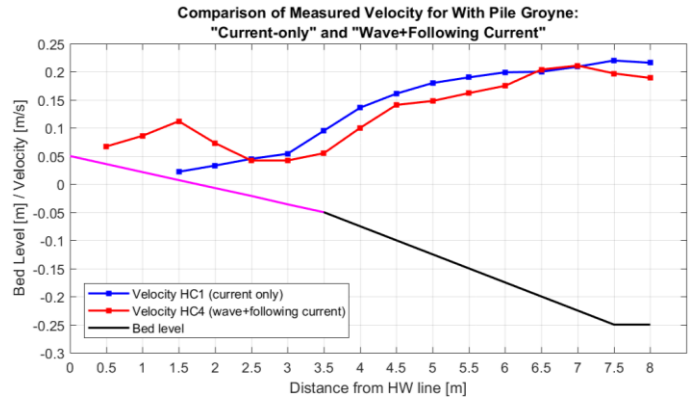


Figure 26        Measured longshore velocity for with pile groyne B configuration

Figure 26 shows the comparison for current-only (blue line) and wave+following current (red line) for with pile groyne B condition. The extent of pile groyne B is from the waterline to x=3.5m (pink line). In general observation, the velocity of current reduce significantly within the pile groyne region. An interesting observation is that even with pile groyne, there is significant longshore current observed (blue line) for the region from waterline to x=2.5m. This could be attributed by the fact that there is sufficient gap between the pile groynes (groyne field). Wave energy (and wave height) could still propagate inside the groyne field and break and consequently induces currents. It is expected that within the groyne field, the longshore current is maximum in the middle point, and lowest at immediately close to each flanking groyne. This means that the tidal flow momentum is effectively reduced by the groyne but the waves bring energy further shoreward and induce extra momentum in that region. This will need to be investigated with numerical modelling. The difference between peak of longshore current and the tidal-driven current is 9 cm/s (approximately 80%).

A point of uncertainty is shown for x>3m. Current velocity for flow-only is seen to be slightly higher than that of wave+following current. An uncertainty is presented by the fact that the measurement for HC1 is done for a section only and it is unsure whether this is representative for the rest of the sections in that hydraulic condition. However, despite the uncertainty above, the pattern of both measurements are as expected, where current is reduced at the region where pile groynes are located.

## 5.5    Current+Wave – With and Without Groyne Conditions

This corresponds to Hydraulic Conditions 3 and 4 of the experiment by Hulsbergen (1973). However, measurements for both with and without pile groyne B configuration were conducted only for HC4. For HC3, the measurement was only conducted for without pile groyne. This comparison, then, is only done for HC4. The measurements are shown in Table 8 and Figure 27. The measurement for the condition with and without pile groyne were done with visually observed surface floats, and for 16 and 5 transects, respectively.

Table 8  Measurement results for current+wave condition: HC4

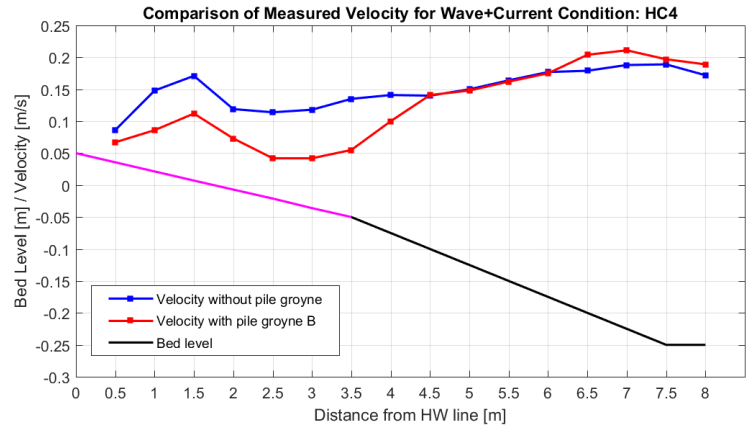| Distance from H.W. line (m) | Without Groyne | | With Pile Groyne B | |
| | H = 0.03 m T = 1.04 s Dir = 15° Flow = 450 l/s (→) | | | |
| | Average velocity (cm/s) | Standard deviation (cm/s) | Average velocity (cm/s) | Calculated standard deviation (cm/s) |
|---|---|---|---|---|
| 0.5 | 8.6 | 4.6 | 6.7 | 0.3 |
| 1.0 | 14.8 | 3.5 | 8.6 | 1.7 |
| 1.5 | 17.1 | 4.1 | 11.2 | 2.4 |
| 2.0 | 11.9 | 2.2 | 7.3 | 1.7 |
| 2.5 | 11.4 | 1.7 | 4.2 | 1.9 |
| 3.0 | 11.8 | 1.5 | 4.2 | 1.4 |
| 3.5 | 13.5 | 0.7 | 5.5 | 1.0 |
| 4.0 | 14.1 | 1.2 | 10.0 | 3.5 |
| 4.5 | 14.0 | 1.2 | 14.1 | 4.3 |
| 5.0 | 15.0 | 1.2 | 14.8 | 1.1 |
| 5.5 | 16.4 | 1.6 | 16.2 | 0.6 |
| 6.0 | 17.7 | 1.8 | 17.5 | 1.4 |
| 6.5 | 17.9 | 1.1 | 20.4 | 1.7 |
| 7.0 | 18.8 | 1.9 | 21.1 | 0.9 |
| 7.5 | 18.9 | 1.6 | 19.7 | 1.7 |
| 8.0 | 17.2 | 1.3 | 18.9 | 0.3 |



Figure 27        Measured longshore velocity for without and with pile groyne B configuration: HC4

In the deeper water, the distribution of current for both conditions are almost similar. The distribution diverge at x=4.5m. The reduction of velocity is most apparent for the condition with pile groyne (red line) where it drops by almost 10 cm/s, due to the resistance by the pile cylinders and bed friction. The condition without pile groyne only drops by about 2 cm/s due to bed friction. This means that in that region, resistance by pile cylinders is dominant over bed friction. Significant shear layer may be present at x=3.5m to x=4.5m for the condition with pile groyne.

Between x=3m and x=2m, due to longshore current contribution, the velocity picks up much earlier (more offshore) for condition with pile groyne than that of without pile groyne. This shows that the lateral penetration of tidal flow towards waterline for the condition with pile groyne is very little compared to that of without pile groyne. The location of peak longshore current is not changed by the presence of pile groynes.

From Section 5.4, the difference between peak of wave-induced longshore current and the tidal-driven longshore current is 9 cm/s (approximately 80%) due to the contribution of wave-induced current to the velocity profile. But in Figure 27 above, the difference between peak longshore current and tidal-driven current is 6 cm/s. This means that a further 3 cm/s, or 33% of the reduction is caused by the tidal flow reduction from pile groynes resistance.

It is seen that the location of peak of longshore current is not changed when comparing between the two conditions. This is mainly due to the fact that wave energy can still propagate relatively unobstructed towards within the groyne field, which makes up the most coverage area within a groyne system, and break at the same location as for the case without pile groyne. It is expected that this will be different for the case with mangrove forest mainly due to the large coverage of vegetation stem, thus dissipating wave energy more efficiently than pile groynes. With the transformation of wave height of a given wave ray propagates further into the mangrove forest, the location of breaker line will shift and this in turn shift the location of longshore velocity peak.

## 5.6  Summary

The analysis and comparisons above show that for a condition with and without pile groyne, (stationary) tidal flow is seen to be significantly reduced. This is consistent with the theory that in the region where stem cylinders are present with significant density, the dominant resistance is provided for by the stems/cylinders rather than by bed friction. However, the tidal flow is not entirely reduced to nil, because as per the findings of Trampenau (2000), for pile groyne with permeability of more than 20%, significant current still flow through the individual stems. This, however, may be different for the case of with mangrove forest, due to the larger coverage of the cylindrical stems, which will need to be investigated by means of numerical modelling.

In contrast, longshore current is present in the groyne field. It is hypothesized that due to the significant gap between each groyne, wave energy still propagates into the groyne field and break and consequently induce current. It was found that the presence of pile groynes does not reduce the magnitude of longshore current significantly, which is the opposite to that of tidal current.

For the case of wave and current in the same direction, longshore current magnitude is slightly increased due to the addition of current and orbital velocity vectorially. For the case of wave and tidal current in opposite direction, it is seen that the wave-induced longshore current is only slightly reduced by the opposing current. Thus, the highest wave-induced longshore current velocity magnitude is observed for wave+following current condition, followed sequentially by wave-only and wave+opposing current conditions.

Also it was found that due to the different extent of penetration of tidal current for with and without pile groyne, the increase of wave-induced longshore current velocity in the groyne region is earlier (more offshore-ward) for condition with pile groyne than without pile groyne.

Despite the above, for a given current+wave condition, the location of peak of wave-induced longshore current is not changed when comparing between the conditions with and without pile groyne. It is expected that this will be different for the case with mangrove forest mainly due to the large coverage of vegetation stem, thus dissipating wave energy more efficiently than pile groynes. With the transformation of wave height of a given wave ray propagates further into the mangrove forest, the location of breaker line will shift and this in turn shift the location of longshore velocity peak.

A comparison of wave+following current for with and without groynes show that roughly 66% of current reduction within a pile groyne field is caused by the presence/absence of the longshore current, and roughly 33% is caused by the velocity reduction due to stem resistance.

# 6 Numerical Simulation

This chapter elaborates on the numerical modelling works for the different hydraulic conditions, i.e. flow-only, wave-only and wave+flow conditions, and for different cylindrical stem conditions, i.e. without pile groyne and mangrove forest, with pile groyne and with mangrove forest. Validation runs are also shown.

Firstly, mangrove forest parameters are established and the schematization into the model is provided. Subsequently, each section that follows provide the validation works and the simulation with mangrove forest. Discussion of results are embodied with these sections. Section 6.5 elaborates on the comparison between different hydraulic conditions.

A complication was faced during the validation for wave-only condition (Section 6.3). Several previous relevant studies were referred to and various methods were attempted. Method 4, which although does not validate perfectly but provides the best representation of wave-induced current, is eventually adopted to further study wave-induced current within mangrove forest. Appendix C provides detailed elaboration on the various methods attempted, the eccentricities of the results as well as the calibration and sensitivity analysis.

For the purpose of discussion, the condition without pile groyne and mangrove is denoted as plain condition. For discussions of cross-shore distributions, the cross-shore distance from waterline (H.W. line) is denoted by the distance x (e.g. x=3m).

A summary is provided at the end of the chapter.

## 6.1 Mangrove Forest Schematization

For the simulation with mangrove forest, the vegetation parameters for Rhizophora mucronata of coastal fringing forest as used by Narayan et al. (2011) will be adopted as shown in Table 9. For current study, the parameters of the tree stem are used to be representative of the forest. Hence, a diameter of 0.25 m and height of 6 m are adopted. Individual stems represent a single mangrove tree. In the numerical model, this translates into 0.00625 m diameter and a height of 0.15 m. A stem density of 0.7 tree/m$^2$ in prototype is equivalent to 0.7 tree/0.000625 m$^2$ in model. Which is equivalent to 1,120 tree/m$^2$, or for a grid spacing of 0.25m x 0.25m, it will be 70 trees/grid.

Table 9       Parameters of Rhizophora mucronata (Narayan et al., 2011)

| Parameters | Control Value | Value Range |
|---|---|---|
| Root diameter (m) | 0.075 | 0.05 – 0.1 |
| Stem diameter (m) | 0.25 | 0.15 – 0.4 |
| Canopy diameter (m) | 0.5 | 0.02 – 1 |
| Stem height (m) | 6 | 0.5 – 1.7 |
| Root height (m) | 0.8 | 0 – 1 |
| Canopy height (m) | 2 | 0.2 – 3 |
| **Density variations** | | |
| Root density (m$^{-2}$) | 60 | 1 – 130 |
| Stem density (m$^{-2}$) | 0.7 | 0.5 – 1.7 |
| Canopy density (m$^{-2}$) | 100 | 1 – 100 |

In the model, the proposed mangrove forest covers the full length of the model domain alongshore and extends to 3.5 m from the waterline. In prototype scale, with Hulsbergen's (1973) scale of 1:40, the size of the mangrove forest is of 140 m wide. According to Truong et al. (2017), the typical width of coastal mangrove forest is more than 100 m. Thus, this is satisfactory. The mangrove forest will cover the upper slope of the bed profile with slope of 1:35.

A study into the variation of mangrove density will be adopting the two extremes of the value range for stem density in Table 9 above. The prototype densities of 0.5 and 1.7 trees/m$^2$ is translated into 800 and 2,720 trees/m$^2$ in numerical model with scale factor of 40. Stem diameter is maintained at 0.00625 m for both density values.

## **6.2**   Tidal Current Only (Hydraulic Condition 1)

Model Setup

A domain of 35.5 m and 13.5 m in the longshore and cross-shore direction was set up. The domain cross-shore length was extended by 1.4 m. This is determined by approximating the extra spaces created by the wave makers in the northern boundary of the domain (Figure 28a). The 1.4 m extension is found at the middle of each wave maker. This is due to the diagonal orientation of the wave makers. As a comparison, a current-only experiment by Trampenau (2000) has a guide wall in the offshore boundary to create a uniform flow. The absence of this guide wall in Hulsbergen (1973) experiment necessitated the extension in the cross-shore direction to obtain a good validation. Grid spacing of 0.1 m x 0.25 m was applied. This model grid and bathymetry was used for the plain condition, condition with pile groyne, and condition with mangrove forest.

The coastline/waterline was located in the southern boundary, the offshore boundary was located in the northern boundary, while the western and eastern boundaries were lateral boundaries (Figure 28c). The western boundary was imposed with total discharge of 0.45 m$^3$/s and eastern boundary with water level of 0.05 m. For HC1, the northern boundary was treated as a closed boundary due to the wave generators in Hulsbergen's experiment (Figure 11). The cross-shore profile of the bed level is shown in Figure 28b. The cross-shore profile is uniform in alongshore.
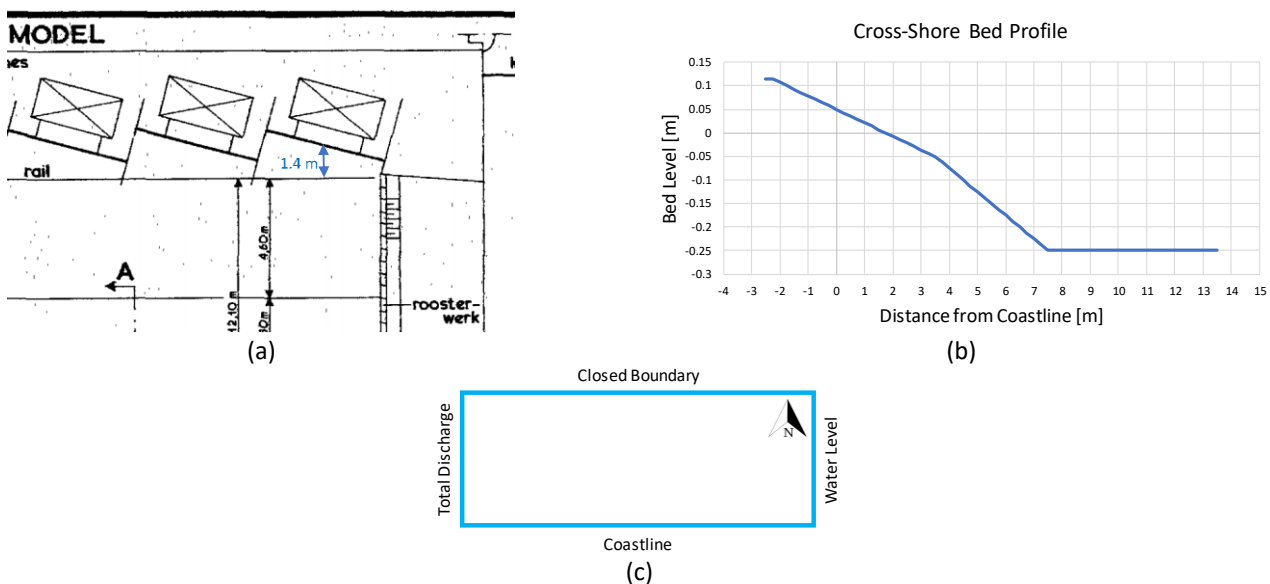


Figure 28    (a) Approximation of cross-shore extension of domain [Adapted from Hulsbergen, 1973] (b) Cross-shore bed level (uniform in alongshore direction) (c) Specified boundary conditions

The simulation was run for 2 hours with time step of 0.005 minutes. Initial condition was imposed with water level of 0.05 m. A roughness of Chezy coefficient with Nikuradse roughness length of 0.001 m was applied across the whole domain. Viscosity of 0.025 m$^2$/s was set constant spatially.

In the condition with pile groyne, the piles were implemented into the model by using a rigid vegetation model file. A depth file was incorporated to input the location of the piles. 5 groyne piles were placed at locations as shown for pile configuration B in Figure 12. The groynes were denoted as Number 1-5 in west-east direction. Turbulence length scale coefficient between stems were ClPlant = 0.80. The stem height from coastline to 2.75 m in cross-shore direction was 0.0425 m, for 2.75 m to 3.0 m from coastline was 0.0454 m, for 3.0 m to 3.25 m from coastline was 0.0518 m, and for 3.25 m to 3.5 m from coastline was 0.059 m. The stem diameter was 0.00625 m. This means that the pile groyne was partially emergent and submerged. $C_d$ value of 2.0 was used, consistent with the formulation used according to Kothyari et al. (2009) in Section 2.5. For this grid size, an adapted stem density of 6400 stems/m$^2$ was used to be able to represent 50% lateral blocking (Figure 29c) as per the blocking of pile groyne in Hulsbergen's (1973) setup (Figure 29a). An adaptation in the density value was done because Delft3D recognizes the density as uniformly distributed in space as per Figure 29b. This stem arrangement renders 1600 stem/m$^2$ to represent lateral flow blocking of less than 50%, and consequently results in higher longshore current velocity. This adaptation only introduces small error because the grids with pile groynes are far in between (5 m gap between two adjacent groynes), thus flow within the groyne field was not very much affected.

(a) 1600 stem/m² as per Hulsbergen (1973) (= 50% blocking)

(b) 1600 stem/m2 as assumed by Delft3D (= 25% blocking)
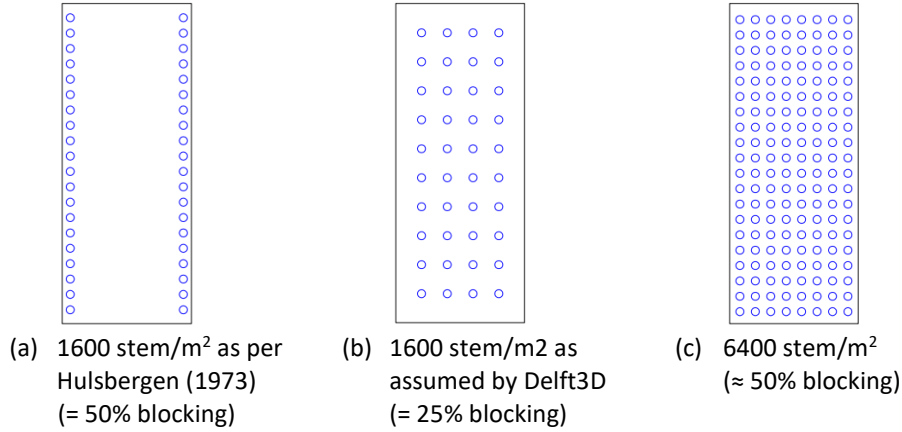
(c) 6400 stem/m² (≈ 50% blocking)

Figure 29          Schematization of pile groyne density in grid size of 0.1 m x 0.25 m

For the with mangrove condition, the mangrove forest was implemented into the model using a rigid vegetation model file. The forest was schematized as fully emerged. As explained in Section 6.1, the stem density was 1120 tree/m² with diameter of 0.00625 m.

Results

The result for without pile groyne condition is shown in Figure 30. Measured data of Hulsbergen is denoted by black dots. The simulated velocity (blue line) between x=2 m and x = 3.5 as well as x>7 m shows good agreement. The simulated velocity between x=3.5m to x=6.75m is slightly underestimated. This could be attributed to the usage of constant eddy viscosity value. Generally, the cross-shore profile of the longshore current is satisfactory.
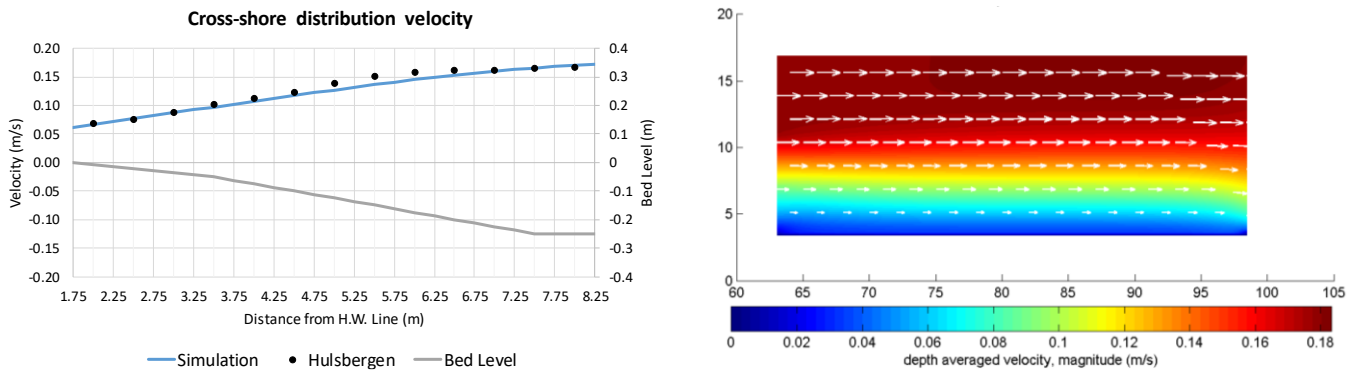


Figure 30      Results for without pile groyne. Left: cross-shore distribution of velocity. Right: flow field
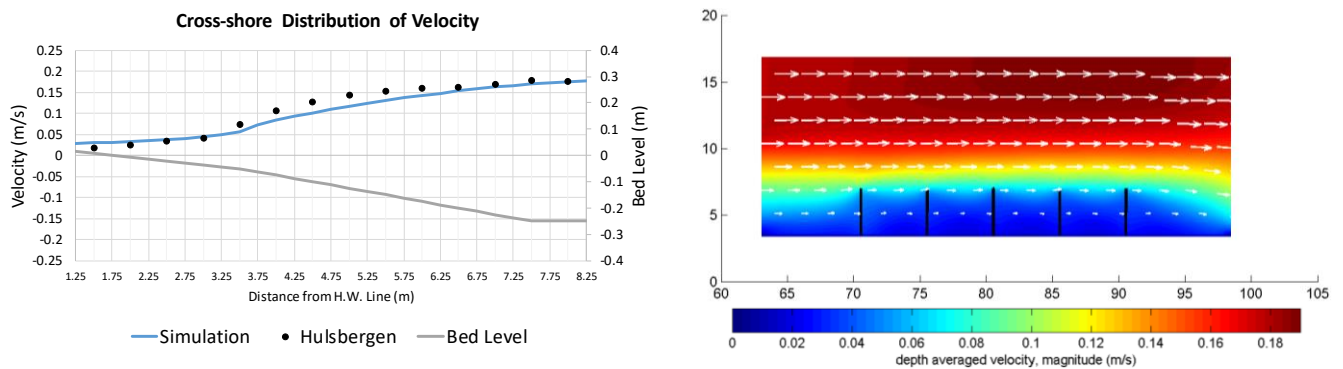


Figure 31      Results for condition with pile groyne. Left: cross-shore distribution of velocity. Right: flow field. Black lines denote pile groynes.

The results for with pile groyne condition are shown in Figure 31. The values of measured data have been corrected for depth-averaged velocity by assuming a logarithmic velocity profile (black dots). In the cross-shore distribution of velocity, the simulated velocity (blue line) for x=1.5 m to x=3.5 m is significantly reduced due to the presence of pile groyne field. The velocity at x< 3m and x>6.5m agrees very well with that of Hulsbergen's (1973) result. The simulated velocity is underestimated for 3<x<6.5m. By using constant horizontal eddy viscosity, the momentum exchange throughout the cross-section is constant. The flow field shows current velocity dampened at the pile groyne field. It has been shown by Trampenau (2000) that for a pile groyne with permeability of more than or equal to 20%, current will still flow through

the pile cylinders, in contrast to when the permeability is less than or equal to 10%, at which point there will be circulation in the groyne field (between a given two pile groynes) (Figure 32). The model then is validated satisfactorily.
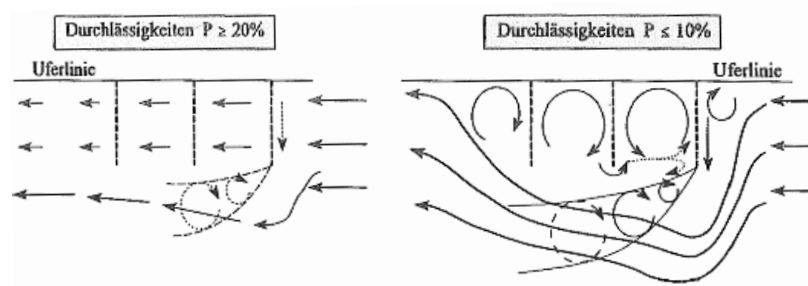


Figure 32    Flow field sketch of the flow conditions in groynes with permeability transitions of P> 20% and P <10% (Trampenau, 2000)



Figure 33    Cross-shore distribution of current velocity: Comparison of plain, with pile groyne and with mangrove conditions

Figure 33 shows a comparison of plain condition(blue line), condition with pile groyne (red line) and condition with mangrove (green line). The velocity profile for condition with pile groyne is extracted in the middle between Groyne 2 and 3 (number 2 and 3 from West Boundary). Pink line denotes the extent of the pile groyne and mangrove forest. As expected, within the pile groyne and mangrove field, the velocity is reduced compared to the plain condition by about 33% and 76%, respectively, at x=3.5 m. At the waterline,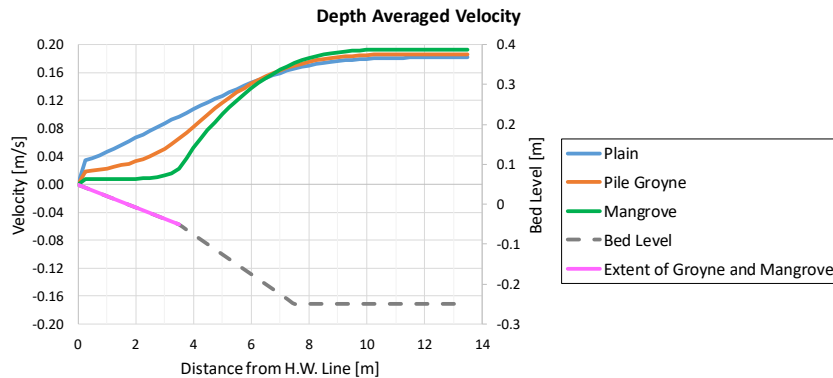 wave-induced longshore current velocity is reduced by 45% and 78%, respectively for conditions with pile groyne and mangrove forest, compared against plain condition.

Although mangrove forest was specified with lower density (1120 stem/m$^2$) compared to pile groyne (6400 stems/m$^2$), the velocity is reduced more substantially because of the much larger coverage area of the mangrove forest. At 3.5m<x<7.5m, velocity gradient increases for with pile groyne and mangrove conditions. At x>7.5m, the velocity is higher for condition with mangrove forest, followed by condition with pile groyne and by plain condition. This occurs due to the flow constriction provided by the introduction of cylindrical stems into the model. For condition with pile groyne, the constriction is less than that of the condition with mangrove because the current flow through the piles are still significant. Whereas, the longshore current within mangrove forest is almost close to 0 m/s. However, the amount of increased velocity at x>7.5 m is not 1:1 proportionate to the decrease of velocity at x<7.5 m due to the momentum reduction by the resistance force provided by the cylinders. In general, the velocity profile for condition with mangrove is consistent with literature (Figure 8).

This is consistent with theory in Section 2.6 and the analysis conducted in Chapter 5, where within the pile/mangrove region, stem resistance is dominant over bed friction.

## 6.3    Wave Only (Hydraulic Condition 5)

This section elaborates on the model setup as per Hydraulic Condition 5 (Table 1). First, the model setup is outlined and the results as well as discussions follow. Simulations were done for plain condition, and conditions with pile groyne, and with mangrove forest.

Model Setup

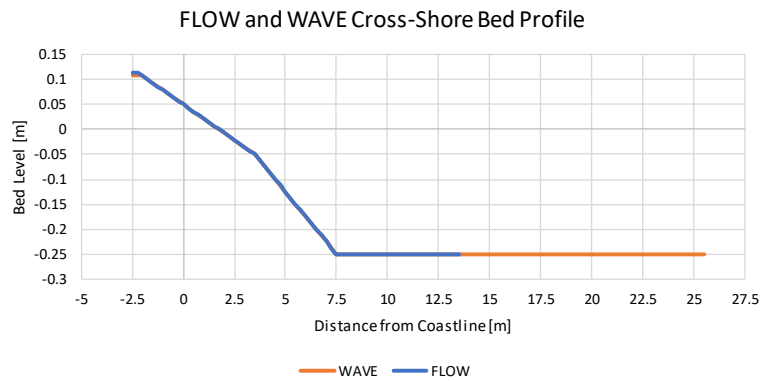FLOW and WAVE Cross-Shore Bed Profile



Figure 34          Domains and cross-shore bed level for FLOW (blue grid) and WAVE (grey grid). The bed level is uniform in the alongshore direction.

The grid of computational domain for FLOW was 54 m x 13.5 m in alongshore and cross-shore directions, respectively, with grid spacing of 0.25 m x 0.25 m (Figure 34). Initial condition imposed was water level of 0.05 m. A Chezy coefficient of 50 $m^{1/2}$/s and eddy viscosity of 0.001 $m^2$/s were applied. Default stress formulation due to wave forces was used, i.e. Fredsoe 1984. Threshold depth of 0.01 m was applied.

The grid of computational domain for WAVE was 162 m x 25.5 m in alongshore and cross-shore direction, respectively, with grid spacing of 1.0 m x 0.5 m (Figure 34). The FLOW domain was located in the middle of the WAVE domain to avoid shadow effect to reach the area of interest. Wave height of 0.03 m, period of 1.04 s and direction of 15° shore-normal were imposed at the boundary. To emulate as close to regular wave condition as possible, a Gaussian-shaped spectrum with spreading of 0.01 Hz and directional spreading of 90 cosine power were specified. This Delft3D-WAVE model setup was run for single time step.

In FLOW, roller model was turned on and wave conditions were defined with a <wavcmp> file. This file required wave direction information from communication files produced by WAVE module. Thus, a dummy FLOW and a normal WAVE module for one time step as specified above were run first. Similar wave conditions as in WAVE module were specified in the wavcmp file. According to Delft3D-FLOW manual (Deltares, 2016), All the flow boundaries had to be set to Riemann type. The input for the Riemann boundary conditions would be generated automatically based on the given wave conditions. Due to the specification of wave conditions through the wavcmp file, a shadow effect is seen at the eastern boundary of the FLOW model domain. This is why the domain was extended by 54 m, in contrast to the 35.5 m alongshore length for current-only condition in Section 6.2.

Appendix C outlines the methods attempted in obtaining a reasonable alongshore current as per Hulsbergen's (1973) measured data and as per analytically calculated velocity (Chapter 4). The reader is strongly urged to refer to the appendix where the details of methods (approaches) including bathymetry, specification of boundary conditions, etc. are elaborated, and the comparison of each respective result are discussed. The appendix provide reasoning on possible numerical and/or physical interpretation of the results.

The methods attempted were online Delft3D FLOW-WAVE with roller (Method 1) and without roller (Method 2), with specification of wave condition through wavecon file (Method 3), as well as the specification of wave condition through wavcmp file (Method 4). Although not a perfect validation, Method 4 showed the best fit amongst the methods as well as showing a correct representation of wave-induced current. In view that the objectives are not to merely identify the shortcomings of the model in simulating wave-induced current, but are geared towards understanding the interaction of wave-induced current in mangrove forest, then despite being short in validation accuracy, Method 4 was then adopted for further analysis in current study. The result of Method 4 is shown below with discussion. Appendix C shows the results of the various methods attempted as well as reference to previous Master's theses as basis of setup.
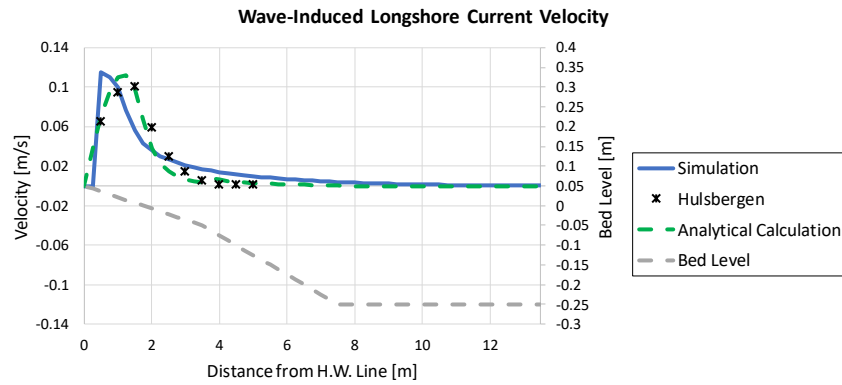
Results



Figure 35    Validation for wave-only condition

Figure 35 shows the simulation result for condition without pile groynes and mangrove forest (plain condition). The magnitude of peak of simulated longshore current velocity is in good agreement with both the analytically calculated and measured data of Hulsbergen. However, due to the wave breaking location being closer to shore (Figure 55 in Appendix C), the simulated velocity peak is shifted closer to shore. It is suspected that since the wave breaks closer to shore, the breaking gamma is very large. Upon further inspection, the wave breaks at 1.25 m from coastline, with wave height of 0.043 m, and at water depth of 0.036 m, which resulted in breaking gamma ratio of 1.21, which is extremely high. However, as shown in Appendix C, the velocity profile of the model result does not show changes despite changing the breaking gamma value. It can also be seen that the simulated velocity outside of the breaker line was overestimated. Treffers (2009) has shown a similar velocity profile for a constant breaking gamma. By adopting breaking gamma as introduced by Ruessink et al. (2003) (Equation 17), Treffers has shown that the overestimation outside of the breaker line is reduced and fits almost perfectly with measured data. However, due to the limitation of current model setup, the value of breaking gamma was unable to change the simulation result. The cross-shore distribution of the longshore current is relatively uniform alongshore, which is important to have in a model result for current study, as mentioned in Section 3.2.



|        (a)         |        (b)         |        (c)         |
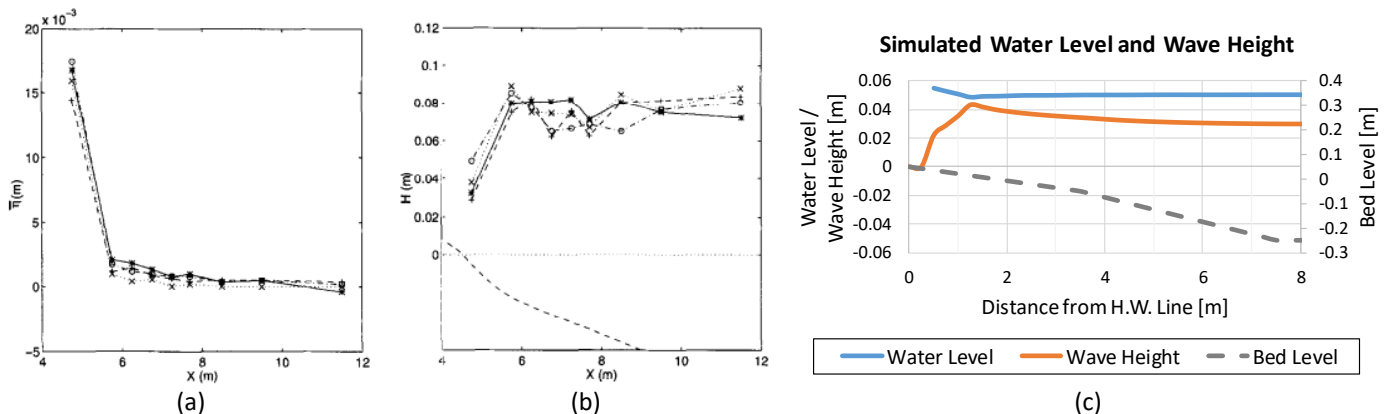
Figure 36    Reniers and Battjes (1997) measurement results for non-barred profile with regular waves (a) water elevation, (b) wave height; (c) Simulated water elevation and wave height from current study

A qualitative comparison look at cross-shore profiles of water elevation and wave height between simulated (blue and red line, respectively, of Figure 36c) and measured water elevation by Reniers (1997) (Figure 36a) shows that the simulated water elevation is representative of water set-up induced by waves and the wave height profile (Figure 36b) is well simulated qualitatively.

Despite the shift of velocity peak shoreward, in view of current study objectives, it is imperative to study the wave-induced current within mangrove forest. Thus, the result of the simulation above is considered a good representation of longshore current and is sufficient to study wave-induced current within mangrove forest.

(a)

(b)

(c)                                    (d)                                    (e)
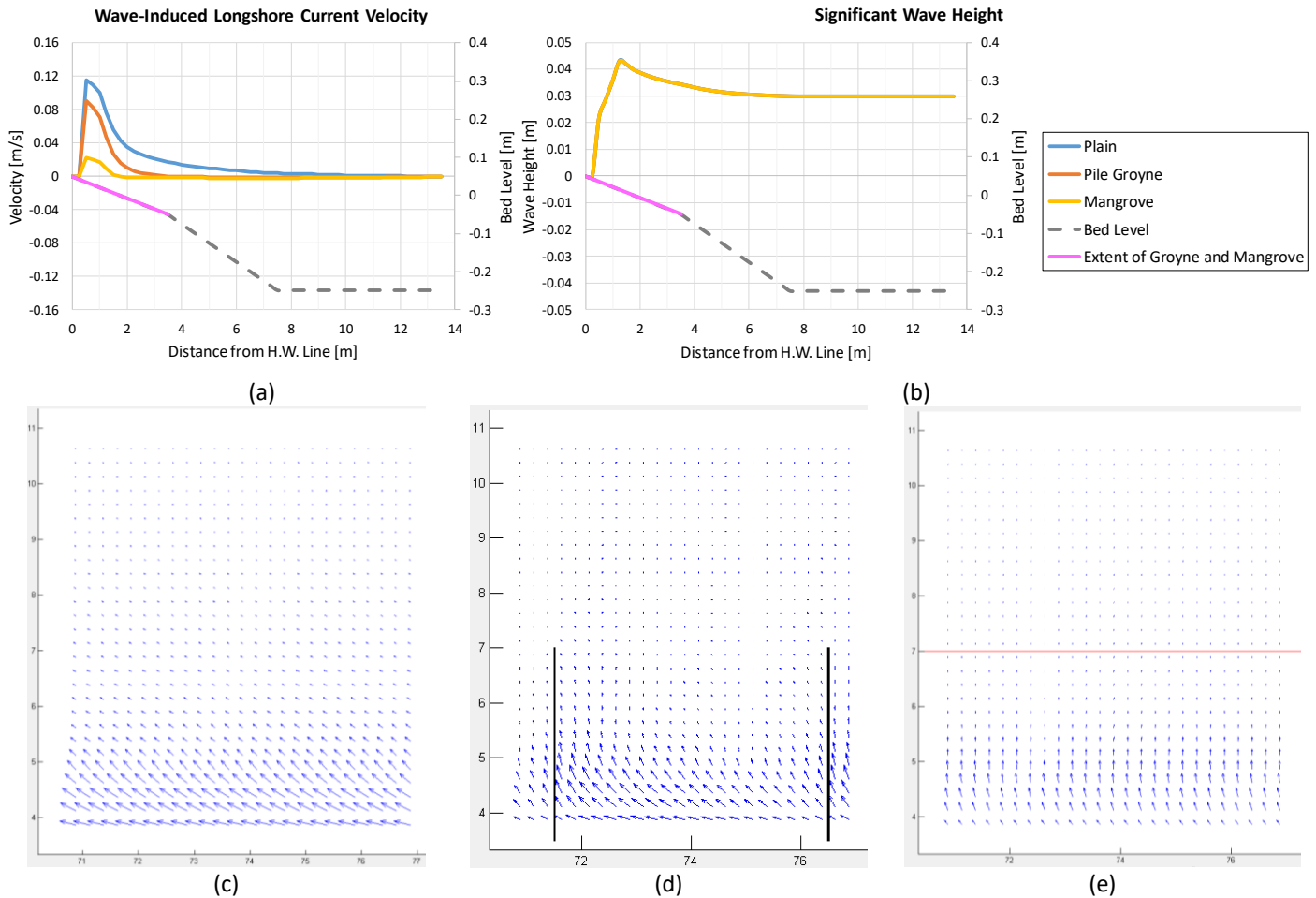
Figure 37     (a) Velocity cross-shore distribution and (b) significant wave height for conditions without pile groyne and mangrove (plain condition), with groyne and with mangrove; Flow field for (c) plain condition, (d) condition with pile groyne, (e) condition with mangrove forest (mangrove interface is denoted by red line); x-axis represents alongshore coordinate in meter and y-axis represents cross-shore coordinate in meter. Origin is 54m, 3.5m.

This paragraph looks into the velocity profile for plain condition (blue line), condition with pile groyne system (red line) and condition with mangrove forest (yellow line) (Figure 37a). The velocity profile for condition with pile groyne was extracted in the middle of groyne number 2 and 3. As expected, it can be seen that for both conditions with pile groyne and mangrove, longshore current velocity is significantly reduced at x<3.5 m. At x=3.5 m, wave-induced longshore current velocity is reduced by 51% and 82% for conditions with pile groyne and mangrove forest, respectively, in comparison against that of plain condition. Whereas, at waterline, the reduction is 27% and 83% for conditions with pile groyne and mangrove forest, respectively.

With the presence of wave-induced current within mangrove forest, this indicates that as long as wave energy is not entirely dissipated by the vegetation and as long as waves break within the forest, this will induce longshore current within the forest. As found by Trampenau (2000), for pile groyne permeability of more than 20%, the current flow through the pile groynes is still quite significant that very little circulation is observed within the groyne field. Longshore velocity is much more reduced by the mangrove forest than by the pile groyne. Although longshore current is consistently being produced within the forest, vegetation stems effectively reduce the current, whereas, for the condition with pile groyne, the groyne field gap allows current to gain momentum due to absence of resistance (bed friction plays significantly smaller role in this case).

A look into the wave height profile for the three conditions (Figure 37b) show that wave height does not change despite having both pile groynes and mangrove tree stems. Theoretically, wave energy should be dissipated by the stems, and the significant wave height should reduce with highest being for the plain condition followed by condition with pile groyne and with mangrove forest. This means that wave energy is only dissipated by breaking and that the velocity reduction is mainly due to the resistance of pile groyne stems and mangrove tree stems against the induced current, and none from reduced wave height due to wave-vegetation interaction. It is uncertain how much further longshore current reduction may be observed in the event that the model takes into account wave height reduction from wave-vegetation interaction. This may need to be addressed in future thesis study with a different model.

Apart from the reduction of wave height, the location of wave breaking for the condition with mangrove forest was anticipated to be more shoreward than the other two conditions with and without pile groynes (Section 5.6). This however is not observed from this numerical modelling result. That is very much due to the absence of wave-vegetation interaction. The change of breaking location was hypothesized to also in return shift the location of longshore current velocity peak.

On top of that, this will affect the magnitude of offshore-directed current as well. This magnitude of cross-shore current will be determined by the gradient of radiation stresses, which among others, is a balance between shorter distance to the waterline and the lower wave height (consequently, wave energy).

In the plan view of flow field plot (Figure 37c-e), longshore current flows from east to west. For plain condition and condition with mangrove forest, the longshore velocity profile is uniform alongshore (Figure 37d and e). In contrast, for the condition with pile groyne, the longshore velocity is highest in the middle of a groyne field and lowest for immediate vicinity to the groynes (immediately downstream and upstream of a given groyne). This is because waves propagate in between the groynes, they break induced by depth limitation, and in return induce longshore current. Also, the offshore-ward current observed for all three conditions is caused by the increase of water elevation at the coastline as shown in Figure 36c, and due to this pressure gradient, water flows in offshore direction. There is only offshore-directed flow in mangrove forest, with almost no longshore current.

It is anticipated that should the simulated wave breaks further from waterline, meaning if the wave breaks at the same location as Hulsbergen's measured data, the energy gradient at the waterline will be smaller, which in turn makes the radiation stress gradient smaller. Consequently, onshore directed wave force, $F_x$, will be reduced. With that, increase of water elevation (setup) will reduce and the magnitude of offshore-directed velocity will reduce.

## 6.4    Wave and Current (Hydraulic Condition 4)

Hydraulic condition 4 corresponds to regular oblique waves of wave height 0.03 m, period of 1.04 s and direction of 15° shore normal, as well as a constant tidal flow from the eastern boundary with 0.45 m³/s.

Model Setup

The model domain and bathymetry was similar to those of wave-only condition (Section 6.3), which is an adaptation of Method 4. General setups were also similar, which is the specification of *wavcmp* for wave conditions and the requirement of communication files for Delft-3D flow simulation by running a dummy FLOW model and a single time step WAVE model. Flow discharge was specified in East Boundary, Riemann type in North Boundary and constant water level in West Boundary. Both pile groyne and mangrove forest were specified similarly, i.e. by means of rigid vegetation model files. Appendix C provides more details regarding the model setup.

Results
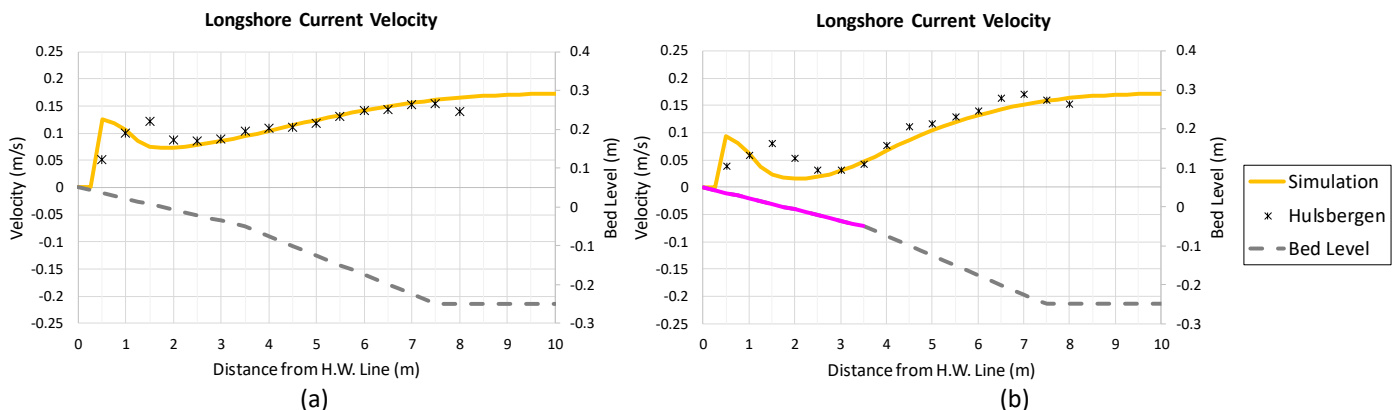


Figure 38    Validation for wave and current in same direction for (a) plain condition; and (b) condition with pile groyne. Pink line denotes the cross-shore extent of pile groyne.

Figure 38a and b show cross-shore distributions of simulated longshore velocity for plain condition and condition with pile groyne, respectively, validated against Hulsbergen's (1973) measured data which have been corrected for depth-averaged values (black asterisks). For plain condition, from deeper water to about x=3m, which is mostly driven by the (stationary) tidal flow, the simulated velocity shows good agreement. For x<3 m, the current flow is dominated by wave-induced current. This means that, similar to that of wave-only condition, due to the more shoreward location of wave

breaking, the magnitude peak of longshore current is in turn more shoreward located. This explains why the longshore current is underestimated in 1m<x<3m and overestimated in x<1m. The velocity profile in the alongshore direction is relatively uniform. As has been elaborated in Section 6.3 and Appendix C, for current model setup, the shoreward shift of the longshore current does not change with the change of roller parameters and breaking gamma. By having the capability to calibrate the breaking gamma alone would be able to give significant improvement to the location of peak of wave-induced longshore current. This limitation to the current model requires attention.

A roughly similar distribution is observed for the condition with pile groyne Figure 38b. At x<3.5 m, similar to measured data, the simulated wave-induced longshore velocity drops due to the resistance provided by pile groynes. At x<2m, the simulated wave-induced longshore velocity increases due to wave-induced current, but with smaller magnitude than that of plain condition. Despite the limitations of the model, the validation results above are considered fit for study into wave-induced current within mangrove forest.

Details regarding the validation of wave and current in same direction are also provided in Appendix C.
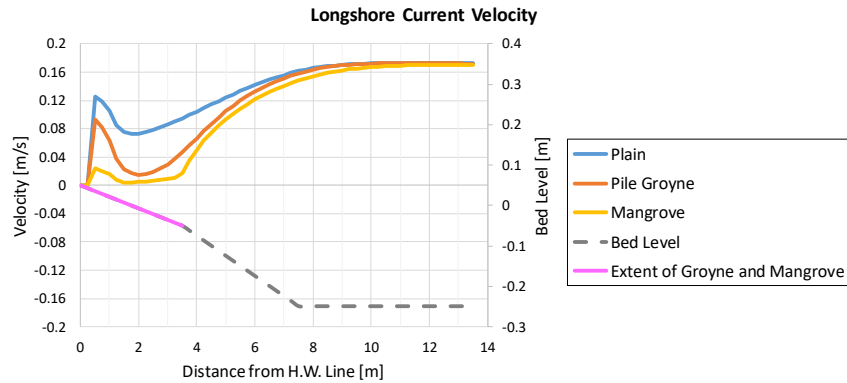


Figure 39          Cross-shore distribution of current velocity for conditions without pile groyne and mangrove (plain condition), with groyne and with mangrove

Figure 39 shows the simulation results for plain condition (blue line), condition with pile groyne (red line) and condition with mangrove forest (yellow line) for wave and current in same direction. Longshore current is induced at x<2m. The magnitude peak of the longshore current is reduced by 26% and 82% for conditions with pile groyne and mangrove, respectively. Similar to the wave-only condition, longshore velocity reduction by mangrove forest is significantly more effective than by pile groyne. The (stationary) tidal flow penetration towards waterline is varying for all three conditions. For plain condition (blue line), the tidal flow penetrates the whole cross-shore profile, for condition with pile groyne (red line), it penetrates to about x=2.5m, and for condition with mangrove forest (yellow line), the penetration is furthest away from waterline, i.e. about x=3.5m, which is the interface of mangrove and open channel flow.



| (a) | (b) | (c) |
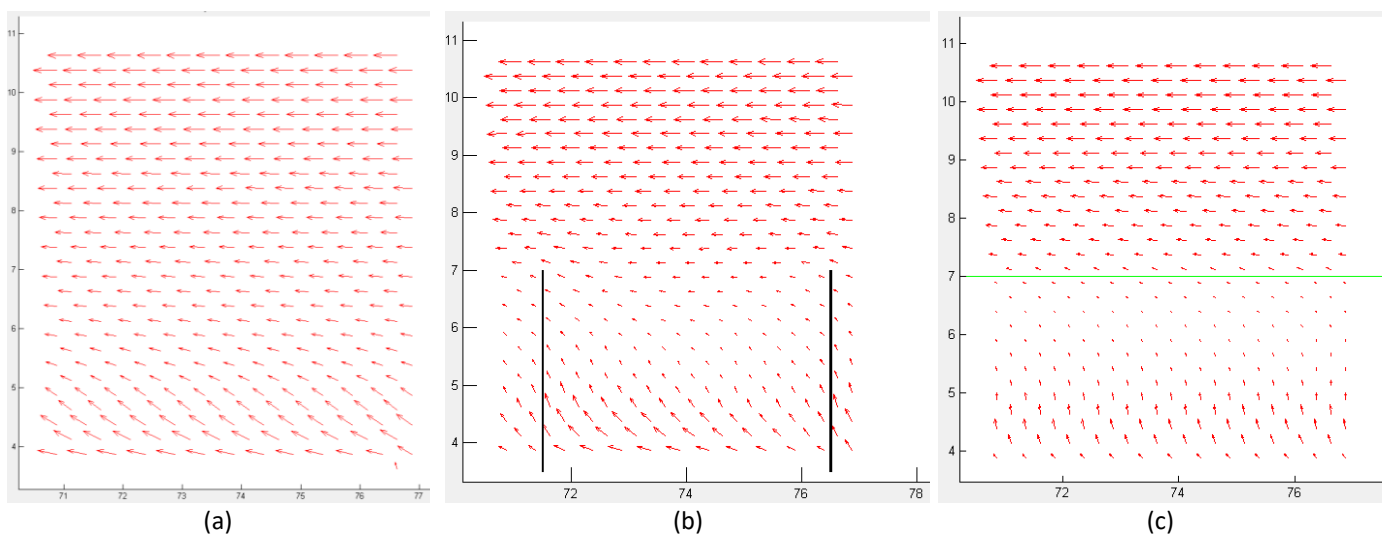
Figure 40     Flow field for (a) plain condition, (b) condition with pile groyne (pile groynes denoted by black vertical lines), (c) condition with mangrove forest (mangrove interface is denoted by green line); x-axis represents alongshore coordinate in meter and y-axis represents cross-shore coordinate in meter. Origin is 54m, 3.5m.

The flow fields for the wave with current in same direction are shown in Figure 40. In this paragraph, cross-shore coordinate in meter is denoted with y. For condition with pile groyne, the flow field is consistent with that of wave-only

hydraulic condition for y<5m. The tidal flow penetration can be seen at y>6m. For condition with mangrove forest, the longshore current is seen at the waterline, and for further distance from the waterline, offshore-directed flow dominates until halfway through the mangrove forest. Outside of the mangrove-main channel interface, tidal flow dominates. Very small longshore current is seen within the mangrove forest.

## **6.5**  Comparison for Different Hydraulic Conditions

In this section, comparisons are made for plain/pile/mangrove conditions across different hydraulic conditions. This is mainly to understand the differences in the interaction between the stem resistance and the various hydraulic conditions.
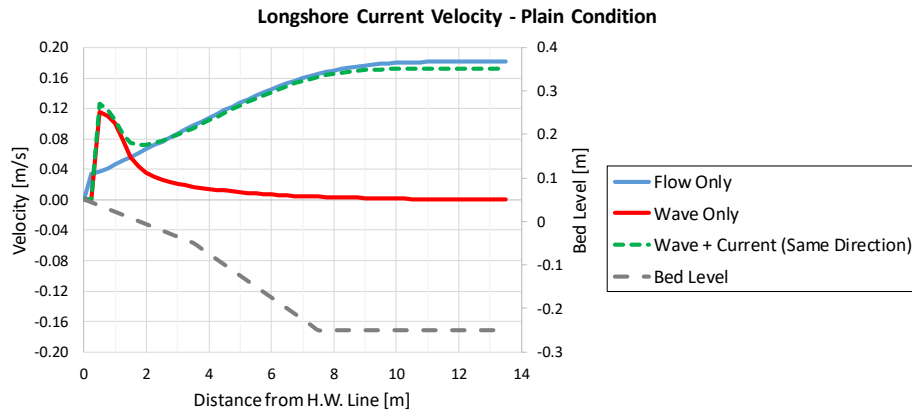


Figure 41     Velocity profile for different hydraulic conditions: Plain condition

In Figure 41, flow-only (blue line) and wave with current (dashed green line) conditions show similar velocity profile in x>2.5m. This region is dominated by tidal flow. In x<2.5m, flow-only and wave+current conditions show similar distribution, with slightly higher magnitude for wave+current condition due to the interaction of waves and current in the same direction. The increase of current velocity due to wave+current interaction is not as significant as expected. A broader look across the cross-shore profile shows that current velocity for wave+current is consistently slightly lower than that of tidal flow-only condition, starting from offshore boundary. An explanation to this might be due to the specification of Riemann type to offshore boundary, where current was seen to flow through the boundary (Figure 57a). This means that should the velocity profile of wave+current is transposed upward by as much as the current velocity difference in the deeper water, the velocity peak of wave-induced longshore current will also be slightly higher. It is also worth noting that Figure 41 shows that in the surf zone, wave-induced longshore current is more significant than tidal current. In this plain condition, wave-induced longshore current accounts for up to 90% of current velocity in the surf zone.
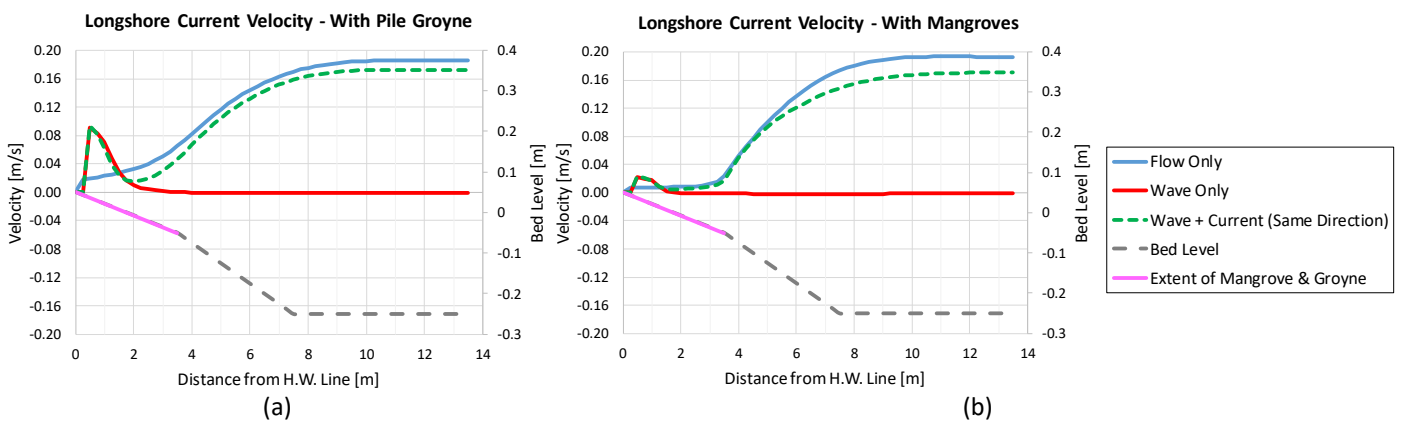


Figure 42     Comparison for different hydraulic conditions: (a) Condition with pile groyne; (b)  Condition with mangrove forest

In Figure 42a, at x<2m, it is generally seen that velocities of both wave-induced longshore current and tidal current are reduced. Tidal current within surf zone does not seem to contribute to the velocity magnitude, although for current-only condition, there is still current velocity in that region. Similar to the case with plain condition (Figure 41), velocity cross-shore profile of wave+current is consistently lower than current-only condition due to Riemann boundary condition for offshore boundary. This means that wave-induced longshore current for wave+current is supposed to be slightly higher than wave-only condition. Should tidal flow be accounted for in the surf zone, the contribution of wave-induced longshore current to the total velocity is up to 93%, which is very significant.

For the condition with mangrove forest at x<1.5m (Figure 42b), current velocity in the surf zone are more damped than for both plain condition and condition with pile groyne. Similar situation due to boundary condition is observed here. Should tidal flow be accounted for in the surf zone, the contribution of wave-induced longshore current velocity to the total velocity is up to 76%. This is still significant, despite reduction in comparison to the condition with pile groyne in preceding paragraph.

Above results show that there is a small extent of error involved which is caused by specifying an open Riemann type boundary in the northern boundary for the wave+current condition. However, the results reflect expected pattern of wave damping and thus is applicable for current study. A question rises as to whether the same longshore velocity magnitude in the deeper water would be observed should the offshore boundary of hydraulic condition of tidal flow only (Section 6.2) is changed to Riemann type instead of a closed boundary. A simulation was run as such and the model ended abnormally. This means that applying Riemann type boundary is unfeasible to a condition without waves being imposed.

It is seen that generally wave-induced longshore current contributes to more than 70% to total current velocity within mangrove forest, and more than 90% for that in the condition with pile groyne and plain condition.

## 6.6    Comparison for Different Bed Slopes

This section discusses on the effects of varying bed slopes to wave-induced current within mangrove forest. The general model setup was similar to that of wave-only condition (Section 6.3). Domain was enlarged to cater for extension of cross-shore domain when slopes are gentler. Mangrove forest density of 1,120 stem/m$^2$ was used for all bed slope variation and the coverage is from waterline to 3.5 m in cross-shore direction, and covers from West Boundary to East Boundary.

Three bed slopes were studied (1:35, 1:40 and 1:45) as shown in Figure 43. Ideally, a much gentler slope is more representative of bed slope for mangrove forest. However, attempts at slopes gentler than 1:45 shows unrealistic result with wave-induced longshore current velocity of up to 0.35 m/s at the waterline with an abrupt change of direction within surf zone (west-directed at waterline and east-directed within 1 m from waterline). This means for Method 4 model setup, there is a limitation on bed slope, with the gentlest slope possible for this setup being 1:45. In light of this, three bed slopes that are still relatively steep were used for discussion and the result of this is being qualitatively extrapolated for gentler slopes.
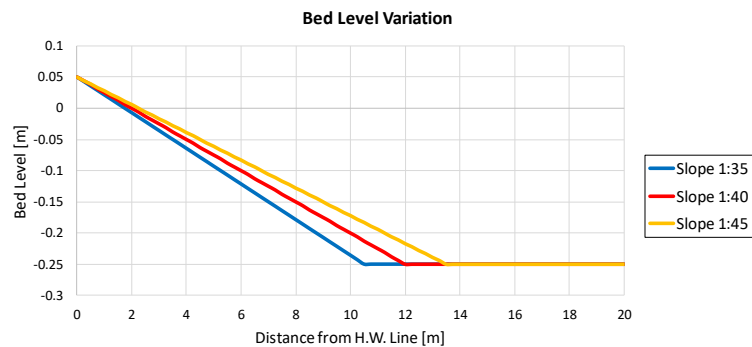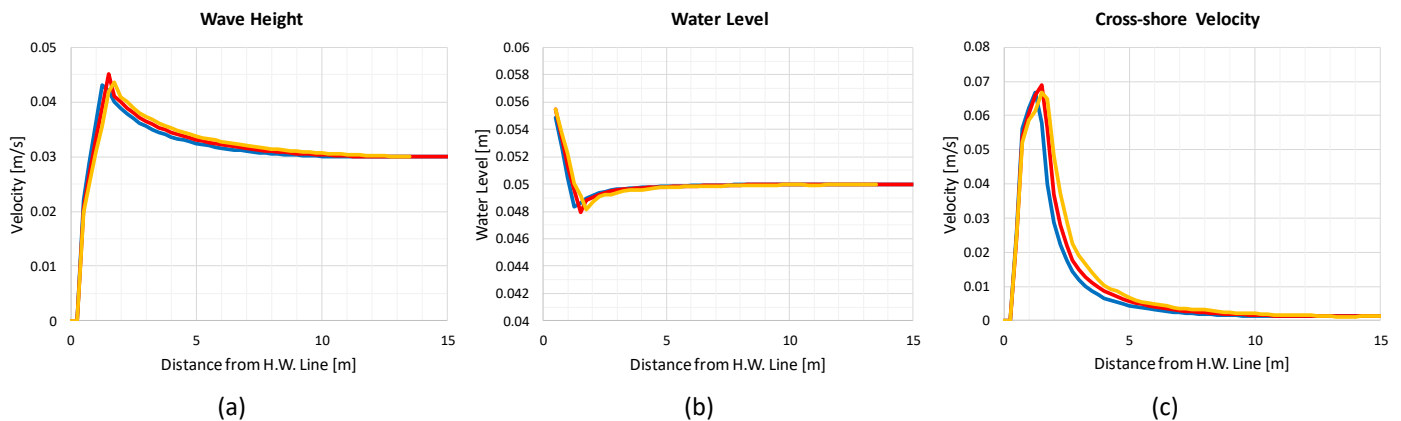


Figure 43            Bed level variation



(a)                                    (b)                                    (c)

**Cross-shore Distribution of Wave-Induced Longshore Velocity**
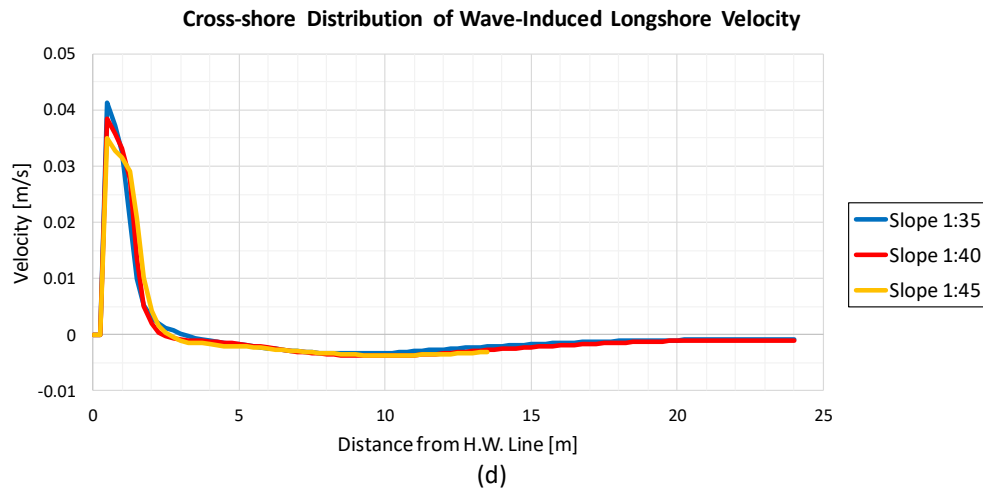


(d)

Figure 44          Cross-shore distribution of (a) wave height; (b) water level; (c) wave-induced cross-shore current velocity; (d) wave-induced longshore current

The result of the simulation is shown in Figure 44. In Figure 44a, wave height for gentler bed slope (yellow line followed by red line) breaks further offshore because water is shallower further offshore for gentler bed slope. It is expected that should the bed slope be much gentler, shoaling will start further offshore, breaking wave height will be lower and the cross-shore profile of wave height will be much wider. Wave set-down and set-up for gentler slopes are further offshore compared to steeper slope Figure 44b. Consequently, both wave-induced cross-shore and longshore currents are induced further offshore for gentler bed slope conditions. For cross-shore profile of wave-induced cross-shore current, the velocity is lower for gentler slope and more widely distributed. This trend is expected to be extrapolated accordingly for much gentler slopes, which can be seen from the formula by Longuet-Higgins (1970) (Equation 39 to Equation 48) which shows that gentler bed slopes affect the wave-induced longshore current firstly by shifting the location of wave breaking, and second by inherently affecting the value of P, the non-dimensional parameter representing relative importance of horizontal mixing.

For all three bed slopes, at roughly x>2.5m, wave-induced longshore current flow in the opposite direction, which is towards east. This persists throughout most of the profile until offshore boundary. A look at wave height profile does not show any reason why such is the case. This is also present in the case of varied mangrove forest density below (Section 6.7), which also is not caused by any variation of wave height in the deeper water. This phenomenon could be caused by the presence of high density stems, which is mangrove forest in this case, because this phenomenon was not observed in the case of condition with pile groyne (Figure 37a). Alternative explanation for this phenomena is that it could be caused by numerical artefact, due to prescription of Riemann boundaries at both lateral boundaries. The explanation for this is better explained in Section 6.7.

In general, the gentler a bed slope is, wave-induced longshore current will be more widely distributed, lower in magnitude and the peak is further from waterline. It needs to be kept in mind that wave-vegetation interaction was not considered due to limitation of current model setup. Should it be taken into account, the magnitude of wave-induced longshore current velocity will be lower. Thus, the damping of wave-induced longshore current above is only due to current-vegetation interaction. The result above means that for the case of the majority of mangrove forest, where bed slopes are gentle to very gentle, wave-induced longshore current is of generally a smaller magnitude and more widely distributed in the cross-shore direction.

## 6.7  Comparison for Different Mangrove Forest Density

In this section, wave-induced longshore current and wave-induced cross-shore current are studied for different mangrove density. Table 9 in Section 6.1 shows the range of mangrove forest density for Rhizophora mucronata. The extreme ends of the spectrum are used, i.e. 0.5 and 1.7 stem/m² of prototype densities, which translates into 800 and 2,720 stem/m² in the numerical model.

Figure 45 shows the result for the variation of stem density, including that of control value, i.e. 1,120 stem/m². Wave height profiles for all three different stem densities are similar (Figure 45a). This means that wave-vegetation interaction was not considered due to limitation of current model setup, as also has been shown in Figure 37b of Section 6.3. The implication of this finding is that the simulated wave-induced longshore current and wave-induced cross-shore current are overestimated. Also, the resulting water level profiles were not affected due to the absence of wave-vegetation interaction (Figure 45b). Due to the similarity of simulated wave set-down and wave set-up for the different stem

densities, the resulting wave-induced cross-shore current are also similar for all scenarios (Figure 45c). In Figure 45d, the magnitude of wave-induced longshore current velocity is more damped for higher density mangrove forest. This is consistent with expectation. Also the width of positive wave-induced longshore current is narrower for higher density forest.

There is also similar pattern of wave-induced longshore current for x=2.5 m to x=12 m as observed in Figure 44d, which is current flowing in the opposite direction, i.e. eastward direction. Equation 30 for alongshore uniform coastline would be simplified to $F_x = -\frac{dS_{xx}}{dx}$ and this means that the variation of alongshore-directed wave force is based on wave height variation only (as intrinsic in $E$, the wave energy). However, for this simulation, wave height profiles show only either constant or increase of wave height (shoaling) in the region of 2.5<x<12m. This means that the presence of eastward directed wave-induced longshore current is not caused by gradient of radiation stresses. This could mean that this phenomenon is a numerical artefact. This is also supported by the cross-shore profile of alongshore-directed wave force (Figure 44e) which shows constant wave force in that region (2.5<x<12m). An alternative model software with similar setups would be able to further explain whether this is numerical artefact or a physical phenomenon.



(a)                                                          (b)                                                          (c)



(d)                                                                              (e)
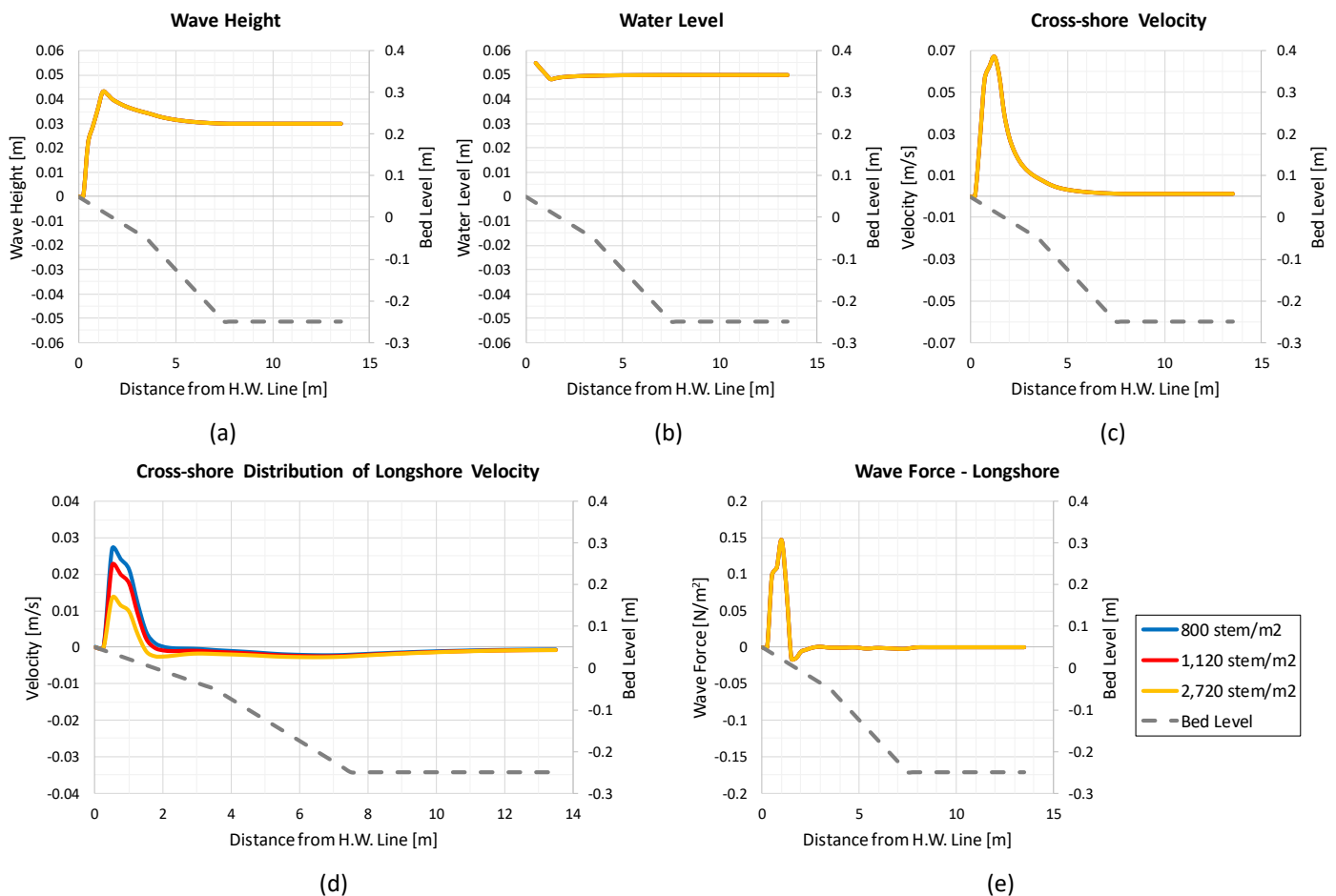
Figure 45            Cross-shore profile of (a) wave height; (b) water level; (c) wave-induced cross-shore current velocity; (d) wave-induced longshore current; (e) wave force

From Table 9, another relevant parameter would be root density, especially in very gentle and shallow mangrove forest. It ranges from 1-130 root/m$^2$ with control value of 60 root/m$^2$. In numerical model, this translates into a range of 1,600-208,000 root/m$^2$ with control value of 96,000 root/m$^2$. However, Delft3D does not allow cylindrical density of more than 80,000 root/m$^2$. This maximum allowable density is smaller than the control value.

## **6.8**  Summary

The stem density for schematization of pile groyne was adjusted to represent 50% lateral flow blocking as per specified by Hulsbergen (1973). The adjustment was necessary because Delft3D understands input of density as uniformly distributed over planar area, whereas Hulsbergen's piles were not uniformly distributed (Figure 29). With this, model validations for without and with pile groyne for hydraulic condition of tidal flow only were satisfactory.

For modelling of hydraulic condition of wave only, the numerical works were not straightforward. Several methods of specifying boundary conditions and communication between Delft3D-FLOW and wave module were attempted to obtain firstly, logical wave-induced longshore current distribution and direction, and secondly to obtain good wave-induced longshore current magnitude. Method 4 presented the best fit for both validation data and analytically calculated wave-induced longshore current. However, the peak of magnitude of wave-induced longshore current was shifted further shoreward due to the late breaking of waves. Calibration of wave height so that it breaks further from the shore was unsuccessful because it does not change despite changing breaking gamma parameter and roller parameter. But, it still simulates a textbook wave-induced longshore current. Seeing that the objective of the study is to understand wave-induced current within mangrove forest, the model setup of Method 4 was adopted for further numerical simulation as the resulting wave-induced longshore current is considered satisfactory for purpose. At x=3.5 m, wave-induced longshore current velocity is reduced by 51% and 82% for conditions with pile groyne and mangrove forest, respectively, in comparison against that of plain condition. Whereas, at waterline, the reduction is 27% and 83% for conditions with pile groyne and mangrove forest, respectively.

For the simulation of hydraulic condition of wave with tidal current, adapted Method 4 setup was used. The adaptations were the boundary conditions prescription. The validation was satisfactory despite shift of wave-induced longshore current velocity peak towards coastline. Reduction of wave-induced longshore current at waterline is 26% and 80% by pile groyne and mangrove forest, respectively. This model setup introduces a slight error for longshore current where longshore velocity along cross-shore profile is consistently lower than for tidal-driven current in the deeper water. It is possible this is caused by the Riemann type in offshore boundary where water was seen to flow through the open boundary.

In cases where waves are present, wave-induced longshore current is more dominant within mangrove forest as waves are able to propagate into the forest and induces current. Whereas, tidal driven current is dissipated from the onset of the interface of mangrove forest and main channel.

A big limitation to the model setup of Method 4 is the absence of calculation of wave-vegetation interaction. Thus, the resulting reduction of wave-induced longshore current velocity by pile groyne and mangrove forest were contributed only by current-vegetation interaction and due to bed friction. This is quite a significant absence, because generally, waves are attenuated by vegetation and cylindrical stems, which will reduce wave height and energy, resulting in breaking of waves closer to shore but with smaller dissipation rate of energy. This not only will affect wave-induced longshore current, but also wave-induced cross-shore current. It is anticipated that should the wave breaks further from waterline, the energy gradient at the waterline will be smaller, which in turn makes the radiation stress gradient smaller. Consequently, onshore directed wave force, $F_x$, will be reduced. With that, increase of water elevation (setup) will reduce and consequently the magnitude of offshore-directed velocity will reduce.

Generally, it was found that current velocity reduction by forest is more effective even for mangrove forest of lower density (1,120 stem/$m^2$) than for pile groyne (6,400 stem/$m^2$). This is due to the large stem coverage for mangrove forest, in contrast to the gap between successive pile groynes (groyne field) where wave energy can reach, dissipate, and induce both longshore and cross-shore current.

# 7 Discussions

Discussions in this chapter are centred on the research questions and the study approach as outlined in Section 1.2 and Section 1.3. Also, a discussion on the practicality of findings from current study is placed at the end of the chapter. In discussing results with respect to cross-shore profiles, cross-shore distance is denoted with x (e.g. x=3m).

## Understanding of Main Validation Data

Understanding into model setup of the experiment by Hulsbergen (1973) is paramount as this leads to a better representation with numerical modelling. Also this will provide an insight into explaining the results that were obtained by the experiment.

From the perusal of Hulsbergen's model setup schematization, it is understood that flow guide along the offshore boundary of the wave basin, which is a standard practise for 3D physical modelling in wave basin post-Visser (1991), is an apparent absence. This adds up water volume in that region, bounded by diagonally placed wave makers. Without the flow guide, it is anticipated that the momentum of current flow closer to the offshore boundary is partially advected to the additional water volume at the offshore boundary, effectively reducing momentum in the main channel. This has been improved upon in more recent experiments. This phenomenon in Hulsbergen's experiment is represented within the numerical model by means of extension of cross-shore model domain, which in turn provides a good agreement on validation.

Also it can be seen that wave guides were not installed. In practice, wave guide is installed along the sides from wave makers to the main channel within the model domain (Figure 14 of setup by Reniers and Battjes, 1997, and Figure 17 of setup by Trampenau, 2000). Wave guides are important to prevent waves from diffracting, and to consequently prevent alongshore variation of wave set-up (Reniers and Battjes, 1997). The absence of wave guide in Hulsbergen's model setup may have contributed to the spatial variation of breaking wave height and breaking location (Figure B. 3). Wave diffraction induces variation of wave height spatially, which with a breaking gamma that is varying with depth, would render the wave height to vary and consequently the breaking location to vary spatially. On top of that, a varying wave set-up would induce spatially varying undertow current, which flow in generally in offshore-ward direction, which is slight opposite of incoming waves. This may cause the steepness of approaching waves to increase in varying degree spatially, which may also affect breaking wave height and location. As a domino effect, the wave-induced currents, both longshore and cross-shore, are varying alongshore.

A pump system is needed to recirculate wave-induced longshore current to obtain alongshore uniformity. On top of that, Visser (1991) has shown that without optimized pumping, current recirculation could contribute to larger measured velocities outside of surf zone. However, a pumping system was not present from the study by Hulsbergen. This could be contributing, to some extent, to non-uniformity alongshore of wave-induced current.

## Reference to Other Similar Experiments

In a study such as current study, apart from a single designated main measurement data for validation purposes, it is useful to refer to one or more other relevant experiments to be able to understand the main designated validation data. Furthermore, this is useful for qualitative comparison, if not also quantitative. Reniers and Battjes (1997) and Trampenau (2000) have conducted extensive experiment using state-of-the-art setups and equipments, which provide high level of confidence. The datasets then are instrumental in analysing the results of numerical modelling, albeit qualitatively.

Reniers and Battjes (1997) have conducted an experiment on longshore current on barred and non-barred beaches. For current study, the case with non-barred beach is most relevant and is referred to. A pump system for optimal current recirculation was installed. Also, multipaddle wave makers with wave guide were installed at oblique angle. A regular incident wave height of 0.08 m, wave period of 1 s, and wave direction of 30° from shore normal was imposed. The result of his measurement for several transects showed slight variation of wave height in deeper water but with wave breaking location at the same distance from waterline. Resulting wave set-up and longshore current were relatively uniform

alongshore. These were facilitated by the pumping system. Due to absence of measured data of condition with pile groyne, this experiment was not adopted as main validation data. However, it provides additional information, especially on the cross-shore profile of wave-induced set-up, which was referred to qualitatively during the analysis of numerical model result. This reference to wave set-up result complements its absence in the experiment by Hulsbergen (1973).

Trampenau (2000) conducted a series of laboratory experiment to understand the hydraulic functioning of permeable pile groins in comparison to impermeable groynes. In the tests, groyne permeability and the ratio of groyne length to the width of surf zone were varied. Similar to Reniers and Battjes (1997), wave guides and pumping system were utilized to facilitate optimal longshore current within the basin. Wave with height of 0.05 m and with direction of 30° from shore normal was imposed. In looking at the results of Trampenau's (2000), it is to be noted that breaker line was located outside of groyne field (either more offshore than the groyne heads or exactly at the groyne head).

Among Trampenau's findings was that for different permeability, flow pattern within the groyne fields were different. This applied to both current-only and wave-only conditions. For a groyne system with permeability of less than 10%, which is highly impermeable, current circulations (vortices) are formed within each groyne field. For permeability of more than 20%, no vortices were formed, with current flowing through the individual pile stems. This finding is important in qualitative validation of current study. Although more recent, this experiment is not adopted due to lack of cross-shore measurement of velocity for the various hydraulic conditions, which is important for a satisfactory validation work for current study. However, the result of this experiment is used qualitatively.


Analytical Calculation

A formulation was introduced by Longuet-Higgins (1970) calculate magnitude of wave-induced longshore current for a regular wave condition and uniform longshore bed profile. Conventionally, wave-induced current will have a peak of magnitude at the exact location of wave breaking, and a triangular shape which means that velocity reduces linearly towards waterline for a single bed slope profile. This formula accounts for the effects of lateral dispersion of momentum by turbulence, which smooths out velocity gradient with a non-dimensional parameter $P$. With $P>0$, the calculated maximum wave-induced longshore current velocity reduces, the peak shifts shoreward, and due to the smoothing, momentum is distributed outside of breaker line.

The above formulation was applied to calculate wave-induced longshore current with wave conditions of Hydraulic Condition 5 (wave-only) and bathymetry as per the experiment by Hulsbergen (1973). Linear wave theory calculation on wave height transformation and breaking agrees with Hulsbergen's (1973) average of measured data. The result of calculation for $N=0.008$ shows good agreement of cross-shore distribution (pattern) of velocity with the measured data and good agreement in the magnitude of peak velocity magnitude, despite peak magnitude shift slightly shoreward and slight underestimation of current velocity outside of breaker line. Two possible causes to the slight deviation are the (1) spatially varying breaking wave height, wave breaking location and (2) some simplifications and assumptions made by Longuet-Higgins (1970) to the formulation involving $N$ and $\alpha$ coefficients. The measured data of Hulsbergen (1973) shows consistency with theory.

Also, the result of analytical calculation is in good agreement with the findings of Trampenau (2000). This increases the reliability and applicability of the main validation dataset despite the standard deviations seen in measured wave-induced longshore current. This also shows that although the formulation by Longuet-Higgins (1970) is decades old with some simplifications using several coefficients such as $N$ and $\alpha$ values, the physics are represented well and serves as good initial estimation of wave-induced longshore current as has been conducted in current study.


Model's applicability for current study

For different hydraulic conditions, boundary conditions were imposed differently. This was particularly straightforward for Hydraulic Condition 1 (tidal flow only). In contrast, for Hydraulic Condition 5 (wave only) and Hydraulic Condition 4 (wave+tidal current), the specifications of boundary conditions were less so.

For tidal-flow-only condition, the setup was treated akin to that of a river, where upstream (western) boundary was imposed with a total discharge, downstream (eastern) boundary with constant water level, while the other two sides (southern and northern boundaries) were specified as closed boundaries. This setup follows closely the experiment setup by Hulsbergen (1973) with slight adaptation in the cross-shore (north-south) length of the domain to compensate for the absence of flow guide in the experiment. The validation result of this hydraulic condition, for both plain condition and condition with pile groyne, were satisfactory. This setup presents the highest level of confidence for subsequent prediction runs with mangrove forest.

In validating for Hydraulic Condition 5 (wave-only), various methods were attempted (Appendix C.1). These methods are schematized in Figure 50. Firstly, two recent master's theses (i.e. Treffers, 2009, and Gil, 2014) were found that utilized Delft3D to simulate wave-induced current with laboratory measurements as validation datasets (Table 10). These theses ran online FLOW-WAVE with roller model. In current study, this method was attempted and designated as Method 1 (without roller model) and Method 2 (with roller model). Apart from that, Deltares Wiki (URL link in Literature List) presents a short report on a simulation of wave-induced current for Egmond aan Zee (Table 10). The setup for this simulation utilized *wavecon* file to specify wave conditions. This was attempted in current study and denoted as Method 3. Another method, Method 4, was similar to Method 3, but instead of *wavecon* file, wave conditions were specified by means of *wavcmp* file. The various methods above were attempted in both Delft3D version 4.00 and 4.02. It was then seen that the results of simulation between the two versions were starkly different, both in magnitude and in cross-shore profile, which will be discussed below.

It was found that all 4 methods simulated with Delft3D version 4.02 gave unsatisfactory cross-shore profile of wave-induced longshore current. Particularly, the peaks of longshore current were in deeper water (h=0.27m) when roller model was imposed. When roller was not imposed, the peak of longshore velocity magnitude was significantly low and further offshore than measured data, with some current within deeper water. Such observations were not consistent with the analytical calculation, measured data of Hulsbergen, as well as longshore current profile from Trampenau's (2000) experiment. It was concluded that these combinations were not suitable for current study.

The results for simulating Methods 1-3 with Delft3D version 4.00 showed the presence of longshore velocity magnitude peaks in various locations and directions as well as significant current velocity in the deeper water all the way to the offshore boundary, where there should not be any velocity present due to constant radiation stresses in that region. These combinations also were not suitable for current study.

By using Method 4 with Delft3D version 4.00, the resulting cross-shore distribution of wave-induced longshore current was resembling a textbook definition of longshore current (Figure 52b). In the deeper water, no current velocity was seen, unlike for the above-mentioned combinations of methods and Delft3D versions. Longshore current was observed within and slightly outside surf zone, which corresponds well with longshore current with lateral mixing as shown by the measured data by Hulsbergen (1973) and Trampenau (2000). Also, the direction of the longshore current was westward, which was as expected. The wave-induced longshore current was relatively uniform alongshore. The magnitude of peak velocity was approximating well to measured data.

However, a very stark deviation was the location of peak of wave-induced longshore current which was more shoreward. This is due to the more shoreward location of wave breaking: at 1.25 m from waterline, in comparison to 1.8 m from coastline for measured data and 1.75 m for analytical calculation. The simulated wave breaks with height of 0.043 m, in contrast to 0.031 m for Hulsbergen's measured data and 0.033 m from analytical calculation. This requires calibration and sensitivity analysis to improve the results.

Before going into the discussion on the calibration process, this paragraph discusses the abnormalities of the results from the various combinations of methods and Delft3D versions. Firstly, by running similar setups for different Delft3D versions, the results were different in cross-shore wave height transformation, which in turn drives the difference in cross-shore profile of wave-induced longshore current. It was later discovered that a Delft3D revision in 2014 for a different purpose inherently rendered erroneous calculation of roller model for the subsequent revisions and versions (Qinghua Ye, personal communication, October 2017). This explains the good validation of wave-induced longshore current for the two previous master's theses (i.e. Treffers, 2009, and Gil, 2014), which are inferred to have been simulated with proper roller model calculation. The erroneous roller model calculation may have been the prime driver for the other abnormalities in wave-induced longshore current results such as the presence of longshore current in the deeper water far from breaker line, the current flowing in opposite direction (eastward) and wave-induced longshore current velocity peaks in deeper water instead of inside surf zone.

A calibration attempt was done to calibrate the cross-shore wave height transformation of Method 4 with Delft3D version 4.00, which was hypothesized would improve the cross-shore distribution of wave-induced longshore current. The main parameter that was targeted was breaking gamma parameter. Treffers (2009) has conducted a comparison for varying breaking gamma, i.e. constant values and a varied breaking gamma based on depth (Ruessink et al., 2003) (Equation 17). In that comparison, he showed that varied breaking gamma based on Ruessink et al. (2003) provides best validation result. In current study, similar attempts were done, i.e. constant and varied breaking gamma. This however, did not change both cross-shore wave height transformation and cross-shore profile of wave-induced longshore current (Figure 56). Attempts to calibrate with roller model parameters, $\alpha$ (wave dissipation due to wave breaking) and $\beta$ (slope in front of roller) coefficients returned similar results, which is no changes to wave height and wave-induced longshore current

velocities. This could be attributed to a faulty numerical implementation, which could be improved upon with subsequent releases of Delft3D revisions.

A major shortcoming of this method is the absence of wave-vegetation interaction. Figure 37b shows cross-shore wave height transformation for various conditions: plain, with pile groyne and with mangrove forest. The resulting wave height are exactly similar for all these three conditions. By right, wave height for the condition with pile groyne should be lower than plain condition, and wave height for condition with mangrove forest should be lower than that. This has a big impact on the consequent wave-induced longshore current. Cross-shore profile of wave-induced longshore current in Figure 37a then theoretically should be lower for conditions with pile groyne and mangrove forest. Also, with the supposed wave height reduction, the location of wave breaking for reduced wave energy would be more shoreward. This would have been accounted for in SWAN model with an additional keyword in the *mdw* file. However, seeing that Methods 1-3, which uses SWAN did not produce reliable result, this was not possible.

In essence, although Method 4 model setup simulates the best wave-induced longshore current compared to the other 3 methods, it exhibits some errors as following:
1. Wave breaks closer to shore with very high breaking wave height. Calibration of this phenomenon was not possible with the model setup.
2. Consequential wave-induced longshore current velocity has peak that is much closer to shore than validation dataset. Also the cross-shore profile of wave-induced longshore current cannot be calibrated with roller model parameters.
3. Wave-height vegetation was not considered in this model setup. This means wave energy was not reduced by vegetation resistance force. Thus, the observed reduction of wave-induced longshore current velocity is only a result of current-vegetation interaction.

Above errors need to be kept in mind when discussing the result of the simulations for wave-only condition.

The model set-up for the condition of wave+tidal current (HC4) was built upon that of wave-only condition (HC5). An adapted Method 4 was utilized. However, in contrast to that of HC5, Riemann boundary was imposed only onto offshore (North) boundary, while total discharge and constant water level were prescribed at East and West Boundaries, respectively. It was later seen that due to this, there is current flowing through North Boundary (Figure 57a). This introduces slight deviation in longshore current velocity across full length of cross-shore profile, as will be discussed below. Also, it was seen that water level was significantly elevated throughout whole model domain if a constant water level of 0.05 m was imposed to West Boundary (Figure 57b). This consequently introduces error to wave-induced longshore current result. The workaround to this abnormality, then, was applying a lower constant water level, so as to produce a logical whole-domain equilibrium water level. With this adaptation, the simulation results showed acceptable validation to measured data (Figure 38a).

Thus, on top of the errors inherent in the model setup of wave-only (HC5) condition, additional uncertainties were introduced by the model setup of HC4:
1. Current flowing through northern (offshore) boundary which was prescribed as Riemann type. The experiment by Hulsbergen does not have current flowing through this boundary.
2. To overcome the simulated high equilibrium water level in whole model domain, a lower constant water level was imposed at downstream boundary. This gives an acceptable result. However, it is uncertain what errors this workaround might have produced.

Above additional errors need to be kept in mind when discussing the result of the simulations for the condition of wave+tidal current.

In addition to the above, in the simulations for varied bed slope angle and mangrove forest density, several more limitations were observed:
1. The setup of Method 4 is not applicable for bed slope that is gentler than 1:45 (Section 6.6). As generally mangrove forests are dominant in very gentle bed slope, the research questions cannot be extended to address wave-induced currents in such bathymetric condition.
2. To simulate roots of mangrove forest, model capability for cylindrical density of up to 208,000 cylinder/$m^2$ is necessary. However, Delft3D only allows up to 80,000 cylinder/$m^2$. Other than density, the main difference between stem and root of mangrove forest is the diameter of the element. In future studies, by having this limitation addressed, it would be valuable to be able to simulate the smaller diameter and higher density of mangrove roots in comparison to the bigger diameter and lower density of mangrove stems for wave-induced currents.

Delft3D model has been utilized numerous times for simulation with vegetation. It utilizes rigid vegetation model introduced by Uittenbogaard (2006, cited by Deltares, 2016). For the simulation with mangrove forest, specification of stem density was straightforward with assumption of uniform distribution in a given plan area. However, for the case

with pile groyne, slight workaround was necessary. In Hulsbergen's experiment, the spacing of double-rowed pile groyne was very small, with lateral flow blocking of 50%. This means that they occupy a very small close-knit, non-uniformly distributed area within a model grid spacing. However, Delft3D only recognizes uniform stem distribution. This means the close-knit stem arrangement was rearranged by Delft3D's assumption in such a way that the blocking is less than 50%. A simulation with this stem density has unsatisfactory validation against measured data. The workaround is by working backwards. With 50% flow blocking as the main criteria, the density of stem per $m^2$ was increased. This gives a good validation against the measured data. This only introduces small error because the grids with pile groynes are far in between (5 m gap between two adjacent groynes), thus flow within the groyne field was not very much affected. With this flexibility, and the result the model gives, the model is considered robust for certain range of vegetation in current study's scope of research. The caveat on stem density in previous paragraph still apply in this case.

A way to tackle the issue of reliability of current model to simulated validation data is by having an alternative model from a different software to calculate similar hydraulic conditions and bathymetry. A different software means that spatial discretization and time integration methods are different, and the formulations adopted may also be different. With this, a comparison can be made between the result of both softwares. Due to time constraint, this was not conducted. It might be a good thesis study for future research.

<u>Damping of wave-induced current within the vegetation</u>

Generally, the introduction of mangrove forest dampens both longshore and cross-shore currents that are generated due to both tidal gradient and radiation stress gradient. The reduction of wave-induced and tide-induced longshore current for pile groynes condition was evident in the measured data of Hulsbergen (Figure 46a&b), which shows both reduction in magnitude of current as well as the width of wave-induced longshore current on top of tidal current. This is being reflected well by numerical calculation in Figure 46c, where the widest contribution of wave-induced longshore current is for plain condition (blue line), followed by condition with pile groyne (red line) and condition with mangrove forest (yellow line). Current-only condition is dashed line, whereas current+wave condition is color-coded similarly with solid line.
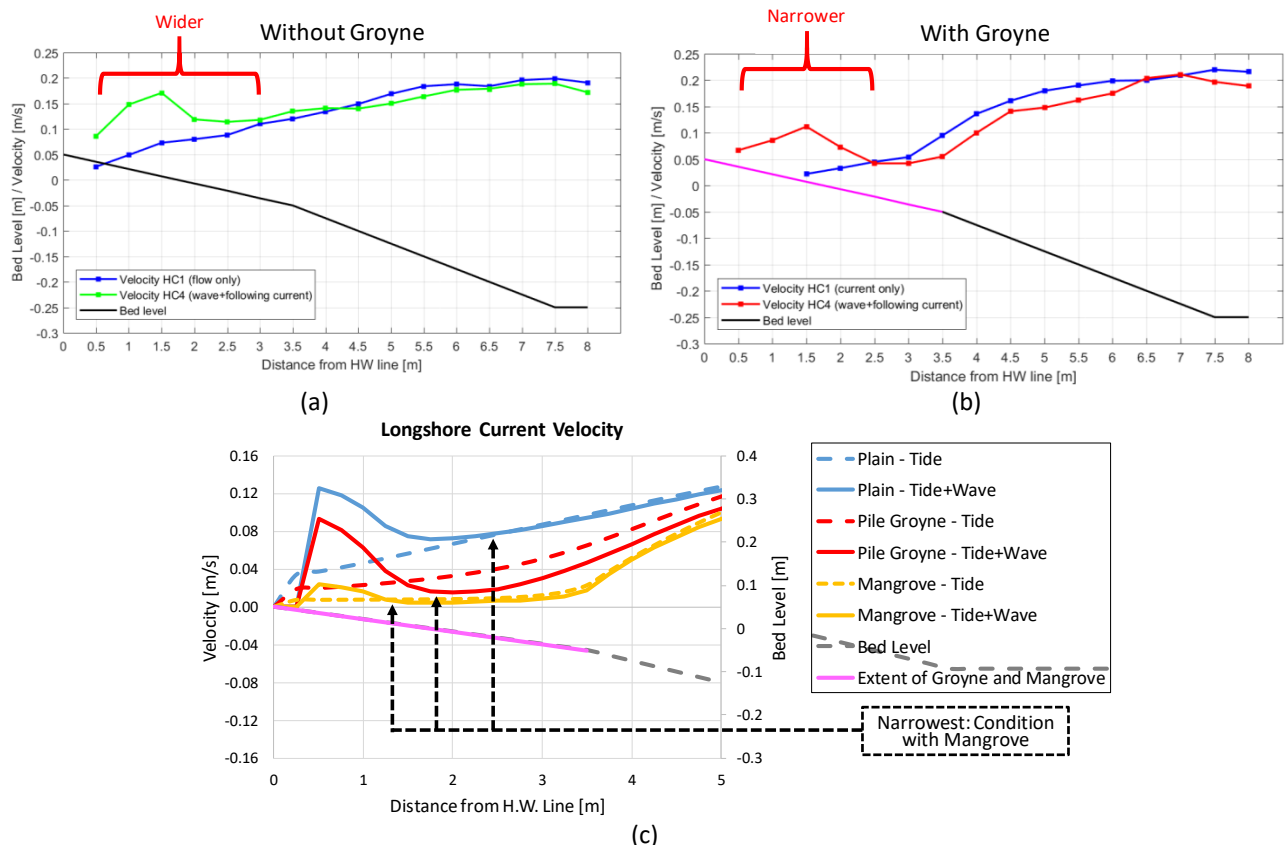


(a)

(b)

(c)

Figure 46            Velocity damping in measured data for with and without groyne

In general, tidal flow is dominant in the main channel. Figure 46 shows that tidal flow penetration into the pile groyne is limited in magnitude (reaches all the way to waterline, but with 50% magnitude only), and more so for the case with mangrove forest (approx. 0.5m into the patch). For all cases (plain condition, conditions with pile groyne and mangrove forest), wave-induced current is observed to be highest in magnitude for the plain condition, followed by conditions with pile groyne (with approx. 30% reduction) and mangrove forest (with reduction of approx. 84%), respectively. Within the

region of pile groyne / mangrove forest, resistance due to stems is dominant over bed friction, which is consistent with theory.

It is to be kept in mind that current model setup does not consider wave-vegetation interaction Figure 37b. This means that simulated wave-induced current velocity is reduced only by current-vegetation interaction. Also from Section 6.5, a discussion followed regarding
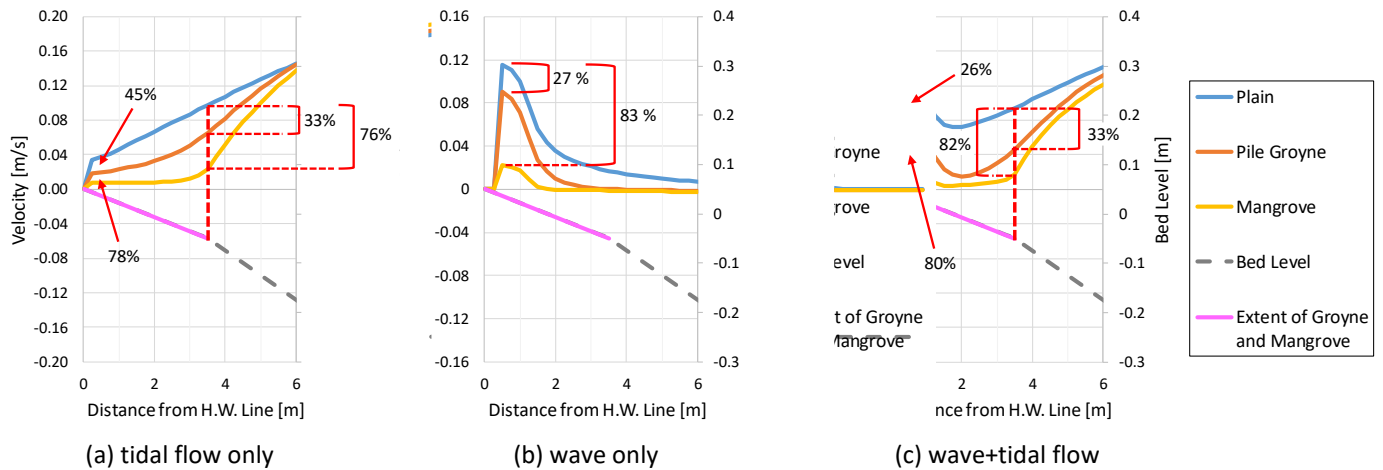


(a) tidal flow only                    (b) wave only                    (c) wave+tidal flow

Figure 47            Zoom-in of Figure 33, Figure 37a and Figure 39 at nearshore region. Cross-shore profile of longshore current velocity.

Figure 47 shows zoom-in of previous plots of wave-induced longshore current in Chapter 6, focusing on the nearshore region. Each extent of velocity reduction is shown with respect to plain condition (blue line).  For the hydraulic condition of tidal flow only (Figure 47a), at x=3.5m, the reduction of velocity by pile groyne and mangrove forest are 33% and 76%, respectively. Moving to near waterline, the reductions of velocity are 45% and 78% for pile groyne and mangrove forest, respectively. Despite lower cylindrical density (mangrove forest with 1,120 stem/m$^2$ and pile groyne with 6,400 stem/m$^2$) mangrove forest provides effective flow damping due to the larger coverage area. In contrast, a pile groyne system consists of gaps (groyne field) in-between each successive groyne, where momentum is not experiencing resistance other than bed friction.

For hydraulic condition of wave only (Figure 47b), reduction of wave-induced longshore current velocity is 27% and 83% for condition with pile groyne and with mangrove forest, respectively. Also, the contribution of wave-induced longshore current is narrower for condition with mangrove forest (waterline to x=1.5m) compared to that for condition with pile groyne (waterline to x=3m).

For hydraulic condition of wave with tidal current (Figure 47c), reduction of wave-induced longshore current at waterline is 26% and 80% by pile groyne and mangrove forest, respectively.

Generally, it is seen that the percentage of reduction wave-induced longshore current by mangrove forest is larger (more than 80%) than of tide-induced current (less than 80%).


Significance of the interaction of wave-induced longshore current with mangrove vegetation

Wave-induced longshore current is dominant within the surf zone region, where tidal flow is effectively reduced, due to bed resistance in the plain condition, and due to additional (and more dominant) resistance by stems (pile and mangrove trees). Figure 48 shows the percentage of contribution of wave-induced longshore current on top of tidal current. Firstly, it is to be reiterated that due to the specification of Riemann type at offshore boundary and total discharge and water level in lateral boundaries for tide+wave condition, current was seen to flow through that the offsbore boundary and this consequently introduces slight deviation in cross-shore profile of wave-induced longshore current velocity. Throughout the cross-shore profile, velocity for the condition of tide+wave at region where tidal current is dominant (deeper water region) is consistently lower than that of tidal-driven condition (Section 6.5).

Current velocity contribution by radiation stresses gradient accounts for more than 70% of total longshore current velocity in nearshore region for all conditions (plain, pile groyne and mangrove). This is quite a significant contribution. In prototype scale, by using Froude scale of 40, the velocity of wave-induced longshore current in mangrove forest (yellow solid line) is up to 0.13 m/s. This velocity may be further broken down into mean velocity and the fluctuating turbulent

velocity. Turbulent velocity may be very significant in mangrove forest due to the complex flow separation and wakes formed by the interaction of flow with mangrove stems. To put in context, the significance of the magnitude of this velocity is mainly important in the context of fine sediment stirring, transport, settling and deposition. On top of the vortices formed by mangrove stems, this settling velocity itself produces wakes trailing above each settling fine sediment floc which may enhance hindered settling. Settling velocity is inherently affected by the concentration of suspended sediment and this is beyond the scope of current study. However, it would be a good topic for next master's thesis.

It is anticipated that the significance of wave-induced longshore current within mangrove forest will reduce for following scenarios:
1. Gentler bed slope, both within the forest and in front of the forest
2. Higher density of mangrove stem and root
3. Bigger mangrove stem and/or root diameter

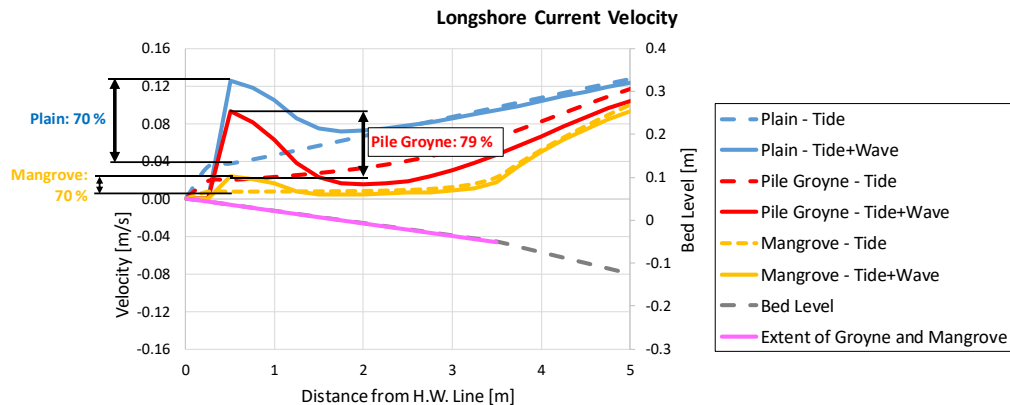This will require further numerical simulation with robust model to investigate.



Figure 48          Significance of wave-induced longshore current

### Wave-induced current for varying mangrove forest properties, i.e. bed slope and density?

Three bed slopes are studied, i.e. 1:35, 1:40 and 1:45. They are considered still on the steeper end for mangrove forest. Gentler slopes are not possible due to the limitation of current model setup for Method 4. Thus, for gentler slopes, the findings are qualitatively extrapolated. For gentler slopes, waves break further from coastline, resulting in wave set-up and set-down that are further offshore. Consequently, for both wave-induced longshore current and wave-induced cross-shore current, the magnitudes are shifted towards offshore and are wider. It is expected that above trends are extended accordingly for much gentler bed slopes.

Three mangrove forest densities are used, which is within the range of Table 9, i.e. 800, 1,120 and 2,720 stem/m$^2$. From the results, it is seen that, as expected, wave-induced longshore current and wave-induced cross-shore current are reduced more for higher mangrove forest densities. A big limitation of this model is the limit of higher density, which is capped at 80,000 cylinder/m$^2$. This means that the wave damping due to the more dense but smaller diameter of roots as per Table 9 is not implementable. A study into this and to compare it against that of stem would be interesting. Different cylinder density with vertical alignment would also be interesting to study.

It is noted that for both simulations into varied bed slope angle and forest density, wave-vegetation interaction was not considered by the model due to the limitation of the model setup.

Also, for both simulations into varied bed slope angle and forest density, it is seen that there is eastward-directed wave-induced longshore current in the deeper water (Generally at x>2.5m). It is argued that since there is no reduction of wave height in that region, which, based on theory, in turn means there is not supposed to be opposite-directed wave force, then this presence of opposite-directed wave-induced longshore current is a numerical artefact due to the Riemann type boundary imposed at all flow boundaries. To verify this, it is recommended in future studies to have other software to simulate similar hydraulic condition, bathymetry and mangrove forest properties.

### Placement and practicality of current study findings in real world

With the findings of current study, the question then is how do they apply to real mangrove forests application? However, before going into the practicality, it is necessary to recap the limitation encountered, and consequently the extra study aspects that need to be done to have a more sound practical use of current findings.

Firstly, the robustness of model setup Method 4 is limited because wave height transformation and consequently, wave-induced longshore current were not subject to changes during calibration of breaking gamma and roller parameters. Secondly, and a very glaring limitation, is the absence of calculation of wave-vegetation interaction by the model setup Method 4. This in turn affects the magnitude of wave-induced longshore current velocity. Also, method 4 model setup was not able to produce reliable wave-induced longshore current for bed slopes gentler than 1:45. On top of that, Delft3D is unable to cater for stem density of more than 80,000 stem/m$^2$.

A potential practicality of current finding is in the improvement of knowledge in rehabilitating mangrove forests or in introducing mangrove forest in suitable coastal areas. Mangrove rehabilitation is widely implemented in areas where the forests are eroding, areas with mangrove squeeze or areas where forests have been detroyed and coastlines are exposed to violent hydraulic forcings. Normally, in such rehabilitation programs, juvenile mangroves are planted in open areas where they are exposed to the hydraulic forcings, thus lowering success rates. Instead of leaving planted juvenile mangroves as they are, it might be possible to plant cylindrical stems at regular intervals to increase stem density in the rehabilitation areas. This may reduce both tidal and wave-induced currents to increase the probability of juvenile mangrove survival rate. Also, with reduction of current velocity, the rehabilitation region may promote fine sediment settling and deposition so that suitable bed level of mudflats for mangrove expansion may develop seaward. There have been quite a number of studies conducted on wave attenuation by mangrove vegetation. More numerical model is necessary to find the optimal balance of cylindrical diameter and density for this purpose. Also, quantification of wave-vegetation interaction may be necessary to be paired to current-vegetation/stem interaction.

It is understood that in certain parts of the world, brushwood dams have been constructed to serve similar purpose as the stem planting proposal in above paragraph, such as in Kien Giang Province, Vietnam, and in Demak, Indonesia (Sediment Dynamics Lecture Notes, 2015). Brushwood dams utilizes the concept of still water basins, which is to create relatively still water where sediment infilling and sediment settling can be promoted. It is uncertain how the comparative effectiveness of either of the methods would be. A comparative study into quantitative effectiveness of both methods would be a good thesis study. One advantage of the planting of stems in regular intervals as proposed above is that there is no need to relocate them further offshore once the forest advances forward, as what is needed to be done for the case of brushwood dams. Also, sediment supply can enter the rehabilitation area from many directions due to the nature of open boundary as opposed to brushwood dam system where there are only one or two inlets for sediment to enter. Numerical simulation for various scenarios (hydraulic condition, stem density, brushwood dams dimension, etc.) is necessary. A cost benefit analysis or a multi criteria analysis would be a great additional way to approach this.

Another question coming from this study is: which is more relevant between pile groyne and mangrove for applicability in real coastal area? For this comparison, the context will be limited to areas where coastline protection is considered to be primary priority. This means that the coastline is aimed either to be maintained or to develop seaward. In both a pile groyne system and a mangrove forest, both tidal-driven and wave-driven longshore currents are reduced. The key difference is the presence of gap between adjacent pile groynes (groyne field) which is absent in mangrove forest. Waves may propagate into the groyne fields and induce currents. The impact of this is that sediments may be stirred by both propagating waves and breaking waves, and in turn they may be transported by both wave-induced current and tide-induced current. Since mangrove forests thrive in mudflats where sediments are predominantly cohesive, once these fine sediments are suspended, their settling and deposition will require very low current velocity for certain extended period of time. A healthy mangrove forest will not have gaps large enough like groyne fields. Thus, no or little wave breaking (possibly spilling breaker, which implies very low rate of wave energy dissipation with respect to cross-shore distance) may occur within the forest. This means sediment stirring and consequently, sediment loss, are kept to a minimum. Not only this may keep mangrove forests stable, but may also encourage expansion seaward.

This brings the discussion to another advantage of mangrove forest over pile groyne for this context. Mangrove forests are able to adapt, and when the conditions are met, the forests may expand. Conditions favourable for forest expansion are mild hydraulic conditions and sufficient or surplus of fine sediments. Additionally, mangrove forests are able to adapt to sea level rise, provided it is rising with sufficient sediment supply and deposition.

# 8 Conclusions and Recommendations

## 8.1 Conclusions

The main conclusion from current study is that in coastal fringing mangrove forests, where they are exposed to tidal waves, tidal currents, short waves and wave-induced current, the short waves may be able to penetrate into the forest and induce both longshore and cross-shore currents that are quite significant. However, the extent of wave breaking and induced currents are subject to the bathymetric condition, hydraulic conditions and mangrove forest properties. For instance, they are subject to increase or decrease depending on the mangrove density and bed slope. Also, critical attention needs to be paid to all aspects of a thesis study, i.e. critical eye on the validation data, numerical model and analytical models.

Numerical modelling has a huge potential in predicting the phenomena related to wave-induced current within mangrove forest should there be robust models that can take this challenge. The main obstacle to this is the ability of models to calculate wave and current processes in very gentle slopes and also in high density vegetation stems.

Another main finding of this study, which in the author's opinion, might be more important than the quantified findings of the other research questions, is the shortcomings of the current numerical model in simulating current study's hydraulic condition bathymetry, and mangrove forest properties. The shortcomings are first reiterated in this section, and later on in Section 8.2, among many others, recommendations on the specific aspects of the numerical model limitations are proposed. A model that achieves better validation will be able to provide more understanding in regards to the transformation of wave height, as well as the damping of longshore current and lateral current.

Research questions are reiterated below to provide a correct frame of mind when perusing the rest of the conclusions.

### What is the extent of the model's reliability for current study?

It is imperative to first re-establish the extent of the reliability of the results that the numerical simulation produced so that the subsequent conclusions are digested with right frame of reference. The issue of model reliability is mainly centred on the simulation of hydraulic conditions of wave-only and wave with tidal current. The simulation for hydraulic condition of tidal current only is reliable, in a sense, that it validates well.

The shortcomings from the model stem from the way the method to impose wave conditions onto Delft3D FLOW, which in essence is one-way communication. This is because online FLOW-WAVE coupling was shown to not be reliable in this study. Hence, the alternative way of imposing wave conditions.

First of all, the main shortcoming of this study is the absence of wave-vegetation interaction. Meaning, wave attenuation by vegetation and pile groynes were not calculated, and damping of wave-induced longshore current is only caused by current-vegetation interaction. Secondly, the wave height transformation is fixed, and calibration with breaking gamma parameter and roller parameters were not able to change the transformation. This renders the waves to break much closer to shore compared to measured data and analytical calculation. This, of course, in turn affects the wave-induced longshore current velocity. Third, the model results are not logical for bed slopes that are gentler than 1:45. Mangrove forests are predominantly located at gently sloping foreshores, and extending the scope of study into this slope spectrum is imperative. However, due to this limitation, this exploration was not possible. Also, Delft3D is unable to cater for stem density of more than 80,000 stem/m$^2$. This means that current study was not able to predict interaction of wave-induced current with mangrove roots, which are smaller in diameter and higher in density compared to mangrove tree trunks/stems.

What is the extent of damping of wave-induced current within the vegetation?

The damping of wave-induced longshore current within mangrove forest is more than 80%. With that, damping both magnitude and width of contribution of wave-induced longshore current to the total velocity are reduced. However, it is to be noted that this damping is very case specific to the bathymetry, hydraulic conditions and mangrove forest properties of current study. It is anticipated that should wave-vegetation is considered by the model, this reduction will be more significant. Such constriction of scope of current study, which in large part was due to the limitation of the model, may provide huge potential for future master's students who are inclined on similar topic of research. This is further elaborated in Section 8.2 below.

What is the significance of the interaction of wave-induced longshore current with mangrove vegetation?

In a situation where both oblique waves and tidal current are present, it is seen that tidal current is mainly dominant in the main channel and less so in the shallower water (especially when mangrove forest is present), while longshore current is dominant in the surf zone for both conditions with and without mangrove forest. On top of that, offshore-directed current induced by setup at waterline is quite significant. Still, it is to be re-expressed that this is case-specific to current study's hydraulic condition, bathymetry and mangrove forest properties.

For current study specific cases, wave-induced longshore current velocity may contribute more than 70% of the total current velocity within mangrove forest. This applies to all conditions: plain, with pile groyne, and with mangrove forest. This is quite significant. It is anticipated that the significance of wave-induced longshore current within mangrove forest will reduce for following scenarios:
1. Gentler bed slope, both within the forest and in front of the forest
2. Higher density of mangrove stem and root
3. Bigger mangrove stem and/or root diameter

In prototype scale, by using Froude scale of 40, the velocity of wave-induced longshore current in mangrove forest is up to 0.13 m/s. This velocity may be further broken down into mean velocity and the fluctuating turbulent velocity. Turbulent velocity may be very significant in mangrove forest due to the complex flow separation and wakes formed by the interaction of flow with mangrove stems. To put in context, the significance of the magnitude of this velocity is mainly important in the context of fine sediment stirring, transport, settling and deposition. On top of the vortices formed by mangrove stems, this settling velocity itself produces very small scale wakes trailing above each settling fine sediment floc which may enhance hindered settling. Settling velocity is inherently affected by the concentration of suspended sediment and this is beyond the scope of current study.

How is the nearshore current affected by varying vegetation properties such as bed slope and density?

Three bed slopes were considered, i.e. 1:35, 1:40 and 1:45. For gentler slopes, waves break further from coastline, resulting in wave set-up and set-down that are further offshore. Consequently, for both wave-induced longshore current and wave-induced cross-shore current, the magnitudes are shifted towards offshore and are wider. It is expected that above trends are extended accordingly for much gentler bed slopes.

Three mangrove forest densities were studied, i.e. 800, 1,120 and 2,720 stem/m$^2$. From the results, it is seen that, as expected, wave-induced longshore and cross-shore currents are damped for higher mangrove forest densities.

## 8.2   Recommendations

The recommendations proposed in this sections is divided into two categories. The first one focuses on the extrapolation from current study. Previous section and chapters have elaborated on the limitation of current study, mostly dealing with the shortcomings of the model. This first category of recommendations is proposed by assuming the model shortcomings are solved. This assumption is inherently held because current study does not delve into trouble-shooting of model. Also, several other recommendations are proposed that are not related to the found current model setup shortcomings but may be good continuation of current study. The recommendations under this first category are:
1. A very important aspect in studying wave-induced current within mangrove forest is the wave and vegetation interaction. This is important because in general, vegetation attenuates wave energy and this in turn affects the induced currents, in comparison for a situation without vegetation. It is recommended to use a suitable model that can simulate both wave-vegetation and current-vegetation at the same time, unlike the model for current study. This will reflect more realistic wave transformation and wave-induced current.

2.  Also, wave transformation for current model setup are not calibratable with breaking gamma. Thus, for a similar study scope, it is recommended that simulations with robust wave height calibration capability is adopted. This is because wave height is the driving mechanism for wave-induced current.

3.  Using model that complies with the recommendation in items 1 and 2 above, it is recommended to simulate for very gentle slopes and for higher mangrove density with smaller diameter so as to mimic mangrove roots. Gentler slopes means that shallower depth is achieved further offshore. Also, as Iribarren number may be smaller, wave breaking type might be more inclined towards spilling breaker type. In turn, this may affect wave-induced longshore current. Also, breaker line might shift outside of mangrove forest.

4.  A comparison into the difference of wave-induced longshore current for regular waves and irregular waves may be able to show different findings. This is especially because irregular waves will produce long bound waves and consequently long free waves. The penetration extent of long waves are more than short waves and this will definitely show different phenomena within mangrove forest.

5.  In Chapter 7, a proposal was made to consider planting of stems at regular intervals in a wide coverage area where mangrove forest replanting is conducted. The main idea is to provide damping of wave-induced current to reduce loading onto the juvenile planted mangrove trees. Also, it was mentioned that among current practice in several parts of the world that are implemented for mangrove rehabilitation is the construction of brushwood dams. This stem planting of course is a very rough idea, the finetuning and feasibility of which would require:

    a.  Robust numerical simulations to compare both stem planting and brushwood dams that takes into account items 1, 2 and 3 above. The numerical simulations need to consider scenarios that includes optimal diameter, optimal distance between stem and also to compare against typical brushwood dams dimensions.

    b.  Multi criteria analysis because cylindrical stems may be sourced from natural or synthetically made materials and this will have wide ranging effects on social, economic and environment.

    c.  A more in-depth numerical simulation would involve morphodynamics study to observe erosion versus deposition for the rehabilitation area.

    d.  Perhaps the practicality aspects of both rehabilitation methods may be studied. This includes the logistics, manpower, durability and cycle of maintenance, etc.

The second category of recommendations focuses on the shortcomings that have been identified in applying Delft3D for the validation of Hulsbergen's (1973) measured data. They merely are a recap and a highlight on the shortcomings:

6.  The interaction of wave and vegetation/cylinders are to be taken into account in Delft3D simulation using *wavcmp* and *wavecon* attribute files. This will ensure a more realistic representation of wave height transformation and wave-induced current within mangrove forest as has been discussed in Chapter 7.

7.  With the implementation of *wavcmp* into Delft3D-FLOW, it is necessary that roller parameters such as slope of roller front and the breaking parameters are able to calibrate both the significant wave height profile and the induced current.

    a.  Firstly, wave height should be calibratable, because in current study, the breaking gamma was more than $\gamma$ = 1.0 and this is considered too high (Section 6.3). A more realistic breaking gamma is the one proposed by Ruessink et al. (2003) (Equation 17). This explains why the simulated wave was breaking much closer to shore.

    b.  Secondly, by changing roller parameters, the wave-induced longshore current did not change and this means that the model is not sensitive to the parameter calibration.

    It is imperative that these parameters are calibratable.

8.  It was seen that *wavecon* file simulated for 2DH model such as current study was unable to be implemented as was by Broekema (2015) and Deltares Wiki which modelled with 2DV domain. Having used *wavecon* with communication files from Delft3D-WAVE shows no difference than an online Delft3DFLOW-WAVE results. A consistent workaround is recommended. *wavecon* file application may have the potential to provide better calculated wave-induced longshore current than by using *wavcmp*.

9.  It was seen that previous Delft3D version (Version 4.00) was able to provide a more realistic longshore current compared to the latest Delft3D version (Version 4.02). It is uncertain why such is the case. It is recommended that the numerical or physical conceptualization within the model to be re-assessed.

# 9 Literature List

Bosboom, J. and Stive, M. J. F. (2015). Coastal Dynamics 1. Delft Academic Press, Delft, 0.5 edition.

Briele, A. C. (2014). Assessment of the application of permeable pile groins as coastal protection. Delft, The Netherlands: Delft University of Technology, Master's thesis. http://resolver.tudelft.nl/uuid:63c53a1d-e768-4e28-9dd5-4147f36eb609

Broekema, Y. B. (2015). Modelling of Grain Sorting Mechanisms in the Nearshore Area for Natural and Nourished Beaches. Delft, The Netherlands: Delft University of Technology, Master's thesis. http://resolver.tudelft.nl/uuid:9815a76c-12ea-415f-9957-5f1993a42b5e

Buckman, L. (2013). Hydrodynamics of partially vegetated channels:stem drag forces and application to an in-stream wetland concept for tropical, urban drainage systems. Delft, The Netherlands: Delft University of Technology, Master's thesis. http://resolver.tudelft.nl/uuid:71f7e38d-a05b-4e6e-bb84-88fa4d6f31b9

Deltares (2016). Delft3D-FLOW User Manual. Technical report, Deltares, Delft.

Deltares (2014). Delft3D-WAVE User Manual. Technical report, Deltares, Delft.

Deltares Wiki, https://publicwiki.deltares.nl/pages/viewpage.action?pageId=90409987

Gil, J. P. d. S (2014). Application of the Delft3D System in the Modelling of Laboratory and Field Longshore Currents. Técnico Lisboa, Lisboa.

Holthuijsen, L. H. (2007). *Waves in oceanic and coastal waters*. Cambridge University Press.

Horstman, E. M., Dohmen-Janssen, C. M., & Hulscher, S. J. M. H. (2013). Modelling tidal dynamics in a mangrove creek catchment in Delft3D.

Horstman, E. M., Dohmen-Janssen, C. M., Narra, P. M. F., van den Berg, N. J. F., Siemerink, M., & Hulscher, S. J. M. H. (2014). Wave attenuation in mangroves: A quantitative approach to field observations. *Coastal engineering*, *94*, 47-62.

Hu, Z., Suzuki, T., Hitman, T., Uittewaal, W., & Stive, M. (2014). Laboratory study on wave dissipation by vegetation in combined current–wave flow. *Coastal Engineering*, *88*, 131-142.

Hulsbergen, C.H. (1973). Effect of permeable pile groynes on coastal currents. Delft Hydraulics

Huthoff, F., & Augustijn, D. C. M. (2005). Channel roughness in 1D steady uniform flow: Manning or Chézy? In A. Makaske, H. P. Wolfert, & A. G. van Os (Eds.), Proceedings NCR-days 2004, Research for managing rivers; present and future issues, NCR publication 26-2005 (pp. 98-100)

Kothyari, U. C., Hayashi, K., & Hashimoto, H. (2009). Drag coefficient of unsubmerged rigid vegetation stems in open channel flows. Journal of Hydraulic Research, 47(6), 691-699.

Longuet-Higgins, M. S. (1970a). Longshore currents generated by obliquely incident sea waves: 1. *Journal of geophysical research*, *75*(33), 6778-6789.

Longuet-Higgins, M. S. (1970b). Longshore currents generated by obliquely incident sea waves: 2, *Journal of Geophysical Research*, 75(33), 6790–6801, doi:10.1029/JC075i033p06790

Longuet-Higgins, M. S., & Stewart, R. W. (1964, August). Radiation stresses in water waves; a physical discussion, with applications. *Deep Sea Research and Oceanographic Abstracts* (Vol. 11, No. 4, pp. 529-562). Elsevier.

Mazda, Y., Wolanski, E., King, B., Sase, A., Ohtsuka, D., & Magi, M. (1997). Drag force due to vegetation in mangrove swamps. Mangroves and Salt Marshes, 1(3), 193-199.

Mazda, Y., Kobashi, D., & Okada, S. (2005). Tidal-scale hydrodynamics within mangrove swamps. *Wetlands Ecology and Management*, *13*(6), 647-655.

McIvor, A. L., Spencer, T., Möller, I., & Spalding, M. (2012). Storm surge reduction by mangroves. The Nature Conservancy and Wetlands International.

McIvor, A. L., et al. Reduction of wind and swell waves by mangroves. The Nature Conservancy and Wetlands International, 2012.

Mil-Homens, J. (2016). Longshore sediment transport: Bulk formulas and process based models.

Narayan, S., Suzuki, T., Stive, M. J., Verhagen, H. J., Ursem, W. N. J., & Ranasinghe, R. (2011). ON THE EFFECTIVENESS OF MANGROVES IN ATTENUATING CYCLONE-INDUCED WAVES. *Coastal Engineering Proceedings*, *1*(32), 50.

Nepf, H. 2012a. Flow over and through biota. In Treatise on Estuarine and Coastal Science, ed. E Wolanski, D McLusky. San Diego: Elsevier

Nepf, H. 2012b. Hydrodynamics of vegetated channels. Journal of Hydraulic Research, 50(3), 262-279.

Van der Linde, P. (2011). Modelling nearshore currents driven by waves and set-up gradients. Delft, The Netherlands. Delft University of Technology, Master's thesis. http://repository.tudelft.nl/islandora/object/uuid%3A2d4c1593-1c77-4445-97f6-f44beddb27ce?collection=education

Reniers, A. J. H. M., & Battjes, J. A. (1997). A laboratory study of longshore currents over barred and non-barred beaches. *Coastal Engineering*, *30*(1-2), 1-21.

Ruessink, B. G., Walstra, D. J. R., & Southgate, H. N. (2003). Calibration and verification of a parametric wave model on barred beaches. *Coastal Engineering*, *48*(3), 139-149.

Schiereck, G.J. (2012). Introduction to Bed, Band and Shore Protection (Second edition), VSSD, Delft.

Tas, S.A.J. (2016). Coastal protection in the Mekong Delta: Wave load and overtopping of sea dikes as function of their location in the cross-section, for different foreshore geometries. Delft, The Netherlands: Delft University of Technology, Master's thesis. http://resolver.tudelft.nl/uuid:2f82f861-73e2-4bb3-8332-e51e917e64cd

Trampenau, T. (2000). Hydraulische Wirksamkeit durchlässiger Buhnen: Laborexperimente und Naturuntersuchungen, Technischen Universitat Braunschweig, Braunschweig.

Treffers, R. B. (2009). Wave-Driven Longshore Currents in the Surf Zone. Delft, The Netherlands: Delft University of Technology, Master's thesis. http://resolver.tudelft.nl/uuid:98c7b974-2c0e-464c-9b9a-2044f018965b

Truong, S. H., Ye, Q., & Stive, M. J. (2017). Estuarine Mangrove Squeeze in the Mekong Delta, Vietnam. *Journal of Coastal Research*.

Uijttewaal, W. S. (2005). Effects of groyne layout on the flow in groyne fields: Laboratory experiments. Journal of Hydraulic Engineering, 131(9), 782-791.

van Rooijen, A. A., McCall, R. T., van Thiel de Vries, J. S. M., van Dongeren, A. R., Reniers, A. J. H. M., & Roelvink, J. A. (2016). Modelling the effect of wave-vegetation interaction on wave setup. *Journal of Geophysical Research: Oceans*, *121*(6), 4341-4359.

Vasarmidis, P. (2016). Assessment of the influence of permeable pile groins on nearshore hydraulics. Delft, The Netherlands: Delft University of Technology, Master's thesis. http://resolver.tudelft.nl/uuid:69682a06-868a-47e0-81a9-34dbff42c950

Visser, Paul J. "Laboratory measurements of uniform longshore currents." *Coastal Engineering* 15.5-6 (1991): 563-593.

Walstra, D. J. R., Mocke, G. P., & Smit, F. (1997). Roller contributions as inferred from inverse modelling techniques. In *Coastal Engineering 1996* (pp. 1205-1218).

# 10    Appendix A

This section provides the layout plan and the respective cross-section profiles. All of the data in this appendix are provided by Phan Manh Hung from Mathematical Modelling and GIS Department of Institute of Coastal and Offshore Engineering - Vietnam Academy for Water Resources.
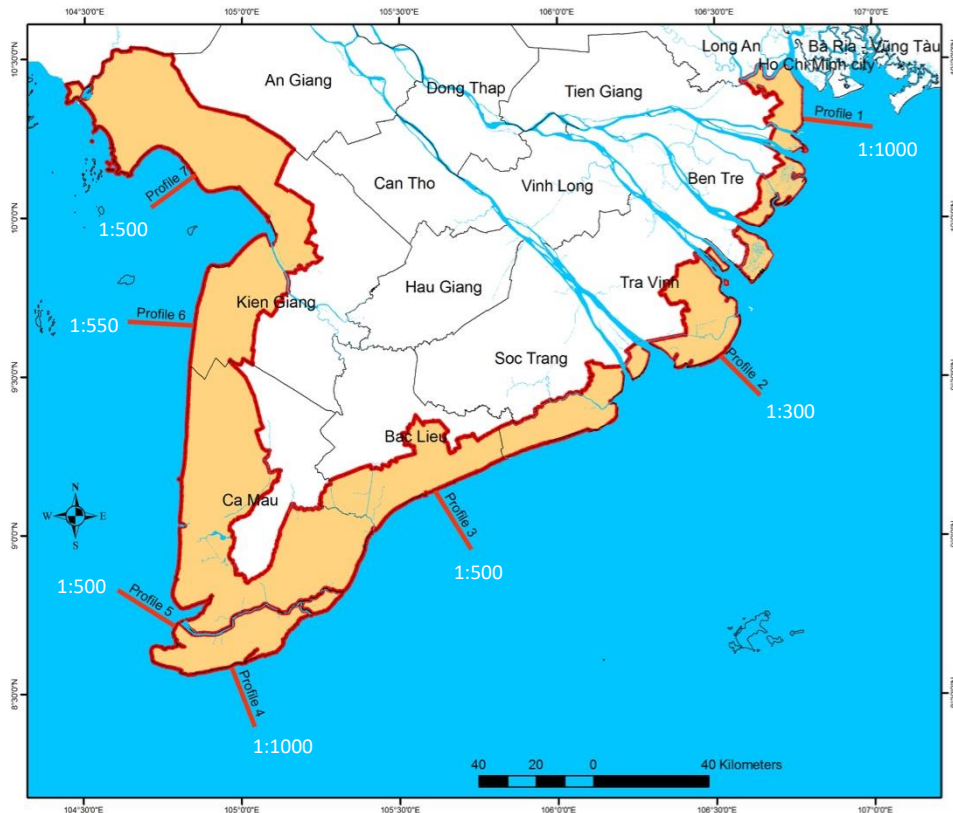


Figure A. 1   Locations of coastal profiles and their respective approximate slopes (Source: VAWR)
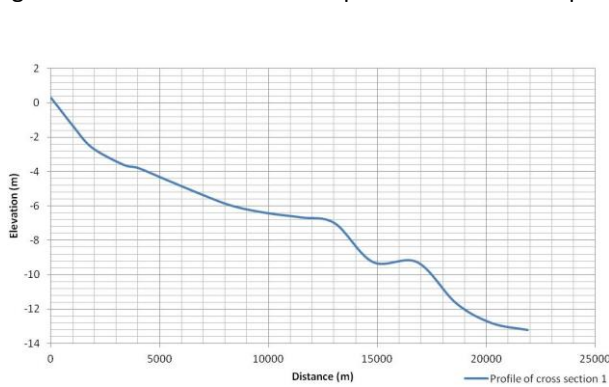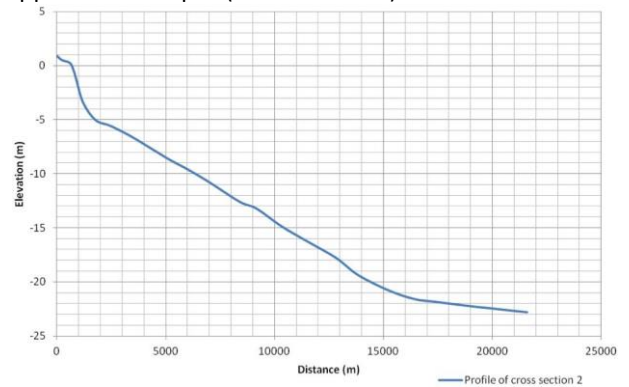


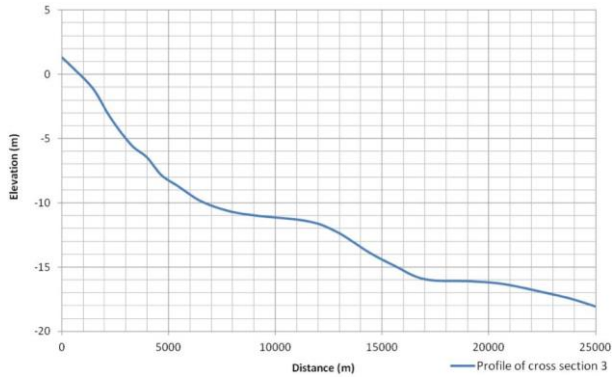Figure A. 2        Profile 1



Figure A. 3        Profile 2

Figure A. 4          Profile 3
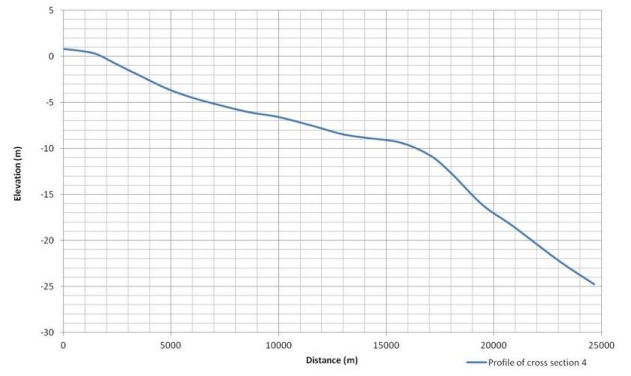


Figure A. 5          Profile 4
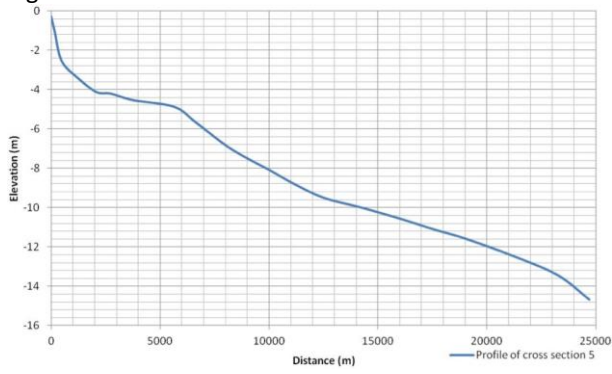


Figure A. 6          Profile 5
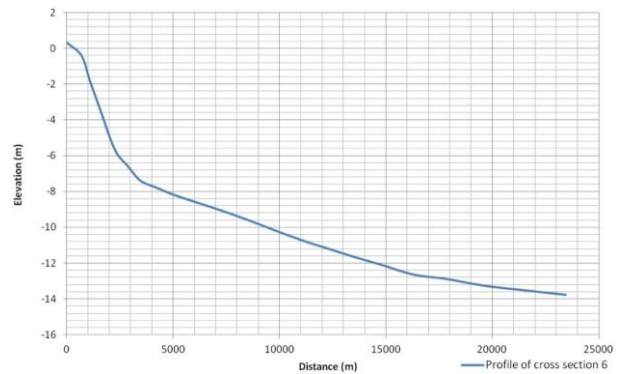


Figure A. 7          Profile 6
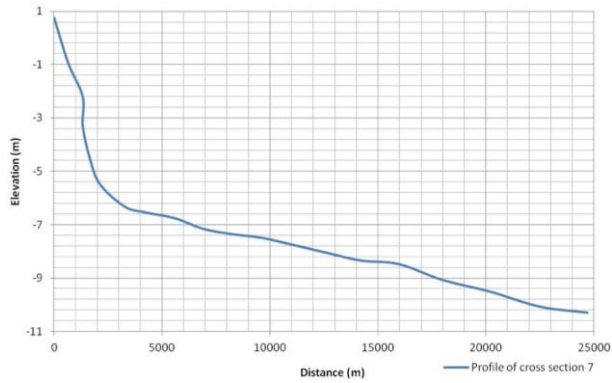


Figure A. 8          Profile 7

# 11   Appendix B

This section provides excepts of results from Hulsbergen (1973) that are proposed for validation of the numerical modelling for current thesis. The corresponding numerical simulations are shown in Table 3.
.
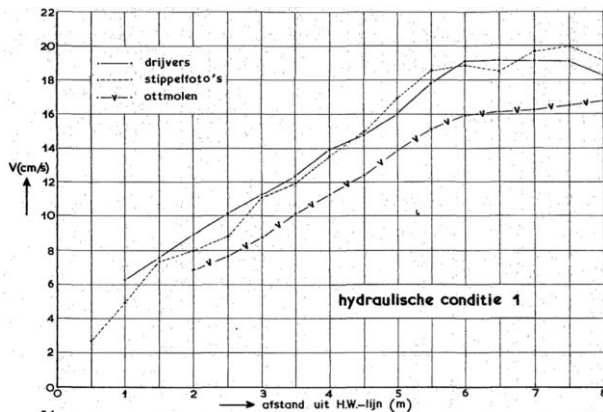


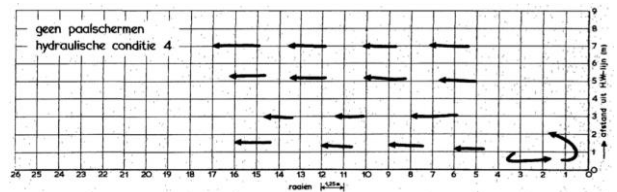Figure B. 1          Velocity distribution for hydraulic condition 1 without pile groyne



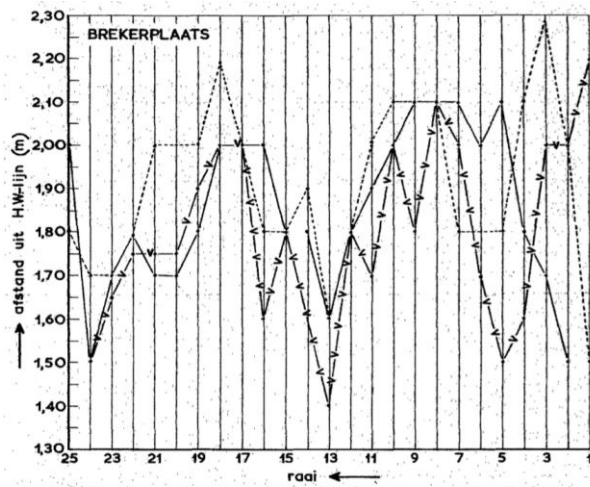Figure B. 2          Sketch of current pattern for hydraulic condition 4 without pile groyne
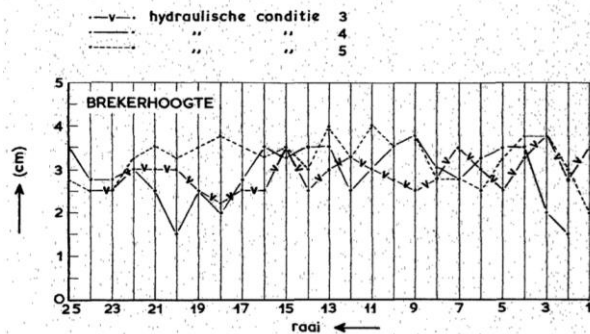


Figure B. 3          Location and height of wave breaking for hydraulic conditions 3, 4 and 5 without pile groynes
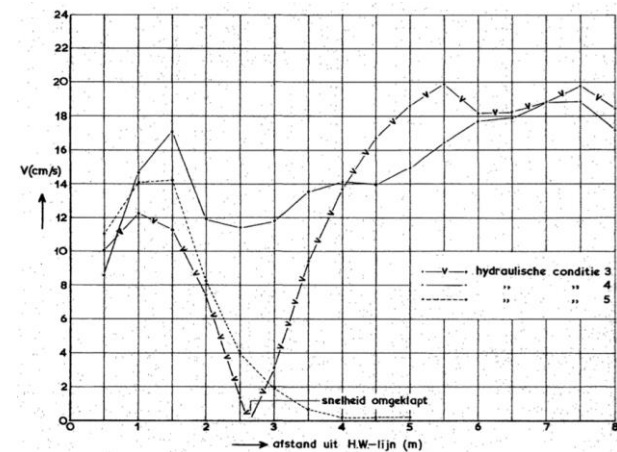


Figure B. 4          Velocity distribution for hydraulic conditions 3, 4 and 5 (measurement with floats) without pile groynes
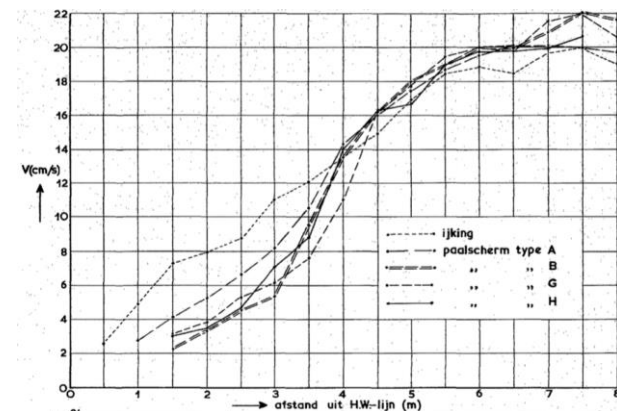


Figure B. 5          Velocity distribution for hydraulic condition 1 with pile groyne configurations A, B, G & H
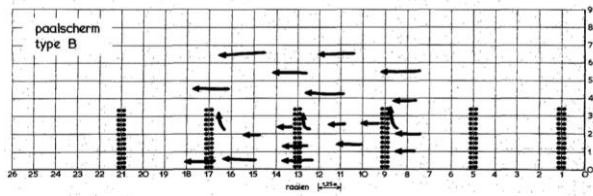
Figure B. 6        Sketch for current pattern for hydraulic condition 4 with pile groyne configuration B
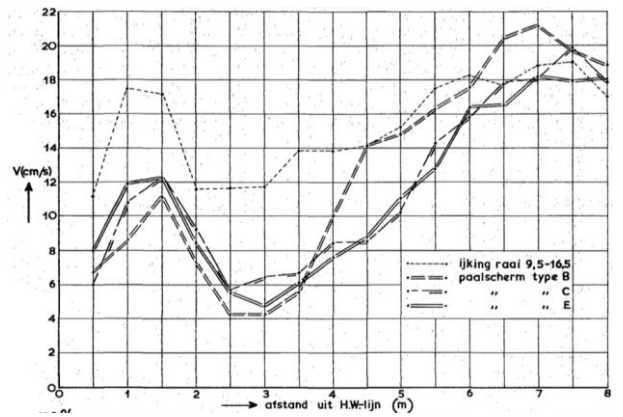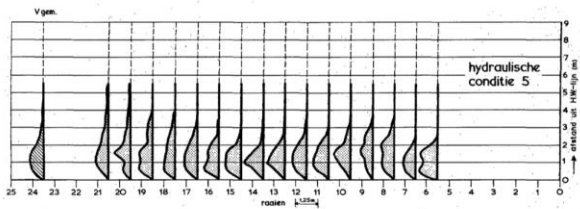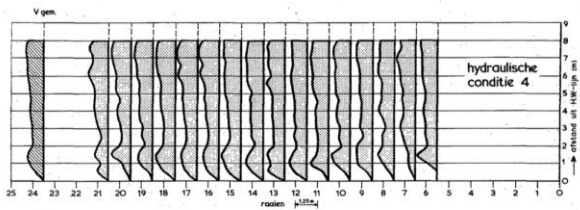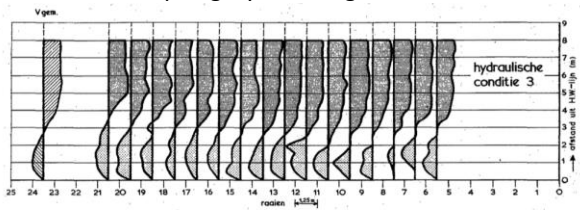


Figure B. 7        Velocity distribution for hydraulic condition 4 with pile groyne configurations B, C & E



Figure B. 8        Velocity distribution for hydraulic conditions 3, 4 and 5

# 12    Appendix C

This appendix outlines the details of validation works attempted for both wave-only (HC5) condition and condition with wave and current in the same direction (HC4) against measured data by Hulsbergen (1973) and analytical calculation. The methods used are shown below. The results and discussion follow. Some of the methods show deviation and eccentricity, which are also elaborated. The final methods of simulation to be adapted for current study (although not perfect, but is fit for purpose) are concluded.

## C.1.    Wave-Only Condition

First of all, two master theses and a setup in Deltares Wiki are summarized. Both theses and the Deltares Wiki have run simulation for wave-induced current for laboratory setups using Delft3D. The subsequent section provides brief explanation of Delft3D setups of current study.

It will be seen that the main parameters of current study setups are similar to that of the two Msc theses and the Deltares Wiki, but with results that are not as expected (based against measured data of Hulsbergen, 1973, and analytical calculation). Subsequently, other methods are attempted. Method 4 shows the best agreement to the expected magnitude and direction, but attempt at calibration using roller model parameters is unsuccessful. Elaboration is provided on the results. Also, simulations were run for different Delft3D versions, and there are some significant result differences. Version 4.00 which is an older version provides better results.

This Section C.1 discusses and concludes that the simulated wave-induced current by the outlined methods for the measured data of Hulsbergen (1973) return results that is far from ideal validation. Having considered that, Method 4 is adopted for the purpose of current study, the justification of which is provided below.

### C.1.1.    Previous Master's Theses and Deltares Wiki

Treffers (2009) and Gil (2014) have conducted Delft3D simulation on wave-induced current (Table 10). The main parameters of their setups are the specification of Neumann condition in lateral boundaries and constant water level in offshore boundary. Then, roller model is imposed. The sizes of Delft3D-WAVE domains are larger than that of the Deltf3D-FLOW domains. Validation of their models were successful.

In Deltares Wiki, a 2DV morphology model was setup for Egmond aan Zee (Table 10). A link to the webpage is provided in literature list (Page 9-1). It also employed Neumann condition at lateral boundaries. Harmonic water level is imposed on offshore boundary, which is not much different than the two master theses. Roller model was also imposed. However, in contrast to the master theses, the wave height, period and direction are prescribed at the seaward boundary through a *wavecon* file.

Table 10    Model Setups: Previous Master Theses, Deltares Wiki and Current Study

| Parameter | Treffers (2009) | | Gil (2014) | Deltares Wiki | Current Study |
|---|---|---|---|---|---|
| | 3D | 2DH | 3D | 2DV | 2DH |
| Calibration data | Reniers & Battjes (1997) | | Hamilton et al. (2001) | Walstra (2004) | Hulsbergen (1973) |
| Flow Boundaries | Lateral = Neumann Offshore = Constant water level | | Lateral = Neumann Offshore = Constant water level | Lateral = Neumann Offshore = Harmonic water level | Method 1, 2 & 3 Lateral = Neumann Offshore = Constant water level<br><br>Method 4 All Riemann (Figure 51a) |
| Wave Boundaries | Random H = 0.1 m T = 1.2 s Dir = 30° Shorenormal | | Irregular (JONSWAP) $H_{m0}$ = 0.225 m $T_p$ = 2.5 s Dir = 10° Shorenormal | *Wavecon* file 4 wave conditions with weightage factor | Regular H = 0.03 m T = 1.04 s Dir = 15° Shorenormal<br><br>Through online FLOW-WAVE, or *wavecon* or *wavcmp* files |
| Bathymetry | Uniform alongshore Barred profile | | Uniform alongshore | Egmond aan Zee | Uniform alongshore (Figure 49) |
| Simulation time (min) | 20 | 20 | 60 | N/A | 300 |
| Time step (min) | 0.005 | 0.005 | 0.3 | 6 | 0.005 |
| No. of vertical layers [-] | 15 | 1 | 10 | 12 | 1 |
| Reflection parameter alpha ($s^{-2}$) | 100 | 100 | 100 | N/A | 100 |
| Roughness | White Colebroook: 6E-4 | Chezy = 55 | $k_s$ = 4E-4 m | Sandy with a $d_{50}$ and $d_{90}$ of 180 μm and 280 μm, respectively | Chezy = 65 |
| Background horizontal viscosity ($m^2$/s) | 0 | 2E-4 | 0.001 | 0.01 | 0.001 |
| Threshold depth (m) | 0.02 | 0.02 | 0.01 | 0.1 | 0.01 |
| Smoothing time (min) | 60 | 60 | | | 60 |
| Roller | Yes | Yes | Yes | Yes | **Yes** / No |
| Cstbnd | Yes | Yes | N/A | Yes | **Yes** / No |
| Gamdis | -1 (Ruessink et al. 2003) | -1 (Ruessink et al. 2003) | -1 (Ruessink et al. 2003) | -1 | N/A |
| F_lam (breaker delay) | 0 | 0 | N/A | -2 (Roelvink, 1995) | N/A |
| FwFac (streaming parameter) | 0.1 | 0 | N/A | 0 | N/A |
| Betaro (angle of roller) | 0.05 | 0.05 | N/A | 0.05 | N/A |
| α (Breaking calibration factor) | 1 | 1 | N/A | N/A | 1 |
| Snelli | N/A | N/A | N/A | Yes | No |
| Fwee (Bottom friction factor) | N/A | N/A | N/A | 0.01 | No |

## **C.1.2.** Numerical Simulation for Current Study

As outlined in Table 10, the main setup parameters are the boundary conditions of Delft3D-FLOW (different for Method 1-3 vs Method 4) and the method the waves are prescribed. Figure 49 shows cross-shore profile of bathymetry for FLOW and WAVE domains which are uniform alongshore, and plan view of FLOW and WAVE domains. FLOW domain was placed in the bottom-centre of WAVE domain to avoid shadow effect due to the oblique angle of wave propagation from offshore boundary. Also, FLOW domain was significantly smaller to avoid boundary effects from reaching area of interest.

In the simulation with Delft3D, 4 methods have been tried (Figure 50). The methods vary mainly in the way waves were prescribed and also difference in the communication method between Delft3D-FLOW and wave specifications, be it SWAN model or attribute files.
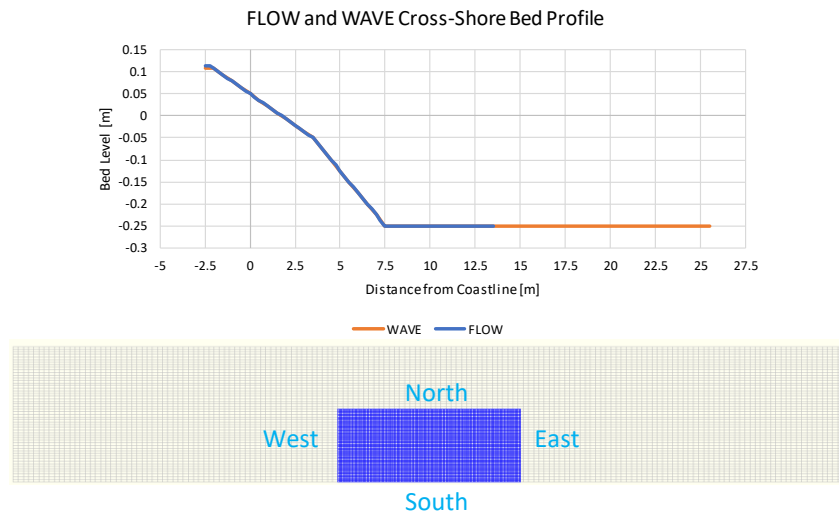


Figure 49    Above: Cross-shore bed profile. Uniform alongshore. Bottom: Plan view or FLOW (blue) and WAVE (grey) domains.
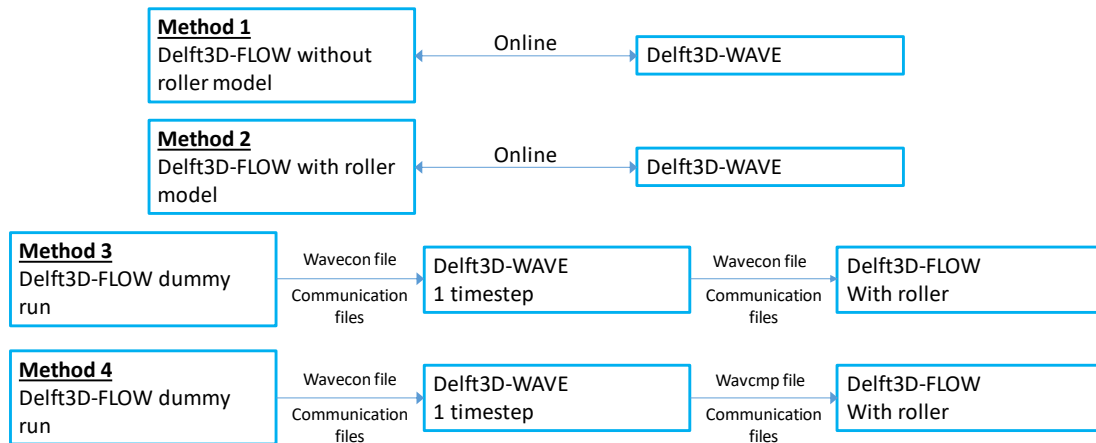


Figure 50    Methods of modelling for wave-only condition attempted in this study

Method 1 was done to observe what the result would be like without roller model being turned on. This applies a direct online Delft3D FLOW-WAVE coupling where communication files act as intermediary for two-way flow-wave interactions. Method 2 was based on Method 1, but with a roller model turned on. It was similar to what the two above Master theses have specified.

Method 3 and Method 4 were as per outlined in Delft3D-FLOW manual (Deltares, 2016). These two methods did not employ online FLOW-WAVE coupling. For a typical small coastal model in stationary mode, Delft3D manual recommends Method 3 to be combined with Neumann condition for lateral boundaries and water level for offshore boundary, which was employed in the model setup. It is suspected that Deltares Wiki has employed Method 3, or it could be that Deltares Wiki had employed a direct Delft3DFLOW-*wavecon* without Delft3D-WAVE, which is what Broekema (2015) had done. Further discussion on Broekema (2015) and Deltares Wiki is also provided in Section C.1.2.4 below.

(a) wave-only                                          (b) wave+tidal current
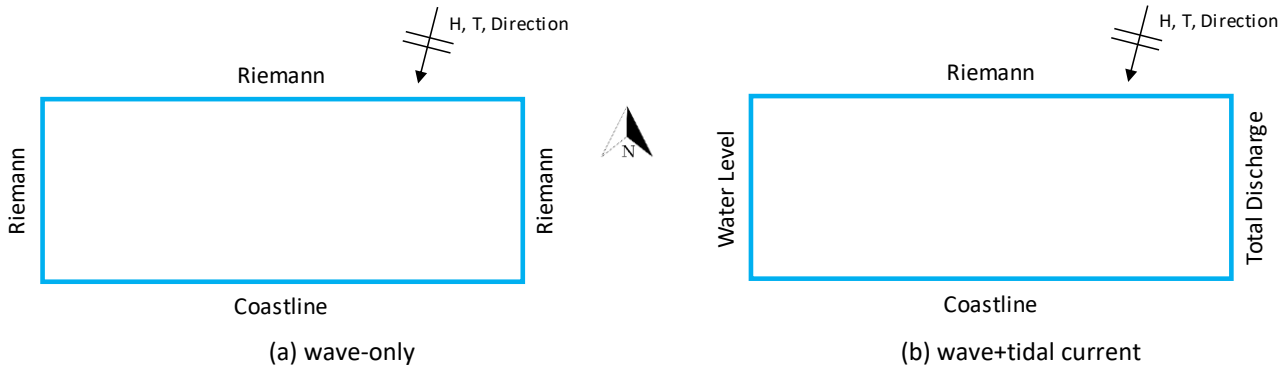
Figure 51    Prescribed boundary conditions for (a) Method 4 for wave-only condition and (b) adapted Method 4 for wave+tidal current condition

Method 4 is for instationary mode. It is necessary that Riemann type was specified to all flow boundaries (Delft3D-FLOW manual by Deltares, 2016), and wave conditions were imposed with *wavcmp* file. This method was attempted because this ss the only method where, upon running, the diagnostic report did not state "No wave components imposed at boundary". It is to be noted, however, that the understanding of this method is that the wave conditions imposed with *wavcmp* file was irregular waves, since there was no communication between the *wavcmp* file and the WAVE module, where spectrum shape and directional spreading can be specified. Both the spectrum shape and directional spreading were not specified in *wavcmp* file, either.

All of the above methods were run for both the latest version (version 4.02) and a previous version that was available in Blackboard and all CiTG (*Civiele Techniek en Geowetenschappen* in Dutch or *Civil Engineering and Geosciences* in English) desktops (version 4.00). This was done because it was suspected that the above-mentioned Master theses were conducted with version 4.00. It will be seen that there were some stark differences between the different versions.

### C.1.2.1.  Results – Longshore Current

The result (cross-shore distribution of wave-induced current) of all above methods are shown in Figure 52, for both Delft3D versions 4.02 and 4.00. It can be seen on first glance that there are significant differences in the result for both versions for each method (each method is color-coded with similar colour across both Delft3D versions).

Positive values indicate westward direction, which is as per measured data of Hulsbergen (1973), and negative values indicate the opposite. Default roller parameters are used. Only in Section C.1.2.3 will some roller parameter changes be attempted and discussed. The cross-shore distance from coastline will be denoted as x- distance in meter (e.g. x=3 m). The breaker line is at approximately x = 1.75 m. The data by Hulsbergen (1973) and the analytical calculation will be henceforth referred to as "*Expectation*" or "*Expected*". This generally refers to the current direction, magnitude and qualitative cross-shore distribution pattern.

Analytical calculation using Longuet Higgins (1970) is plotted in green dashed line. Hulsbergen (1973) measured data is plotted in black asterisks.



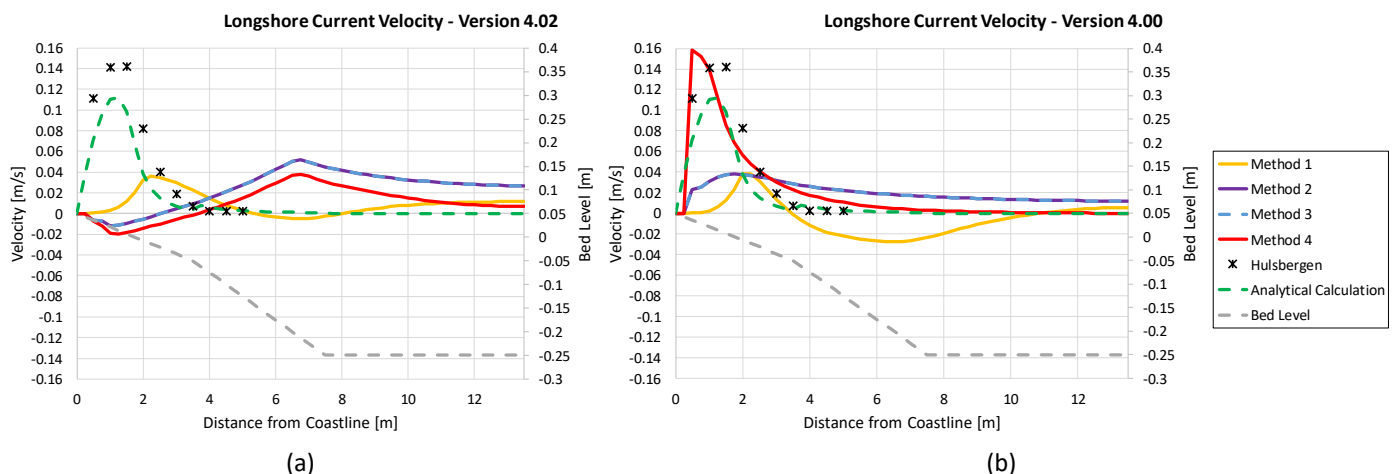(a)                                                          (b)

Figure 52    Result: Longshore current velocity with Delft3D (a) version 4.02 and (b) version 4.00

In version 4.02, **Method 1 (yellow line)** shows that the magnitude of the current nearshore is small (about 0.04 m/s). It is anticipated that by imposing roller model, the peak of the longshore current will be more shoreward, and will be higher (in magnitude), as theoretically understood, and as shown by the two master theses above. The main problem with this Method 1 is the existence of current in deeper water (x>5m). Theoretically, and also based on Hulsbergen data, there should not be current outside of breaker line other than the current due to the horizontal mixing of wave-induced current in the surfzone. For Delft3D version 4.00, **Method 1 (yellow line)** shows that in the surfzone, the longshore current is of expected direction but with smaller magnitude. However, at x>3.5 m, there is current in eastward direction (negative values), which is not as Expected.

**Method 2 (purple line)** and **Method 3 (dashed blue line)** show similar magnitude and pattern to each other for both versions 4.02 and 4.00, as can be seen by the overlapping of both plot lines in Figure 52. In version 4.02, however, in the surfzone, the direction of the current is opposite of Expectation. Also the current in opposite direction that is at x>3m is not as Expected. In version 4.00, the cross-shore profile is consistently flowing westward. First of all, even though roller model is imposed, the magnitude within surfzone is of similar order with **Method 1**, which is without roller model. And secondly, the existence of current outside of breaker parameter all the way to the offshore boundary is not as Expected. This means that although **Method 3** introduces *wavecon* for both Delft3D-WAVE and Delft3D-FLOW (not the dummy run), it is suspected that the FLOW module still calculates current from the communication file instead of the *wavecon* file.

Detailed look at the wave heights are shown in C.1.2.2 (Figure 53 and Figure 54). What is stark is that between Method 2 and 3, the wave heights are exactly the same. But between Delft3D versions 4.02 and 4.00, the calculated wave heights are different. This drives the difference in longshore current between the two Delft3D versions.

The distribution of longshore current in **Method 4 (red line)** of version 4.02 shows pattern that is similar to **Method 2** and **3**, but with slight difference in magnitude. However, it is still different than Expectation. For version 4.00, the longshore velocity resembles closest to Expectation. However, it appears that the peak of longshore current magnitude is at the coastline. Calibration is needed to lower the peak of longshore current, to shift it further from shore and to lower the current outside of the breaker line. This is done in Section C.1.2.3.

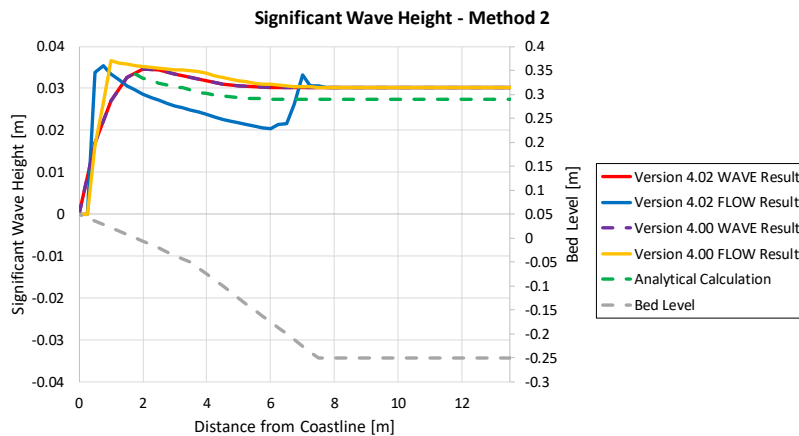### C.1.2.2.  Results – Significant Wave Height



Figure 53     Result: Cross-shore distribution of significant wave height: Method 2
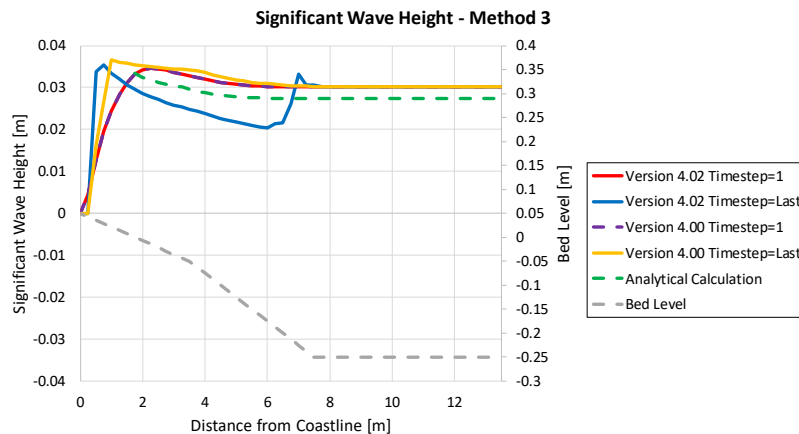


Figure 54     Result: Cross-shore distribution of significant wave height: Method 3

Figure 53 shows the evolution with time of wave height in Method 2 for both different Deltf3D versions. The **red line** and **purple line** represent the significant wave height values from the coupled WAVE run. They are exactly the same. Figure 54 shows the evolution with time of wave height within Delft3D-FLOW for both different Delft3D versions. The **red line** and **dashed purple line** represent the wave height values at time step 1 that are received from the communication file produced by the standalone WAVE run. They are both the same.

For both Method 2 and 3, once FLOW receives the information, and simulation is run, the wave height (**blue** and **yellow** lines) change with time, and both change differently. There seems to be two wave breaking locations observed for version 4.02. The offshore breaking occurs in water depth of about 0.27 m. This is a consistent problem. Changes to the bed slopes at the deeper water have been attempted, and it was seen that the wave height (offshore) breaking is consistent at water depth of 0.27 m. This should not theoretically manifest. Wave breaking for bathymetry of current study should only occur in one location along the cross-shore profile.

**Dashed green line** shows the analytically calculated wave height distribution in cross-shore direction. The breaking wave height is 0.033 m, which approximates well to Hulsbergen's measured data, which averages to wave height of 3.10 m. The calculated location of breaking at 1.75 m from the waterline also agrees well with the measured data of 1.80 m from waterline.

What is stark is that between Method 2 and 3, the wave heights are exactly the same. But between Delft3D versions 4.02 and 4.00, the calculated wave heights are different.
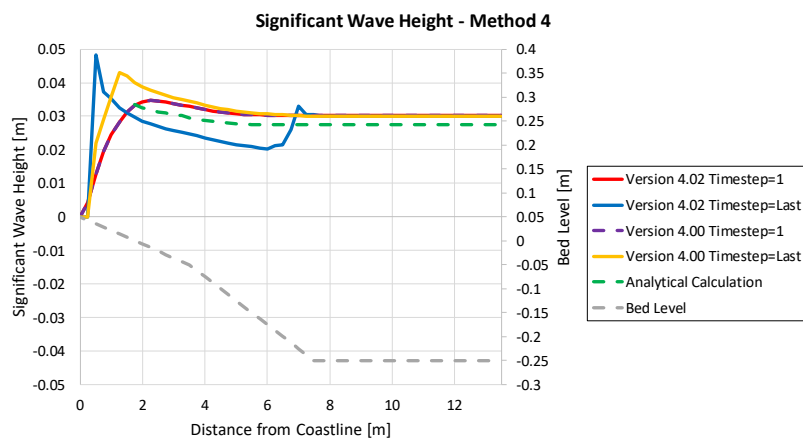


Figure 55      Result: Cross-shore distribution of significant wave height: Method 4

Figure 55 shows the cross-shore distribution of wave height for Method 4 for different time steps and different Delft3D versions. Similar to Method 3, the first time steps are exactly the same for different versions (**red line** and **purple line**). **Version 4.02 (blue line)** still shows double wave breaking locations, meaning it is still incorrect. **Version 4.00 (yellow line)** shows a single breaking location, but it breaks at a higher wave value than **analytically calculated (dashed green line)**.

### C.1.2.3.  Sensitivity Analysis / Calibration of Roller Parameters

Generally, from Figure 52, it can be seen that using Method 4 with Delft3D version provides the closest pre-calibration longshore current to the Expectation. However, it can be seen from Figure 55 that the wave (**yellow line**) breaks closer to shore and with much higher breaking wave height (0.043 m) than analytically calculated (0.033 m) and Hulsbergen's data (0.031 m). This causes the longshore current to peak at the coastline (due to roller) and with higher peak value (**Red line** of Figure 52).

The first calibration parameter attempted is the breaking gamma (keyword is Gamdis in mdf file). The default value is 0.55. For sensitivity analysis, the breaking parameter by Ruessink et al. (2003) is attempted, which is also used for both above-mentioned Master Theses and Deltares Wiki. Also, a value of the other end of the spectrum of breaking gamma is taken to observe the changes (Gamdis = 0.9). α coefficient (Alfaro) calibrates the wave dissipation due to wave breaking, default value of which is 0.1 and a sensitivity analysis value of 0.01 is done. β (Betaro) is the slope in front of the roller. The default value is 0.1, while a sensitivity analysis value of 0.01 is given.
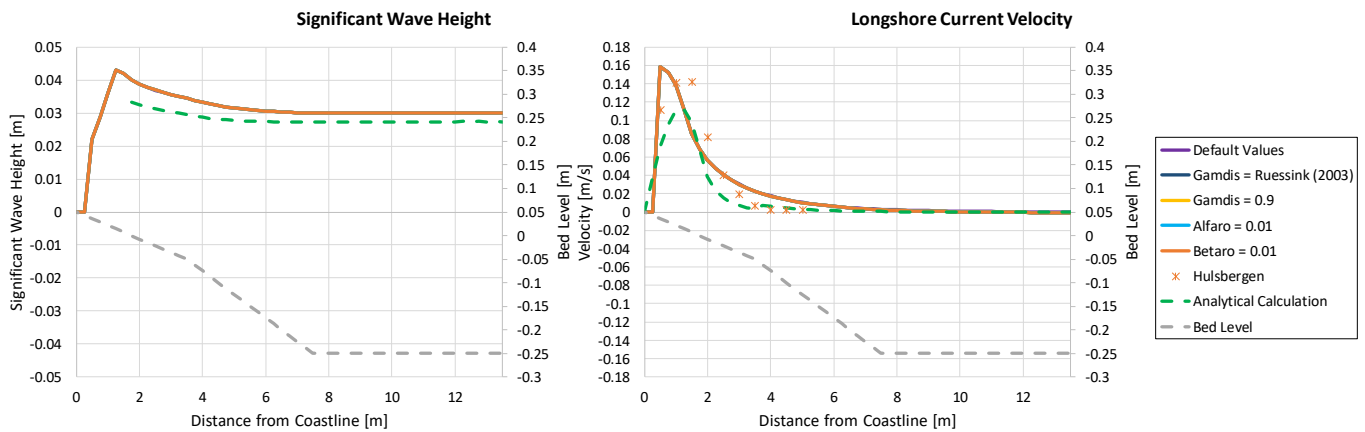
Figure 56      Sensitivity analysis / calibration of roller parameters

Figure 56 shows the result of the sensitivity analysis. For both the analysis on significant wave height and longshore current velocity, despite that the attempted roller parameters are considered on the extreme end, the results show that they are not changed even with the change of roller parameters as shown by the overlap of the plot lines.

In contrast, by using Method 2, the changes done to roller parameter inputs will result in the change of the velocity profile.

Figure 56 shows that the wave breaks at 1.25 m from waterline, with wave height 0.43 m, water depth 0.036 m, which means that the breaking gamma value is 1.21.

### C.1.2.4.  Other Attempted Parameters

Boundary conditions and the way waves are specified are not the only parameters that have been attempted in validating for wave-only condition. With Method 2, 3D model with 10 layers have also been attempted, with no difference in result. Also, with Method 2, the following parameters have been changed:
1. Wave energy dissipation rate & radiation stresses
2. The usage of FLOW HD result in WAVE: water level and current: On & Off
3. Cyclic, Waqua, Flood
4. Whitecapping, refraction, frequency shift
5. Partial slip. Requires very small timestep (smaller at least by order of 10), run becomes very expensive.
6. 3D with wave streaming, FwFac=0
7. Different roughness
8. Higher wave height: Sensitivity analysis. Resulting in increased intensity of above flow field.
9. Wave spectrum: JONSWAP and Gaussian

None of the above parameters return results that are better than Method 4.

The method employed by Broekema (2015) have also been attempted. Generally, it was a shorter version of Method 3. He simulated Delft3DFLOW-*wavecon* directly, without the need of a communication file from Delft3D-WAVE. For current setup, however, the Delft3D-FLOW model cannot calculate without communication file even though *wavecon* file has been placed in the same setup folder. It was understood this might be due to the fact that Broekema (2015) ran 2DV simulation, and not 2DH like in current study. It is worth noting that Deltares Wiki also ran 2DV, which is why perhaps they were able to simulate with *wavecon* file (Method 3).

## C.1.3.  Discussion

Previous section shows that Method 4 resembles closest to the measured data of Hulsbergen (1973) and analytical calculation. However, the longshore current peak is shifted shoreward and this cannot be improved by means of roller model parameters and breaking parameters.

Some might argue that peak velocity of wave-induced longshore current was shifted shoreward due to the specification of roller model. An attempt to run a simulation as per Method 4 without roller model being turned on was done. The simulation, however, ended abnormally. This means that to employ Method 4, it was necessary to have roller model turned on in the first place. Otherwise, there is no other model results that come close to simulating a proper wave-induced longshore current other than Method 4.

Despite above-mentioned limitations, to achieve current study objectives, Method 4 is employed. This is considered sufficient as the cross-shore velocity profile is relatively uniform alongshore, and the distribution of longshore current is theoretically sound.

Further validation was conducted. It was found that a Chezy coefficient of 50 m$^{1/2}$/s achieves good magnitude of peak of longshore current in comparison to measured data of Hulsbergen (1973) that has been corrected for depth-averaged values (Figure 35).

## C.2. Wave and Current Condition

This section describes the model validation for Hydraulic Condition 4, wave and current in the same direction (Table 1). General model setup is similar to that of wave-only condition by employing Method 4. Due to the requirement to impose discharge in the eastern boundary, not all flow boundaries can be specified with Riemann as required by FLOW manual (Deltares, 2016). Riemann was prescribed in the northern offshore boundary, total discharge was prescribed in the eastern boundary, while water level was prescribed in the western boundary (Figure 51b).

Figure 57a shows the flow discharge with time through all three open boundaries. Due to this setup, the discharge though the eastern boundary (blue line) is consistent with input (0.45 m$^3$/s), but it can be seen at the end of simulation, inflow through the northern boundary is observed and in return, extra outflow through western boundary to compensate the northern inflow discharge is observed. Such is not observed for the flow-only condition because close boundary is prescribed for that hydraulic condition. For HC4, there is no workaround for this because with specification of *wavcmp* file for wave conditions in the northern boundary, Riemann type boundary has to be specified.
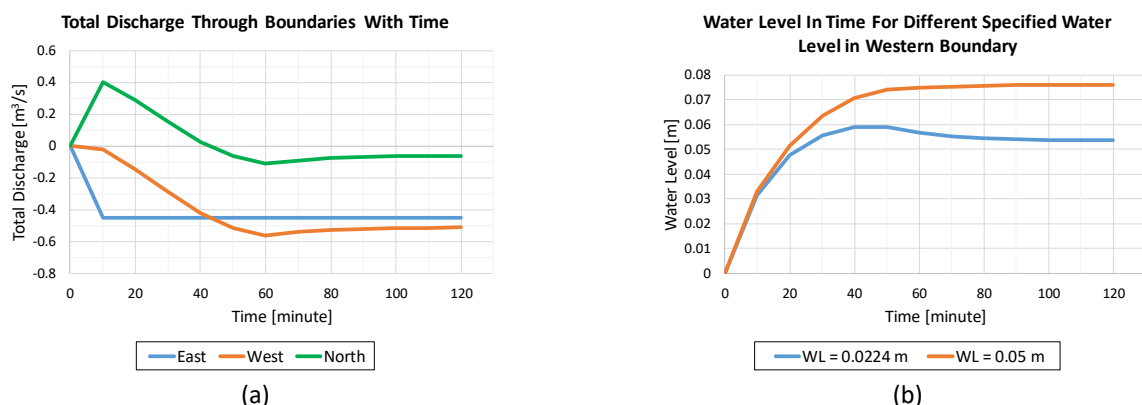


Figure 57    (a) Total discharge through boundaries with time; (b) Water level in time for different specified water level in western boundary

It was found that by specifying constant water level of 0.05 m in the western boundary, the water level at the end of the simulation is very high (Figure 57b). This is in contrast with flow-only condition (without *wavcmp* file and without Riemann type in northern boundary) simulation, where the water level at the end of simulation is approximately 0.05 m. This means that the specification of *wavcmp* file and Riemann boundary induces and increase of water elevation in the domain. It could be that because when Riemann invariant is not zero, the boundary causes artificial reflection of the characteristics. According to Delft3D manual (Deltares, 2016), the input for the Riemann boundary conditions will be generated automatically based on the given wave conditions. Hence, it is possible that the Riemann is eventually not zero and causes reflection within the domain.

In order to simulate a logical cross-shore distribution of longshore velocity, the water level at the end of simulation has to be approximately 0.05 m. This is achieved by specifying a lower constant water level at the western boundary, i.e. 0.0224 m (Figure 57b). Furthermore, it was found out that by specifying varied Chezy coefficient based on nikuradse roughness, $k_s$, of 0.001 m in the domain makes the model unstable. With that, a Chezy coefficient value of 50 is adopted. This setup gives a good validation of longshore current for both plain condition and condition with pile groyne (Figure 38). This is then adopted as the model setup for other the condition with mangrove forest.

## C.3. Conclusion

Despite the limitations elaborated above, Method 4 is considered fit for purpose and is employed for the study of wave-induced current within mangrove forest. Whereas, for wave+current (HC4) condition, offshore boundary is remained as Riemann type, while one lateral boundary is imposed with total discharge and the other is imposed with a lowered constant water level, i.e. 0.0224 m instead of 0.05 m. For future studies, it is recommended to at least adopt a model that is capable of overcoming the limitations of current model setup.